

AD-A127 873

LOW LEVEL CONVERGENCE AND THE PREDICTION OF CONVECTIVE
PRECIPITATION(U) ILLINOIS STATE WATER SURVEY DIV URBANA
B ACKERMAN DEC 82 SWS-CR-316 ARO-15529.10-05

1/2

UNCLASSIFIED

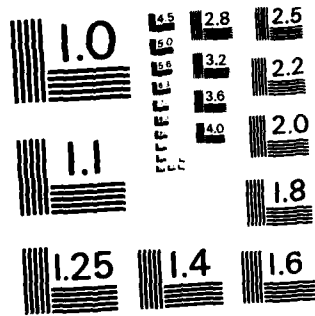
NSF-ATM78-08865

F/G 4/2

NL

11
11

11
11



MICROCOPY RESOLUTION TEST CHART
NATIONAL BUREAU OF STANDARDS - 1963 - A

Unclassified

SECURITY CLASSIFICATION OF THIS PAGE (When Data Entered)

Handwritten initials and marks at the top right of the page.

REPORT DOCUMENTATION PAGE

READ INSTRUCTIONS BEFORE COMPLETING FORM

1. REPORT NUMBER 15529.10-GS		2. GOVT ACCESSION NO. AD-A127073		3. RECIPIENT'S CATALOG NUMBER	
4. TITLE (and Subtitle) Low Level Convergence and the Prediction of Convective Precipitation			5. TYPE OF REPORT & PERIOD COVERED Final: 1 May 78 - 30 Jun 81		
7. AUTHOR(s) Bernice Ackerman			6. PERFORMING ORG. REPORT NUMBER		
9. PERFORMING ORGANIZATION NAME AND ADDRESS University of Illinois Champaign, IL 61820			8. CONTRACT OR GRANT NUMBER(s) ARO MIPR 21-78		
11. CONTROLLING OFFICE NAME AND ADDRESS U. S. Army Research Office Post Office Box 12211 Research Triangle Park, NC 27709			10. PROGRAM ELEMENT, PROJECT, TASK AREA & WORK UNIT NUMBERS		
14. MONITORING AGENCY NAME & ADDRESS (if different from Controlling Office)			12. REPORT DATE Dec 82		
			13. NUMBER OF PAGES 132		
			15. SECURITY CLASS. (of this report) Unclassified		
			15a. DECLASSIFICATION/DOWNGRADING SCHEDULE		
16. DISTRIBUTION STATEMENT (of this Report) Approved for public release; distribution unlimited.					
17. DISTRIBUTION STATEMENT (of the abstract entered in Block 20, if different from Report)					
18. SUPPLEMENTARY NOTES The view, opinions, and/or findings contained in this report are those of the author(s) and should not be construed as an official Department of the Army position, policy, or decision, unless so designated by other documentation					
19. KEY WORDS (Continue on reverse side if necessary and identify by block number) precipitation (meteorology) convection rainfall					
20. ABSTRACT (Continue on reverse side if necessary and identify by block number) Researchers at the University of Virginia, the Office of Weather Research and Modification (OWRM) of NOAA (formerly the cumulus group of Hurricane and Experimental Meteorological Laboratory), and the Illinois State Water Survey, have engaged in a collaborative effort to study the relationship between surface convergence and subsequent precipitation from convective clouds in both subtropical marine and mid-latitude continental climates. The overall goal of the research was to increase the understanding of the dynamics involved in the					

DTIC FILE COPY

DD FORM 1 JAN 73 1473 EDITION OF 1 NOV 68 IS OBSOLETE
83 05 03 028

UNCLASSIFIED
SECURITY CLASSIFICATION OF THIS PAGE (When Data Entered)

UNCLASSIFIED

SECURITY CLASSIFICATION OF THIS PAGE(When Date Entered)

Abstract cont.

development of convective clouds and in cloud interactions on the mesoscale. More specifically, the research focused on the role of low level and surface convergence in the evolution of precipitating convective systems and on developing methods by which this increased knowledge could be used for nowcasting convective precipitation. The research studies were based both on existing data sets from Florida and the Midwest and on measurements made in a special field project carried out during the second year of the three year project.

SECURITY CLASSIFICATION OF THIS PAGE(When Date Entered)

State Water Survey Division
METEOROLOGY SECTION
AT THE
UNIVERSITY OF ILLINOIS

ENR

Illinois Department of
Energy and Natural Resources

SWS Contract Report 318

**LOW LEVEL CONVERGENCE AND THE
PREDICTION OF CONVECTIVE PRECIPITATION**

Edited by
Bernice Ackerman



FINAL REPORT
Grant: NSF ATM 78-08888

Bernice Ackerman
Principal Investigator

Champaign, Illinois
December 1982



88 05 03 026

The project "Low-level Convergence and the Prediction of Convective Precipitation" is a coordinated research effort by the State Water Survey Division of the Department of Energy and Natural Resources, the Office of Weather Research and Modification in the National Oceanic and Atmospheric Administration, and the Department of Environmental Sciences of the University of Virginia. Support of this research has been provided to the State Water Survey by the Division of Atmospheric Sciences, National Science Foundation, through grant ATM-78-08885. This award includes funds from the Army Research Office and the Air Force Office of Scientific Research of the Department of Defense.

State Water Survey Division

METEOROLOGY SECTION

AT THE
UNIVERSITY OF ILLINOIS

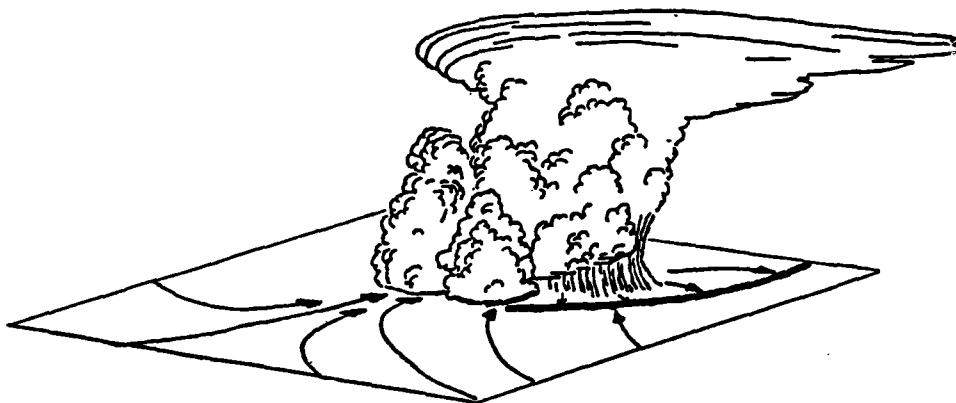
ENR

Illinois Department of
Energy and Natural Resources

SWS Contract Report 316

**LOW LEVEL CONVERGENCE AND THE
PREDICTION OF CONVECTIVE PRECIPITATION**

*Edited by
Bernice Ackerman*



FINAL REPORT

Grant: NSF ATM 78-08865

*Bernice Ackerman
Principal Investigator*

Champaign, Illinois
December 1982



Table of Contents

	<u>Page</u>
ACKNOWLEDGEMENTS-----	iv
I. INTRODUCTION-----	1
Project Organization-----	2
II. MEASUREMENT PROGRAM, ILLINOIS 1979-----	3
Surface Measurements-----	7
Measurements Aloft-----	11
III. RESEARCH SUMMARIES-----	14
University of Virginia-----	14
Illinois State Water Survey-----	16
NOAA, Office of Weather Research and Modification-----	27
References-----	36
APPENDIX A. Project Reports and Publications-----	38
APPENDIX B. Case Study: July 30, 1979	
Preface-----	41
1. INTRODUCTION-----	42
2. SYNOPTIC-SCALE CONDITIONS-----	46
3. REGIONAL-SCALE PROCESSES-----	52
4. MESOSCALE METEOROLOGICAL FIELDS AND PROCESSES-----	71
A. Visual Cloud Fields (NOAA)-----	71
B. Mesoscale Weather Fields and Precipitation (NOAA)-----	72
C. Surface Fields and Subnetwork Scale Processes (U. of Virginia)-----	89
D. Surface Kinematics and Cloud Evolution (Ill. State Water Survey)-----	108
5. SUMMARY-----	124
References-----	127

ACKNOWLEDGEMENTS

The editor of this report wishes to acknowledge the major contributions of the Principal Investigators from the University of Virginia, Michael Garstang and the NOAA Cumulus Group, and Ronald Holle, in all phases of this project, and the efforts of our many colleagues, among whom were: U. Va., Henry Cooper, George Hornberger, K. J. Beven and Omar Lucero; from ISWS, Gary Achtemeier, Robert Scott, Nancy Westcott and John Vogel; from NOAA, Andrew I. Watson, John Cuning and Patrick Gannon. In addition Joanne Simpson, Rob Sax, and Stan Changnon, all of whom were Principal Investigators in the first year of the grant provided valuable input in the initial planning and implementation of the program. We also wish to express our appreciation to the field crews whose dedication has provided a data base which will be a source for research for many years to come. Special recognition must go to Gene Mueller and the ISWS CHILL crew and to Fred Brock and the NCAR PAM crew, all of whom moved from an intensive Spring field effort in SESAME to the summer VIN program without a break. We also wish to recognize the efforts of many unnamed others who have contributed so much to this project: the students and programmers who reduced, processed and massaged the massive collections of measurements.

SECTION I

INTRODUCTION

Some thirty years ago, measurements made during the Thunderstorm Project showed that deep moist convection was accompanied by measurable convergence in the middle and lower troposphere (Byers and Braham, 1949). Moreover local surface convergence was often found to precede the first appearance of a radar echo and/or the onset of convective precipitation. In the years since then a number of investigators have looked for the effect of convergence on cloud systems not only of the summer convective type but also for winter time cyclonic systems (e.g., Matsumoto *et al.*, 1967). Ulanski and Garstang (1977) took the association between the surface convergence and subsequent convective rainfall one step further. Using data for south Florida they developed statistical relationships between these two variables. This new development opened up the possibility that the surface convergence field may provide predictive information on the onset and intensity of convective precipitation on the order of one hour in advance.

Under this grant, researchers at the University of Virginia, the Office of Weather Research and Modification (OWRM) of NOAA (formerly the cumulus group of Hurricane and Experimental Meteorological Laboratory), and the Illinois State Water Survey, have engaged in a collaborative effort to study the relationship between surface convergence and subsequent precipitation from convective clouds in both subtropical marine and mid-latitude continental climates.

The overall goal of the research was to increase the understanding of the dynamics involved in the development of convective clouds and in cloud interactions on the mesoscale. More specifically, the research focused on the role of low level and surface convergence in the evolution of precipitating convective systems and on developing methods by which this increased knowledge could be used for nowcasting convective precipitation.

The research studies were based both on existing data sets from Florida and the Midwest and on measurements made in a special field project carried out during the second year of the three year project. Most of the results of the research carried out by the three groups appear in technical reports and papers. These are listed in Appendix A. In addition the intensive analysis of a single day during the field project, to which all three organizations contribute, appears in Appendix B.

Project Organization

The three participating organizations were individually responsible for their own portion of the research under this project. The project was familiarly known as VIN from the first letter of the three participating organizations (University of Virginia, Illinois State Water Survey, NOAA) to indicate the independence of the three. Each identified their own goals and submitted independent research plans. The Illinois State Water Survey acted as general administrative body, receiving grant awards and distributing it to the other two organizations as subcontracts in the amounts as indicated in their proposals. In addition the ISWS managed the implementation and operation of the field program during the summer of 1979.

Although the three organizations each identified areas of special interest, overlap in certain aspects of the research was expected and indeed occurred. We considered this overlap as desirable since much can be gained from attacking this difficult problem from more than one perspective.

Although there was some change in the principal investigators of the organizations, many of the personnel assigned to the project continued throughout the three years of the project. Principal investigators at the time of expiration of the grant were:

University of Virginia: Professor Michael Garstang
Illinois State Water Survey: Dr. Bernice Ackerman
NOAA, Office of Weather Research and Modification: Mr. Ron Holle

Although each agency carried out their research independently, the overall research program was coordinated through meetings of the principal investigators and principal scientists once or twice a year. In addition all three organizations participated in the field program and in the reduction of the data.

The main elements of the field program are described in Section II of this report which also contains information on data archival. Daily summaries of operations and weather can be found in Technical Report 1. Brief summaries of the research activities of the three groups are given in Section III and publications are listed in Appendix A. Research based on the field data is continuing, but with independent funding.

SECTION II

MEASUREMENT PROGRAM, ILLINOIS 1979

The field program was carried out 28 June - 28 August 1979 in a 5400 km² area in central Illinois. The rainfall distribution during the summer was somewhat unusual, in that the rain periods were interspersed with relatively long periods of dry weather. June was extremely dry, the fourth lowest June rainfall recorded at Champaign-Urbana. July and August were above normal in precipitation, however, with the rainfall in the network occurring primarily on several consecutive days separated by several days of dry weather.

During the period of operations there were about 56 individual storm periods occurring on 31 days. Point rainfall maxima ranged from 1 mm to nearly 150 mm. The times and dates of these storms and the fraction of the raingage network that had rain are shown by the vertical bars in the top section of Fig. 1. The point maximum for each storm period is shown just below the vertical bar, and the number of stations with hail (when hail fell) in the third horizontal section. The very long storm periods were generally due to two or more storms or cloud systems.

The VIN network experienced a wide variety of cloud systems, from small airmass showers to lines of large thunderstorms to the extensive cloud layers with embedded convection of decaying tropical hurricanes. Despite the relatively small size of the network and frequently (relatively) rapid motion of the cloud system, the network was the location of several different types of cloud developments: new shower clouds, mergers of small clouds into complexes or lines, development between two large clouds and formation of new lines ahead of squall lines.

Brief summaries of the general weather conditions and the data that were collected are given for each day in VIN Technical Report 1, along with details of the equipment and the data set that was generated. The principal features of the field program are summarized below. A summary of data availability is given in Fig. 1.

Whenever possible measurements were made in a more-or-less standard mode, which was specified by the requirements of the individual researchers. Because of limitations in resources, measurements which were not obtained by a continuously recording sensor were made only when the forecasted weather was favorable for convective precipitation.

The main field facilities were as follows:

- High density network of 260 raingages with continuous analog recording

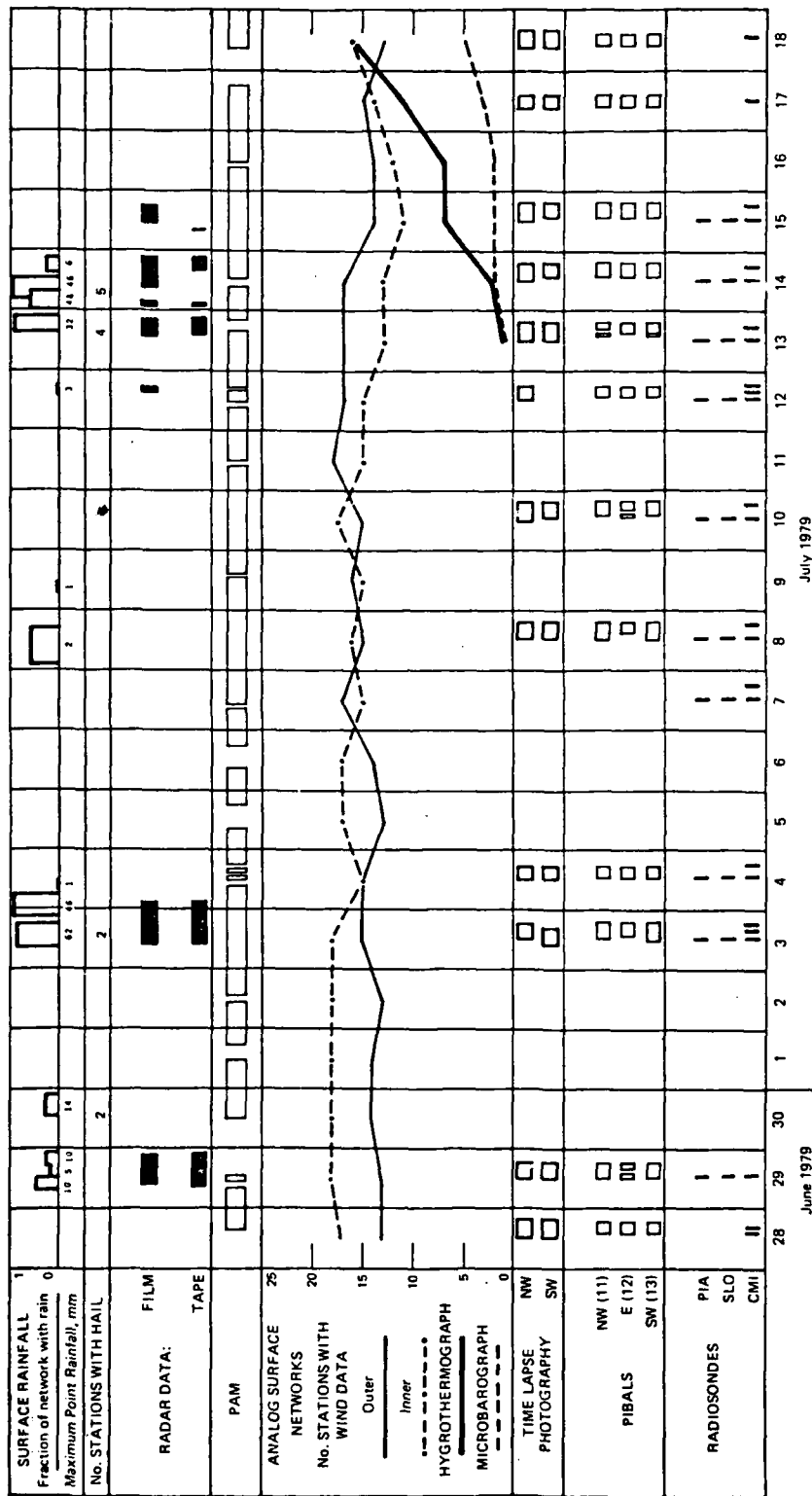


Figure 1. Calendar indicating availability of data, and times, intensities and coverage of rain storms.

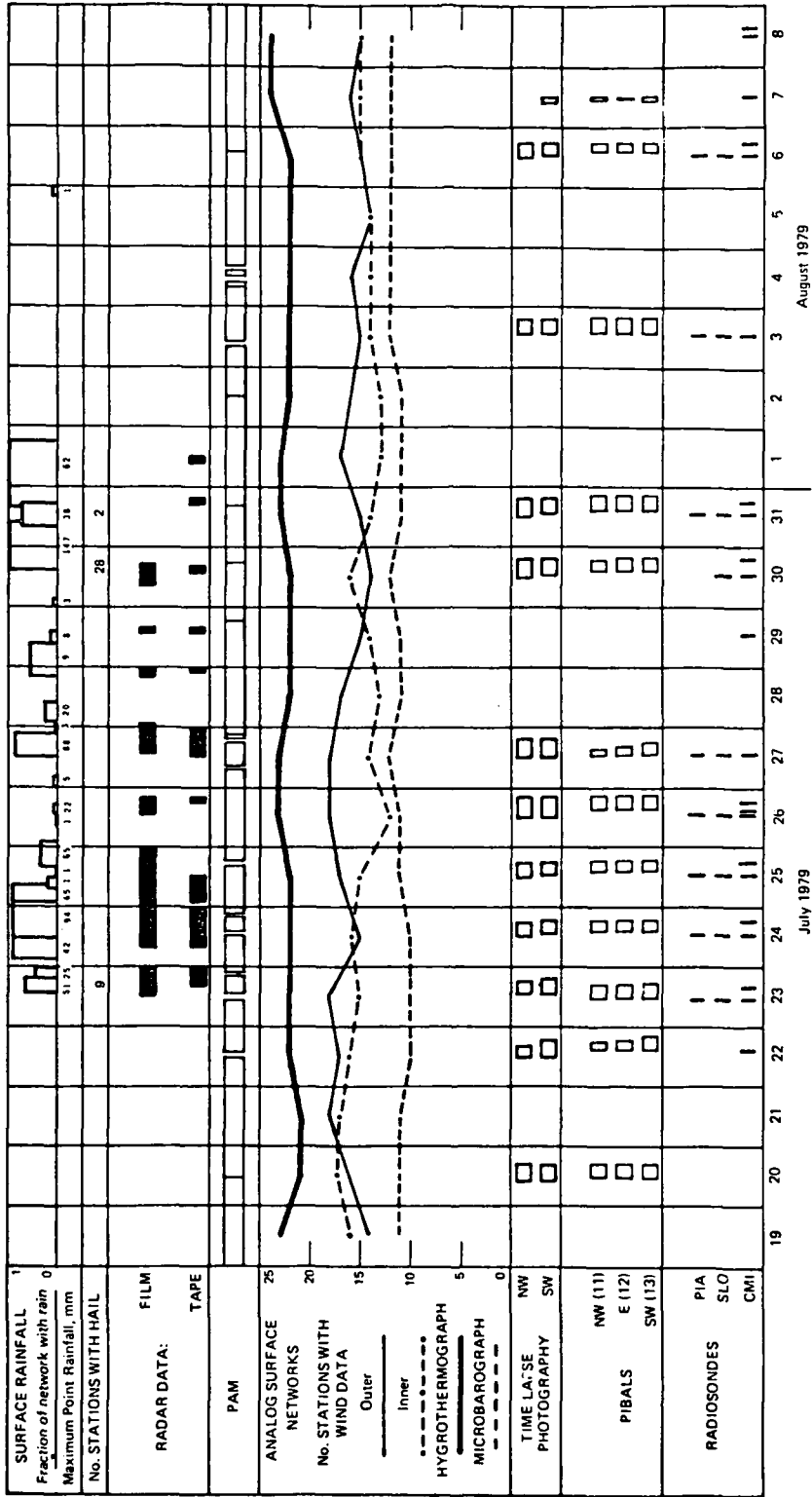
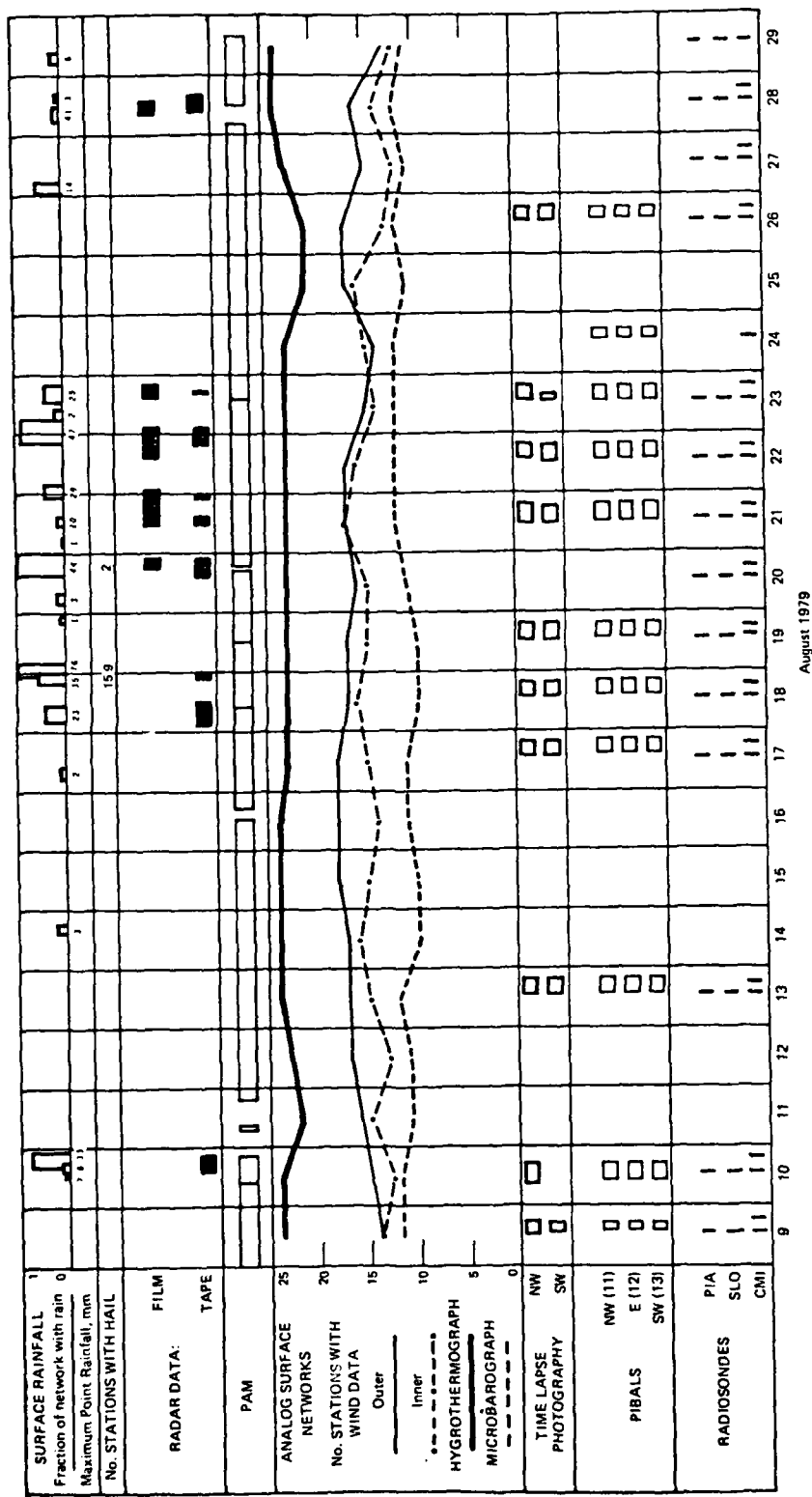


Figure 1. Continued.



August 1979

Figure 1. Continued.

- The 27-station NCAR Portable-Automated Meso-net (PAM) with real time telemetry
- A network of wind sensors with analog recording
- Dual wavelength, Doppler radar with digital recording
- A 3-station pilot-balloon network
- Special radiosonde observations
- Time lapse photography

Field headquarters were located in an University of Illinois building on the east side of the surface network. The NCAR PAM base station and trailer and the radar antenna, base station and electronics trailer were located adjacent to the headquarters building. Daily operations were based on morning weather briefings and forecasts and were transmitted to remotely-based field personnel by telephone and radio.

Surface Measurements

PAM, The Portable Automated Mesonet

The PAM (Brock and Govind, 1977) consisted of 27 stations, sited in a fairly uniform array, with spacing of about 13 km in most of the network (Fig. 2). The variables measured were pressure, temperature, relative humidity, rainfall and wind speed and direction. The wind measurements were made at 4 m and most of the other variables at about 2 m. All variables were sampled at 1-sec intervals with 1-min averaging by on-site microprocessors. The latter were telemetered to the base station where they were recorded on magnetic disk (for real time analysis) and tape (for archiving). The field tapes were processed at NCAR and scaled tapes are archived at the ISWS.

Real-time processing and analysis of the PAM measurements permitted a test by the University of Virginia researchers of their nowcasting scheme for precipitation. Unfortunately the PAM computer was not up to the continual interactive use required for this test and there were frequent "crashes", with some loss of data. About midway in the field program, U. Va. frequently went to a "passive" mode, i.e., one in which the forecast was made after the fact, in order to avoid the loss of data.

Raingage Network

Surface rainfall was monitored by a 260-station network of recording weighing-bucket raingages in a uniform rectangular grid with station density of about $1/23 \text{ km}^2$ (Fig. 3). The gages had daily chart recorders and were serviced weekly. The charts have been reduced using an electronic digitizer. The digital data and the original charts are archived at the ISWS. Rainfall was measured in the PAM system by tipping bucket raingages and is recorded with the other PAM data.

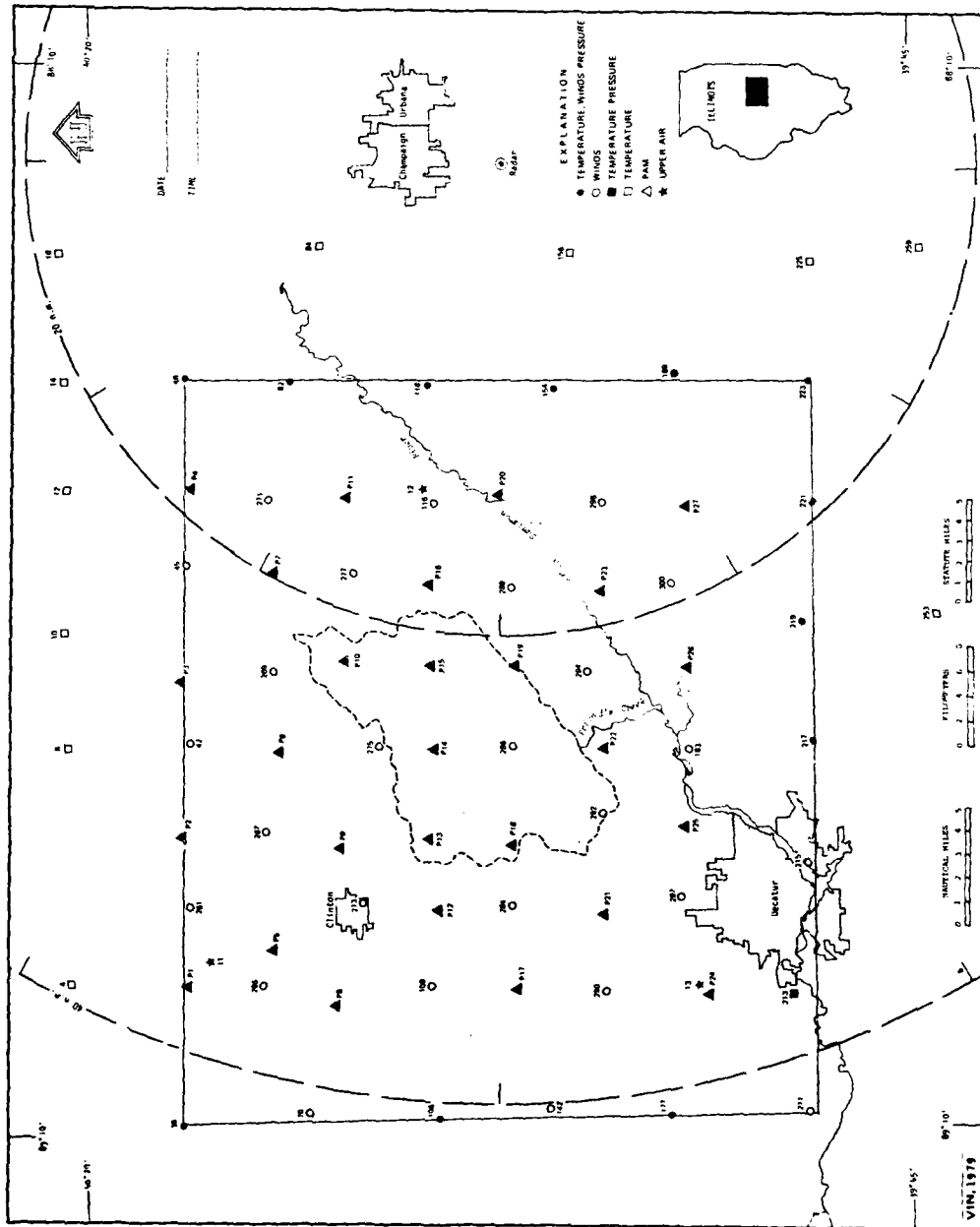


Figure 2. Surface wind network upper air stations and supplementary hygrothermograph/microbarograph stations. PAM stations are indicated by triangles. Pibal stations are shown by stars (numbered as station 11, 12 and 13).

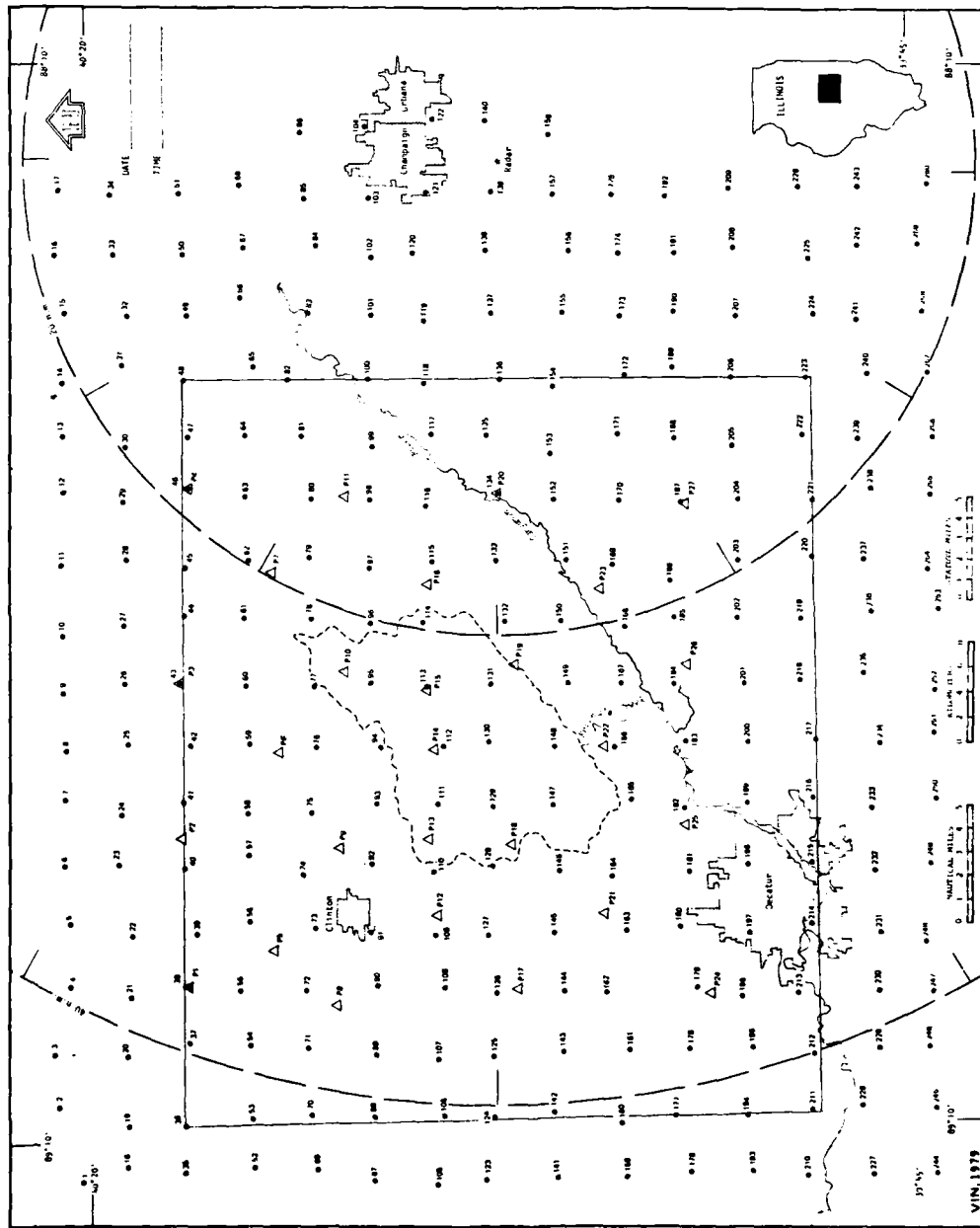


Figure 3. Map of raingage network. PAM stations shown by triangle. Arcs show range from radar, inner box wind network, and dashed outline the Friend's Creek watershed.

Hailpads were co-located with the 260 weighing-bucket raingages. These pads were foil-covered 12-in styrofoam squares set on 18-in high metal stands. The hailpads were replaced only when there was evidence that hail occurred. All pads have been examined by ISWS for occurrence of hail and for qualitative estimates of amount and size of hail. These are in the form of handwritten reports in ISWS files.

Surface Winds

The wind network consisted of a high density inner network of 49 recording wind sensors arrayed in an approximately square grid, with density of about $1/40 \text{ km}^2$. The winds were measured and recorded digitally by PAM at 27 sites; the remaining 22 wind stations had analog recording. Additional wind stations (with analog recording) were spaced at 6 mile intervals along a linear array 6 miles from the inner network on the west, east, and south (Fig. 2).

The analog wind charts from the inner network were digitized on a case-study basis at U. Va. and NOAA. The latter also digitized the wind charts from the stations along the perimeter of the wind network. Digitized data are archived at NOAA/OWRM and at ISWS; original charts at U. Va. and OWRM.

There was a mix of wind instruments: Climets, Lambrechts, C-sets, and aerovanes. Due to slippage of several months in the start date of the project, the digital systems to be developed by U. Va. were not ready for deployment at the start of the field operations. However, they were field-tested and modified as required.

All wind sensors were mounted at 4 m, to coincide with the exposure of the PAM instruments. It was usually necessary (for reasons of security and economy) to locate the instruments on rural homesteads, or on the corners of agricultural fields. Thus, it was not possible to locate all instruments with unobstructed fetch in all directions for the long distances that is preferred for such a low exposure height. Since the prevailing surface winds in situations favorable for the development of convective rains are SSE through SW to W in this area, the instruments were sited such that there was a long unobstructed fetch in the SW quadrant and, if at all possible, to the W and NW also. Least weight was given to exposure in the NE and E since ambient surface winds from those directions were generally associated with suppressed convection. It was recognized that local effects associated with upwind obstructions could distort the analysis. Therefore, the U. Va. photographically documented each station, including those in the PAM, to provide information needed to determine possible errors due to instrument exposure. These photographs were retained by U. Va. A set of 35 mm slide photographs of the sites are available at ISWS and NOAA/OWRM.

State Parameters

The 27-station temperature, humidity, and pressure networks provided by PAM in the 1500 km^2 inner-network were supplemented by a number of

hygrothermographs and microbarographs in a low-density outer network, co-located with wind instruments when possible (Fig. 2). In this secondary network, temperature and relative humidity were recorded on hygrothermographs operated with weekly gears. The pressure instruments were Bendix microbarographs, operated with 24 hour gears.

Although we view these as important measurements, limited financial resources were not adequate for these supplementary stations to be part of the basic field effort. Instruments available at ISWS were checked and installed as time permitted and they became part of the data set on different dates. The original records are archived at ISWS; they have not been digitized or analyzed in any systematic manner.

Measurements Aloft

Radiosonde

Special radiosonde releases were made from NWS stations at Peoria and Salem (Fig. 4) at 1800 Z (1300 CDT), on request. Radiosondes were also released from the field headquarters at Willard Airport, simultaneously with the NWS specials and with the routine NWS radiosondes at 0000 Z (1900 CDT) as well as at intermediate times when conditions warranted. It would have been highly desirable to have radiosonde measurements with higher resolution in time and space. Unfortunately grant funds did not permit this and supplemental resources could not be obtained. These special soundings are archived at ISWS.

Boundary Layer Winds

Winds in the lower troposphere were measured at 3 locations, forming a triangle over the inner wind network (Fig. 2). The winds were obtained on days favorable for convection and on the day prior using single theodolite pilot balloon observations with readings taken every 30-seconds. Balloon releases at half-hour intervals started at 1130 or 1200 CDT and terminated at dark or at the end of the convective activity. Some of the balloon observations were made with recording theodolites (ditital recording on a carbon imprinted tape). However, due to delays in delivery of supplies, most observations were made with standard theodolites and voice recording on cassette tapes of azimuth and elevation angles. The basic pibal data are archived at ISWS.

Cloud Photography

Time-lapse cloud photographs were taken at the two pibal stations near the northwest and southwest corners of the inner wind network. The 16-mm cameras were pointed inward toward the center of the network and operated at about 1 frame per 10 seconds. Photographs were taken when pibal observations were scheduled and there were clouds in view. The film is archived at NOAA/OWRM.

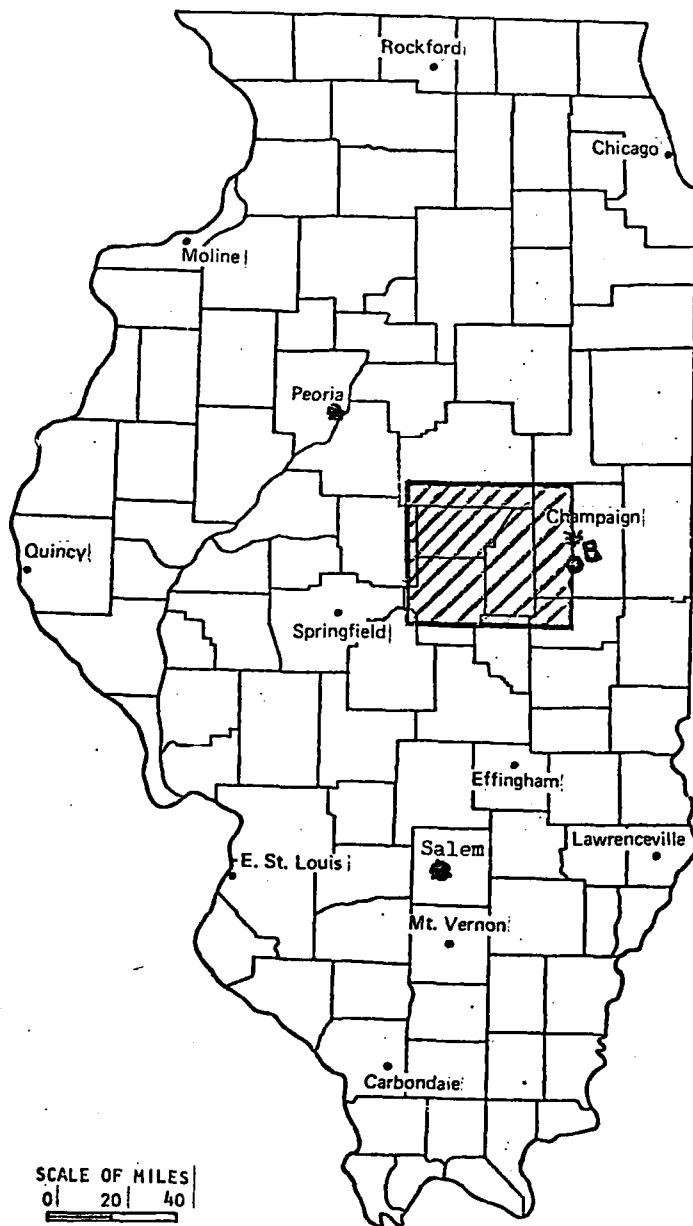


Figure 4. Map of Illinois showing radiosonde stations and VIN network.

Radar

The cloud volume over the network was continuously monitored by the ISWS CHILL radar. The CHILL is a combination of 10-cm Doppler and 3-cm incoherent radars which are matched with respect to pulse length, pulse repetition frequency and beam width (1 degree) and are operated from the same pedestal. The radar was located at the Willard Airport on the eastern edge of the raingage network (Fig. 3). It was operated routinely in a volume scan over the 180° sector covering the surface network, with occasional 360° scans at a low elevation (0.5°), with maximum range of 80 nm. On occasion the sector was increased to cover the later development of the clouds that initiated over the network and then moved east.

Radar surveillance was scheduled on the basis of a forecast of convective precipitation and continued as long as convective echoes were present on the scope or were moving into radar range. The radar scanned at a rotation rate of 16°/second, for every 1° elevation, from 0.5° to 11.5° and every 2° elevation from 11.5 to 25.5°. This permitted a cycle time of just under 4 minutes for a volume scan over the network. The data were recorded digitally on magnetic tape when echoes of interest occurred with occasional scope photography of reflectivity.

The radar operated on all forecasted (and some unforecasted) rain days, except for a serious interruption following a lightning strike on 30 July which caused major damage to all of the electronics. The radar was back on line in a very limited way (base elevation only) for rains on 31 July and 1 August, but the system was not fully operational until the latter half of August. (Fortunately few rains occurred in early August, Fig. 1). Nevertheless, it was not possible to bring the system up to full performance under field conditions and the radar data subsequent to 30 July, although retrievable, requires special handling. An earlier lightning strike during SESAME in Oklahoma did major damage to two of the antenna drive motors, decreasing the precision of the antenna control. This introduced some instability when elevation angle was changed at the end of the azimuth scan. This does not cause any serious problems in data analysis for the main parts of the scan.

Problems occurred in the recording of the Doppler velocities during the summer of 1979 which were not detected until analysis commenced after the field program ended. The cause of these problems has not been identified, nor has a satisfactory way of correcting them in software been found. Thus, as of this date, the velocity data are not considered retrievable.

The original radar tapes in the CHILL recording format are archived at ISWS.

SECTION III

RESEARCH SUMMARIES

University of Virginia
Michael Garstang, Principal Investigator

The University of Virginia (U.Va.) research has focussed upon the convective scale processes in the atmosphere and as they effect the modelling of streamflow hydrographs.

The role of near surface outflow in maintaining convective activity has been examined in terms of the detailed surface measurements taken in the Florida Area Cumulus Experiments (FACE) and in the Virginia-Illinois-NOAA (VIN) experiment (Garstang and Cooper, 1981). Feedback between storm outflow at the surface and the generation of new convective cells is shown. Once a storm begins raining the outflow is clearly visible in the surface fields of divergence. The signal in the surface divergence field is common to storms in the distinctly different meteorological environments of summertime Florida and Illinois. This signal precedes the occurrence of rainfall and radar echo in the location of the new cell by some tens of minutes up to more than 100 mins. Given surface measurements with a spacing of no more than 10 km, the direction of propagation, timing of the future occurrence of rainfall and the intensity of the rainfall generated in the new cell can be determined.

Examination of the daily time series of divergence averaged over the 30x25 km FACE grid showed that on days with deep convective activity over and around the network, a definable sequence in the network averaged surface wind divergence is observed (Cooper, Garstang and Simpson, 1982). The sequence consists of five stages: persistent convergence, peak convergence, non-divergence, peak divergence and the return to a non-divergent state.

Use is made of observations of individual cases and of radar composites built around the above sequence in the network averaged divergence fields to demonstrate that a convective-scale feedback mechanism consisting of outflows from previous storms triggering new growth is frequently observed during both experimental periods.

It is shown that the observations taken over the FACE 1975 network are consistent with the model results of Pielke (1974) and estimates of peninsular scale convergence. Comparison of the convective scale vertical transports over the network at the near surface (4 m) level with the peninsular scale forcing reveals a relationship between the two. After the initiation of convective processes by the peninsular scale forcing, downdraft-induced convergence maintains and intensifies the convective scale activity long after the peninsular scale forcing has passed its peak. The daily cycle of initiation, intensification and the eventual decline of convective activity is related to the rate of change of the peninsular scale divergence.

The links established between the various scales are of fundamental importance to the understanding of the initiation, maintenance and decay of deep precipitating convection and to its theoretical parameterization.

A composite Florida storm is constructed to show that the cumulo-nimbus clusters sampled generated horizontal mesoscale gradients of sensible heat, moisture and moist static energy across the storms in the layers between the surface and 400 mb (Cooper and Garstang, 1982). There is a loss in moist static energy of the storm immediately ahead of the maximum rainfall rate between 700 and 400 mb. There is a general increase in moist static energy at these levels immediately behind the maximum rainfall rate. Surface outflows from the storms are shown to stabilize the subcloud layer, but increase the instability in the layer immediately above cloud base in advance of the storm. The increased instability makes the air in front of the storm more susceptible to triggering by convective scale convergence in the subcloud layer. The average life-time precipitation efficiency of the composite storm is estimated to be between 10-15% and maximum efficiency of the composite storm never exceeds 40%.

There is a strong relationship in the composite storm between the surface rainfall and the downward and upward convective mass transport, through the surface layer. Similarly, the surface rainfall is well correlated with the moisture transported into the subcloud layer across cloud base.

In most approaches to modelling the rainfall/runoff process, a spatially lumped description of precipitation has been assumed adequate for modelling the important characteristics of catchment response. However, theories of catchment hydrology as well as some recent modelling studies suggest that spatial variability in precipitation may be important in determining the characteristics of streamflow hydrographs. Data from two intensive rainfall recording experiments in Illinois have been used to examine the effects of rainfall pattern on stream hydrographs for summer convective storms. A threshold analysis was introduced to distinguish storms of markedly different pattern. A mixed deterministic/stochastic modelling procedure was used to differentiate the hydrograph characteristics resulting from storms of different patterns. It was found that differences in peak timing were highly significant, differences in the distributions of peak flow were significant and differences in the distributions of stormflow volumes were insignificant even given a long period of synthetic record. Rainfall pattern per se seems to have only a second order effect on hydrograph characteristics. Assessing the correct volume of input in a highly spatial variable pattern is far more important in predicting stream hydrographs.

Illinois State Water Survey
Bernice Ackerman, Principal Investigator

The ISWS research subsequent to the 1979 field program focused on the relationship between regional and meso (network) scale convergence and cloud development. Small studies dealt also with a) thunderstorm outflow, and b) the hydro-morphology of an isolated severe rainstorm that occurred in the VIN network. In the initial year of the project the relationship between surface convergence and rainfall was investigated using data collected in 1975. This is summarized in the first section below; all other sections summarized research based on 1979 data.

Case and Statistical Studies: Midwest Data, 1975

Measurements obtained in high density networks around St. Louis during the 1975 METROMEX field program formed the basis for seven intensive case studies and for statistical analyses. The former focused on the physical relationships while the latter were directed toward determining "Nowcasting" potential. Details of the assembly of the data sets, the methods of analysis, and the results are given in VIN Technical Report 2 (Achteimer, 1980) and in Achteimer, 1982.

The seven case studies were representative of a variety of precipitation producing mechanisms that frequent the Middle West. They included ninety-eight raincells that occurred over or sufficiently close to the network to influence the wind field. It was found that, in general, the relationship between the surface convergence and rainfall was highly variable from day to day, from storm to storm, and within the storm period. Very strong convergence centers were present during some rain periods and were almost totally absent during other periods.

On some occasions there was good correspondence between location and strength of convergence and rainfall but this was far from universally the case. Sometimes areas of convergent flow existed for over an hour before rain was recorded at the ground whereas at other times the convergence appeared almost simultaneously with the rainfall.

Major findings of the case studies were as follows:

- a) The nocturnal raincells were more weakly identified in the surface wind field than were the daytime raincells. This result has important practical significance since 40% of the summer rains in the upper Middle West fall at night.
- b) Convergence centers that formed prior to the occurrence of rain were only about 50% as strong as those that formed after the wind field had been modified by downdrafts.
- c) On most case study days raincells did not develop within strong convergence areas when they were associated with rain-cooled airmasses, indicating that a heated surface layer is a factor in raincell development.

Sub-cloud layer wind measurements were not always available in the vicinity of the rain area. However, on three occasions when such data existed, mesoscale convergence systems occurred well into the sub-cloud layer. These systems were 500-750 m deep and persisted for several hours. The convergence was strongest at the surface and gradually diminished upward. In one case the convergence zone maintained its structure after shower outflows lifted it from the lowest one-half kilometer to levels above 750 m.

The statistical analysis was carried out on both network scale and raincell scale. In the network scale studies, correlations were sought between 5 wind parameters (mass inflow, average and maximum divergence, average and maximum convergence) and 3 rain parameters (network average rainfall, network total rainfall, and maximum point rainfall) for "lags" up to 75 minutes before and after the rain began. The best predictor of rain appeared to be the average convergence, for which correlations with total rainfall systematically increased from 0.30 at 75 minutes before first rain to 0.55 at 15 minutes before the rain began. The highest correlation coefficient (0.62) was found between the average divergence and the maximum point rainfall. The network inflow (outflow) was poorly correlated with all rainfall variables for the 75 minutes prior to the rain and became weakly related to rain (correlation coefficient 0.42) after divergent rain-cooled airmasses covered the network.

The statistical analysis on the raincell scale was applied to 19 raincells that formed within the network and could be tracked continuously across the network. Grid-point divergence (convergence) within a 25-km box centered on the location where the rain first appeared was correlated with the sum of the maximum 15-min rain amounts for the cell, for 15-min "negative" lags up to 60-min prior to the time the rain began. This study indicated that strong convergence first appeared about 30 minutes before the rain began, it strengthened at lag 15-min and changed to divergence at lag 0-min (rain start time). The magnitude of the convergence was not related to rainfall amount until 15-min before the rain began and then only weakly (correlation coefficient -0.50). These results as well as the other statistical results tend to confirm the existence of the highly variable relationship between convergence and rainfall which was found in the more subjective case study analysis.

Regional Scale Kinematics and Storm Development

Warm season rains in the Midwest are commonly highly variable in space, with locally heavy rains of small areal extent. Nevertheless, most rainstorms of any significance are associated with meteorological systems occurring on a "regional" (meso β) scale. Thus an exploratory study was made to examine the relationship (if any) between the development or evolution of the cloud systems and the surface convergence on this scale.

The hourly surface data from the regular stations in Illinois and parts of the adjoining states were objectively analyzed for an area of about 617 by 662 km with grid resolution of approximately 47.5 km. The cloud development was traced using the NWS WSR-57 photographic records when available

and the digital records from the SWS "HOT" (10 cm) radar in northern Illinois and from the SWS CHILL radar which was part of the VIN field operation. The study was carried out for two rain days during the field experiment, 24 and 30 July. Rain in the network was heavy on both days but there were significant differences in the cloud systems.

On 30 July, a solid heavy squall line extending E-W across the entire state of Illinois, evolved from a line of widely scattered clouds over a period of 3 or 4 hours. The location of the cloud development remained nearly stationary just downwind of a persistent region of convergent surface winds in central Illinois. The cloud area did not move away from this nearly stationary, apparently preferred, location until the system had fully matured, at which time the surface wind field changed radically with strong divergence replacing convergence over much of central and southern Illinois. (This evolution is discussed in greater detail in Appendix B).

Persistent convergence occurred over central Illinois on 24 July as well. However, on this day the rains in the VIN network were due to a series of cloud lines moving across the area. These lines either formed over central Illinois or moved in from the west. The synoptic situation was quite complex, with a cold front about 400-450 km to the west, and a tropical storm centered over the Louisiana coast. Moderately-sized convective complexes tended to generate in the vicinity of the front at the latitude of northern and central Illinois and move eastward fairly rapidly. Exploratory analyses of the regional scale wind fields in Illinois indicated that new lines formed in or just downwind of persistent regions of mesoscale convergence, either as "appendages" to large storms or as new lines ahead of convective complex. There is also evidence suggesting intensification or reformation of cloud lines as they moved into the regions of convergent flow on the mesoscale.

Network-scale analyses, although covering a smaller area, provide supporting evidence for a positive correlation between mesoscale surface convergence and cloud development. The VIN network data also indicate that evolution from scattered clouds to solid masses accelerated as the local wind fields are modified by outflow from individual clouds or cloud cells. More "solid" cloud lines or larger cloud masses were observed to develop from "merging" of individual clouds due to new cloud development in regions of strong convergence arising from interacting outflows.

An examination of the weather systems on a longer time scale indicates that on both days large storms passing through northern Illinois prior to the period studied probably played an important role in establishing the persistent convergence over central Illinois, as well as temperature and moisture gradients that were favorable for cloud development.

Boundary Layer Convergence, VIN Network

The objectives of this study were to obtain some understanding of the kinematics of the sub-cloud layer prior to and during local convective

precipitation events and to determine the relationship between sub-cloud layer structure and rainfall. Sub-cloud layer divergence, vorticity and vertical velocity and surface divergence were calculated for the triangle formed by the 3 pibal stations for 9 days. Time-height sequences of these parameters, and of rain formed the basis of case-studies. In addition statistical analyses were used to study the relationship between the kinematic parameters and the rainfall in and downwind of the pibal triangle. These analyses are described in detail in Technical Report 8 (Vogel, 1982); they are briefly summarized here.

Rain occurred on eight of the nine days, in a total of 12 identifiable "storms." For the statistical studies the sample size was reduced to 7 cases because of occasionally missing sub-cloud layer winds at one of the pibal stations. The correlation coefficients, r , were calculated for the paired values of rainfall and a number of kinematic parameters. These parameters are given below; the correlation coefficients are listed in Table 1. It should be noted that time resolution for upper air winds was 30 min., whereas time resolution of surface data was 5 minutes.

I. Sub-cloud layer kinematic parameters: (divergence parameters are average values for the layer, surface to 700 m MSL).

- a) D-: Minimum divergence (equivalent to maximum convergence) value within the period 2 hours before the start of rain in the pibal triangle.
- b) D : Value of divergence within 30 minutes of the start of rain.
- c) W (max): Maximum value of vertical velocity at 700 m MSL, calculated from divergence, in the 2-hour period before the start of rain.
- d) W : Vertical velocity at 700 m MSL within 30 minutes of start of rain.

II. Surface kinematic parameters for pibal triangle.

- a) d-: Minimum divergence in the 30 minutes prior to the start of rain.
- b) d : Divergence at the time that rain started in the pibal triangle.
- c) ΔC : Increase in convergence in "typical" divergence "event" (see Figs. 8 and 9, for examples of such events).
- d) Δc : Increase in convergence occurring in the 1-hour period before rain started.

III. Rainfall parameters.

- a) R (A): Total storm rainfall falling within the pibal triangle (coverage A).

- b) R (B): Total storm rainfall falling within the area covered by the pibal triangle and 1-hour transit in the direction of storm movement (coverage B).
- c) Max R (A): Largest 30-min rainfall accumulation in area coverage A.
- d) Max R (B): Largest 30-min rainfall accumulation in area coverage B.

Table 1. Correlation coefficients, r , between rainfall and kinematic parameters. The size of the sample is given in parentheses; symbols are defined in text.

Kinematic Parameters	Rainfall Parameters			
	<u>R (A)</u>	<u>R (B)</u>	<u>Max R (A)</u>	<u>Max R (B)</u>
I. Sub-cloud layer				
a) D-	-.87(7)	-.86(7)	-.87(7)	-.85(7)
b) D	-.83(7)	-.82(7)	-.83(7)	-.83(7)
c) w (max)	.82(7)	.81(7)	.83(7)	.81(7)
d) w	.84(7)	.84(7)	.85(7)	.84(7)
II. Surface				
a) d-	-.04(9)	.46(8)	-.11(9)	.49(8)
b) d	-.52(9)	-.53(8)	-.60(9)	-.53(8)
c) ΔC	.06(8)	.34(7)	.11(8)	.34(7)
d) Δc	-.36(9)	-.28(8)	-.37(9)	-.18(8)

Because of the very small sample, the magnitudes of the correlation coefficients are highly suspect. However, they do indicate positive relationship between the amount of rainfall and the magnitude of the convergence around the time that the rain starts (i.e., negative relationship for divergence) at both the surface and in the sub-cloud layer. Also there appears to be a relatively strong positive relationship between rainfall and the strength of the inflow in the sub-cloud prior to the start of rain, estimated from the maximum value of both layer-average convergence and the vertical velocity in the upper part of the sub-cloud layer. This is not, however true for the surface. In general the relationships appear to be much stronger for sub-cloud layer kinematics than for surface kinematics. This may not be too surprising since the cloud "feeds" on the whole layer below it and, at least prior to initiation of significant downdrafts, one would expect an integration of the inflow for that layer to provide

the most realistic estimate of inflow into the cloud. The large difference between the correlation coefficients for sub-cloud and surface parameters suggests that frequent "de-coupling" of the surface and sub-cloud layer may occur in the Midwest. This has some support from the studies of the individual days described in Technical Report 8 (Vogel, 1982), and from the intensive case studies based on the METROMEX data summarized above.

Periodicity in the divergence and vorticity patterns was indicated on most of the nine days; i.e., the sub-cloud flow tended to alternate between divergent and convergent flow and cyclonic and anticyclonic flow. Examples of these features are shown here for two days, 24 July, which was a rain day, (Fig. 5) and 19 August on which no rain fell (Fig. 6). The upper-air patterns of divergence and vorticity appear well organized in the sub-cloud layer on the rain day. The cyclic behavior is very well defined in the mid- and upper-parts of the sub-cloud layer, but only weakly at the surface on this day. The divergence and vorticity patterns behaved in a similar manner, with maxima in convergence associated with cyclonic vorticity and maxima in divergence with anticyclonic vorticity. The patterns suggest a period of about 4 hours.

There was little organized convection, and no rainfall, in the VIN network on 19 August. From Fig. 6, it is clear that the magnitudes of the divergence (convergence) and the vorticity were less than on 24 July when there was an organized cloud system in the area. Periods of positive and negative divergence occurred, but the vertical depth of the circulations tended to be less than on the rain day. Moreover the "cycling" in both divergence and vorticity is more frequent, of the order of 1 to 2 hours, rather than the 4 hours suggested by the measurements on 24 July.

Time-height series such as these generally indicated that prior to rain, maxima of convergence tended to occur in the upper part of the sub-cloud layer and not at the surface. There is also some indication from the profiles that the height at which the maximum occurred decreased as the time of first measurable rain at the ground approached.

Dry Nocturnal Gust Front

Several times during the 1979 field experiment significant perturbations were noted in the network wind field which were not associated with rain in the local area. One such instance occurred in the early hours of August 9 and was found to be due to outflow from a thunderstorm some 30 km distant from the nearest station in the VIN network. The gust front was traceable through the network for some 2 to 3 hours after the storm started to dissipate.

A detailed analysis of this case is given in VIN Technical Report 3 (Scott, 1980), and a version may be found in Scott and Ackerman, 1983. A brief summary is given below.

A pronounced shift in wind direction from southerly to northerly which occurred at the northern edge of the network at 0300 CDT could be tracked across the network for the next three hours. The wind shift was

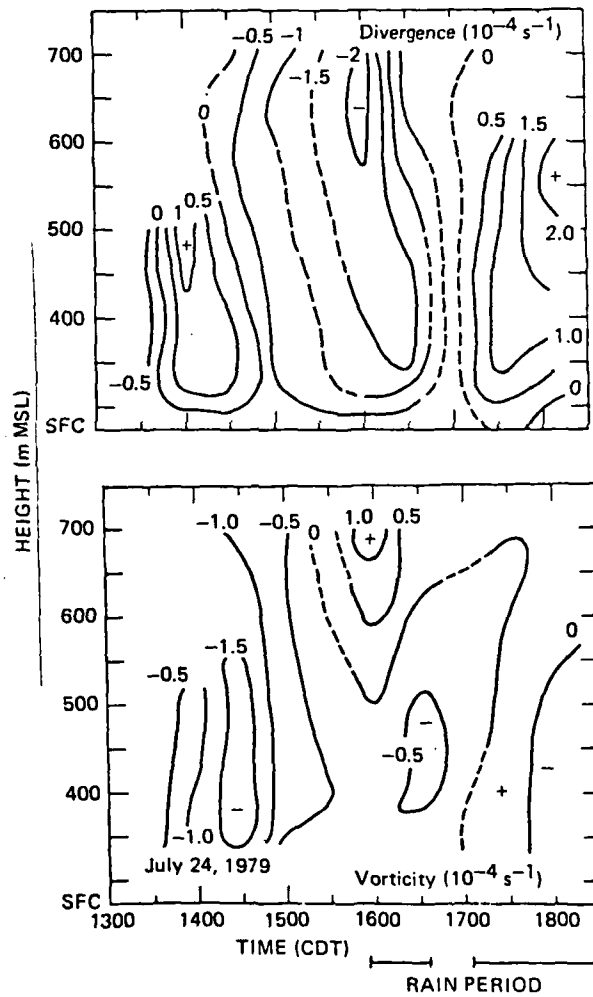


Figure 5. Time-height plot of divergence (top) and vorticity (bottom) in units $10^{-4} s^{-1}$ on 24 July 1979. Dashed lines indicate regions where measurements were sparse or lacking.

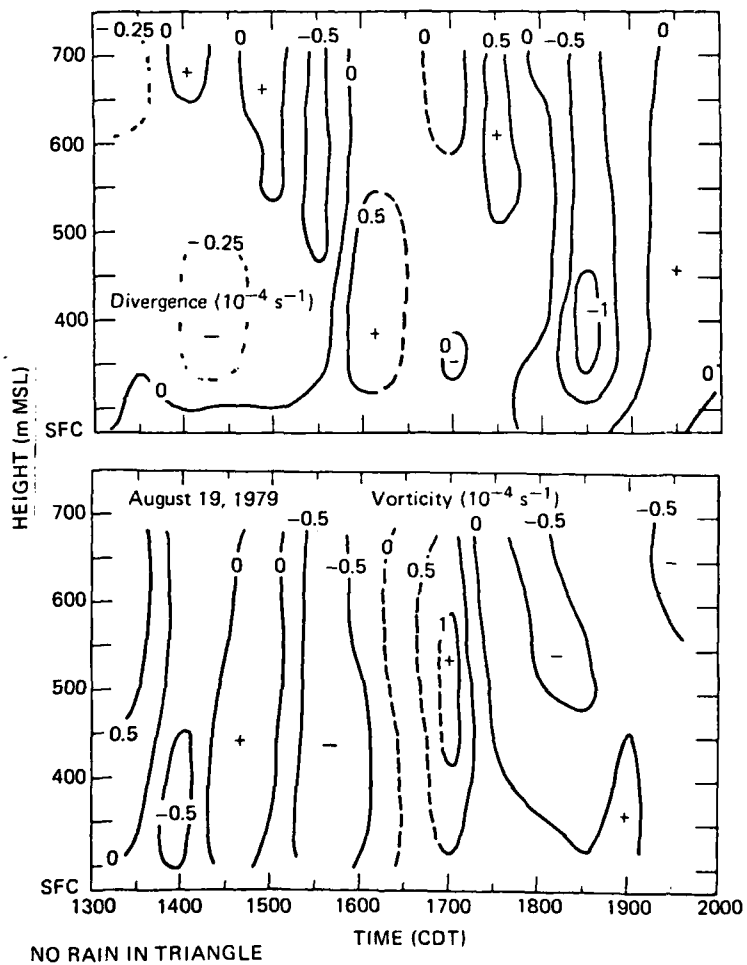


Figure 6. Time-height section of divergence (top) and vorticity (bottom) in units 10^{-4} s^{-1} on 19 August 1979. The short-dashed lines are intermediate contours, the long dashes indicate regions where measurements were lacking.

followed by changes in pressure, temperature, and humidity. These changes were consistent with a change in airmass of the type common to thunderstorm outflow, even though no significant thunderstorm was in the vicinity during the passage of the wind shear line. Using "backward extrapolation" of isochrone analysis, the initiation of the outflow was estimated to have occurred at about 0215 CDT. A potential source of the outflow was identified as a precipitating cloud in northern Illinois, about 30 km from the northern edge of the network. Measurements from the ISWS, 10-cm, digitized radar located at Joliet in northern Illinois indicated that the radar reflectivity in this cloud reached a maximum at about 0210 CDT. The reflectivity decreased rapidly after 0230 CDT, with subsequent dissipation of the cloud as it moved east.

The change in wind and thermodynamic parameters was relatively rapid and monotonic at the northern stations of the network. As the gust front moved farther from the source of the outflow, the structure at the leading edge became more complex. This complexity may have stemmed from a number of causes. Mixing by frictional and shear-generated turbulence, and downward mixing of "prefrontal" air (Charba, 1974), appear to be the most likely processes.

This analysis of the gust front from a nocturnal storm, very common in the Midwest during the spring and summer, demonstrates how lasting the effects of even a moderate thunderstorm can be on surface meteorological conditions. The thunderstorm outflow was still well defined after traveling over 100 km and up to 3 hours after the parent storm decayed. Although there was obvious convergence along the gust front, no cumulus development was observed because of strong subsidence and very dry air above 850 mb. However, under more favorable thermodynamic stratification, the thermal, moisture and velocity gradients established by such outflows may provide a favored site for convection to develop as solar heating warms and destabilizes the surface layer, much as has been proposed by Purdom (1979) from his analyses of satellite data.

Hydrometeorology of a Severe Rainstorm

The locally very intense rains which occurred on 30 July was analyzed in conjunction with a study of the hydrometeorological characteristics of isolated severe rainstorms (Changnon and Vogel, 1981). The dynamics of the storm are discussed in Appendix B; this study focused on the hydrologic aspects.

The morphology of the surface rainstorm was traced using measurements made in the VIN network, supplemented by a number of reports from local cooperative observers in the area around Champaign-Urbana. The heaviest rain occurred just to the east of the network, with maximum point rainfall of 17.5 cm. The core of this rainstorm was very small, with rainfall in excess of 4.5 cm covering an area of less than 1000 km². The storm in its entirety covered a period of nearly 12 hours, but most of the rain fell in about 4 hours. There were three distinct precipitation periods: 1) an

early period when precipitation cells moved rapidly eastward, 2) a second period, which accounted for most of the rain, when a number of rain cores moved from the northwest over approximately the same small area, and 3) a late period of more-or-less steady light rain.

The morphology of the rains during the first and second periods is illustrated in Fig. 7. None of the maximum rain rates for 5 to 30 minutes achieved recurrence values which exceeded 11 years, and the 60-minute maximum rainfall was only equivalent to the 37-year recurrence value. However, the 2- and 3-hour point rainfall was well in excess of the values for a recurrence interval of 100 years.

This morphology, which is traceable to a succession of new convective elements developing in a stagnating storm, is similar to that found in many small localized heavy storms in the Midwest. The storm itself has many of the "model" characteristics for small rainstorms which have been developed by Huff (1979).

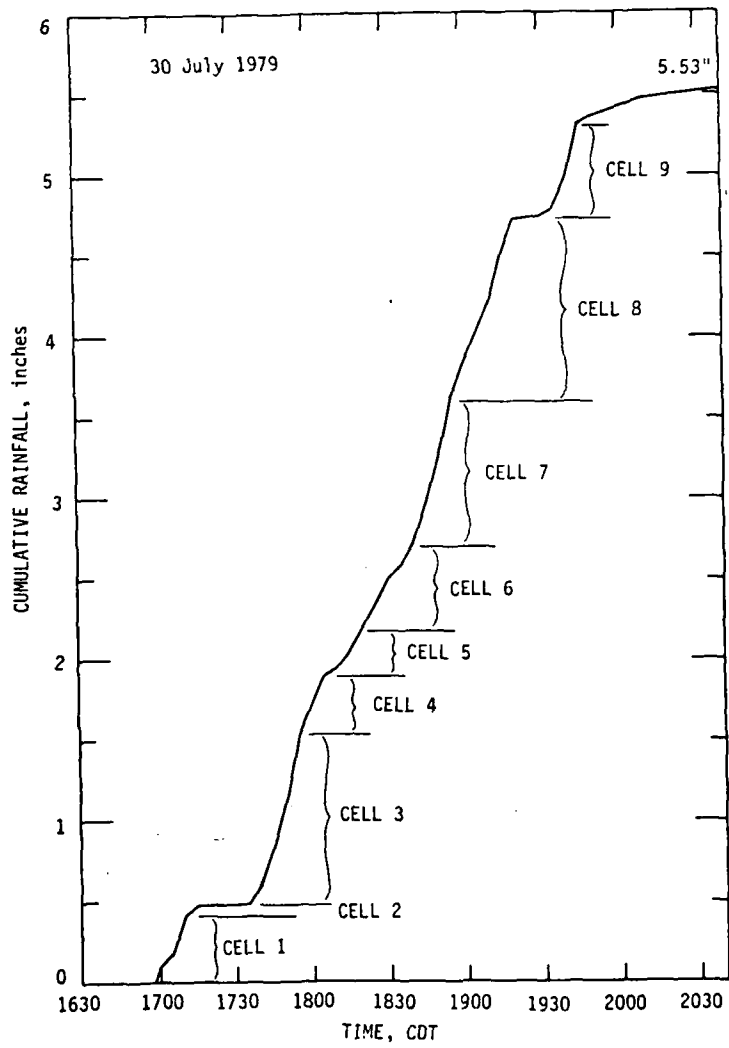


Figure 7. Total rain mass curve for gage 104 with raincells identified.

Office of Weather Research and Modification, NOAA
Ron Holle, Principal Investigator

Introduction

The main direction of NOAA research under the grant has been the relationship of area-average convergence to precipitation; several additional studies were also performed in relation to this topic. Data from mesonetworks in Florida (FACE) during 1975 and in Illinois (VIN) during 1979 were the bases of all studies. Similar methods were applied to both data sets to examine and compare the nature of the convergence preceding rainfall in these two rather different locations. It was determined that a consistent, repetitive convergence signal precedes most rainfall events, and that the magnitude of convergence is a good predictor of the amount of precipitation in the same area.

Florida Area Convergence-Rainfall Research

The initial stage of the project consisted of analyzing Florida data for July and August 1975. A large amount of analog data from FACE was reduced at 5-minute intervals for 46 stations over a 1400 km² area (6.4 km station spacing) south of Lake Okeechobee. Rainfall data were derived from the Miami WSR-57 radar and digitized every 5 min during the FACE program. Details of this data collection and analysis are given in Technical Report 4 (Watson et al., 1981) of the VIN series. Based on earlier research by a) the Thunderstorm Project in Florida and Ohio, b) by NOAA studies of the development of a major cloud system during FACE, and c) by Ulanski and Garstang of the University of Virginia examining FACE cell-scale convergence zones that preceded the onset of rainfall, it was apparent that further research with a large sample would clarify better the extent of the mesonetwork-scale convergence/rainfall relationship. Criteria were tested and established to define an event as one with 1) a sustained change in total area divergence less than $-25 \times 10^{-6} \text{ s}^{-1}$, 2) for more than 10 minutes, and 3) applied to a 15-minute, 3-point running mean of total area divergence. The calculation of total area divergence was made from a) the mean of all grid-point divergence values in the 6 by 8 mesoscale grid after objective analysis, b) the line integral of the wind along the border of the mesonetwork after objective analysis, and c) the line integral without objective analysis. The latter method can be applied to a mesoscale area with the advantage of requiring measurements only around the border. The first method requires interior stations but can better specify the location of the resultant rainfall from the convergence.

A typical convergence event is shown in the time series of Figure 8 (from Watson, et al., 1981). The top panel shows the time series of both measures of area-average convergence. Weak divergence prevails over the network until 1400 EDT, when convergence begins to increase until a maximum at 1605 EDT, then a rapid change to divergence occurs to a peak at 1815 EDT, and a return follows to quiescent values. The radar-measured rainfall (lower panel) indicates that very little rain fell until 1600 EDT, then a major rain event occurred with a peak at 1740 EDT. The middle panel shows two other measures of divergence. Weighted convergence consists of the average of all grid

DATE.... 81975

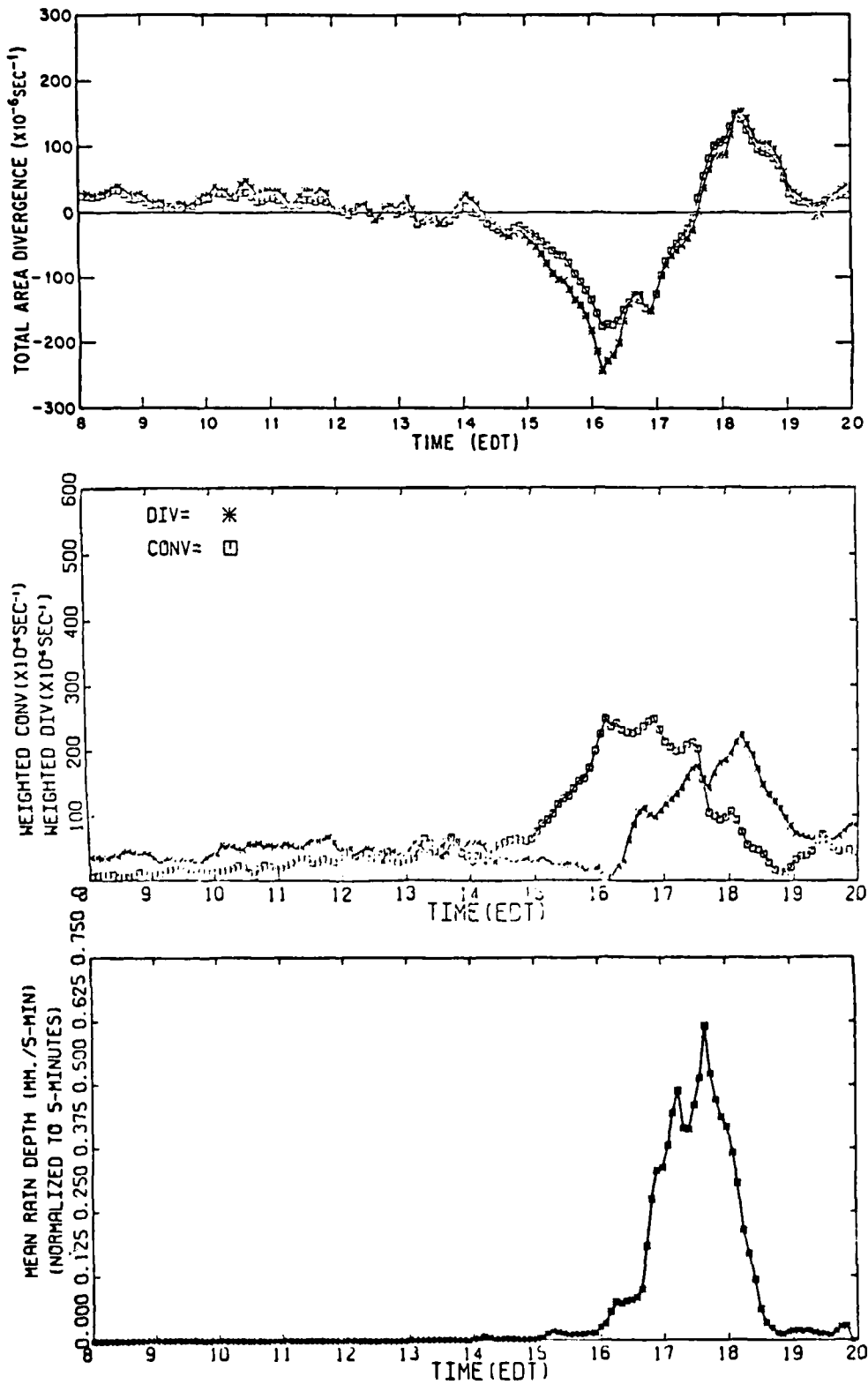


Figure 8. See text for explanation.

points with convergence divided by the total number of grid points. It indicates an increase of convergence from 1500 to 1700 EDT, then a rapid decrease by 1730. An analogous definition applies to weighted divergence, which peaks at 1815 EDT. It is apparent that convergence steadily built to rather large values before any significant rainfall was measured in the same area. Also, the weighted divergence was invariant until rainfall occurred. The relation between the magnitude and timing of convergence, divergence, and rainfall was examined by similar time series for other FACE days.

A total of 59 events similar to that shown in Figure 8 was analyzed in August 1975. For the total ensemble, a correlation coefficient of $-.60$ applied between magnitude of convergence and magnitude of rainfall. Table 2 shows that 38 of the 59 convergence events had associated rainfall, and there were only 5 weak rain events during August that were not associated with a convergence event. The correlation of $-.60$ for all events changes when events are subdivided by other parameters. During light winds ($<4 \text{ ms}^{-1}$), the correlation was the same, but when stronger winds prevailed, the correlation was poor and the rainfall was light. Events occurring with no echo motion had more rain and a better correlation than when echoes were moving. The best relationship ($-.76$) between convergence and rainfall occurred when 850-500 mb humidity was high.

Weighted convergence was also calculated for the same categories as shown by Table 2, and did not have quite as high a correlation in each category as total area divergence.

Table 2. Total area divergence versus area rainfall based upon FACE 1975 mesonetwork data.

Criteria	No. of Cases	Rain Events	$\overline{\text{Rain}}$ (mm)	Rain Misses	$\overline{\text{Rain}}$ (mm) Misses	r
All	59	38	1.72	5	.18	-.60
$V_{1-10} < 4 \text{ ms}^{-1}$	27	22	3.22	1	.71	-.60
$V_{1-10} > 4 \text{ ms}^{-1}$	32	16	.45	4	.05	-.18
No Motion (echo)	21	14	2.98	2	.37	-.63
Motion (echo)	38	24	1.02	3	.05	-.46
RH > 52% (850-500 mb)	28	23	2.55	3	.26	-.76
RH < 52% (850-500 mb)	31	15	.96	2	.06	-.51

Additional Convergence-Related Research

The average time lag between beginning convergence and initial rain was 35 minutes; between maximum convergence and rain maximum, the lag was 38 minutes. These periods indicate that an important time predictability was formed with this method in Florida.

A high correlation between thunderstorm outflow (measured by divergence) and area rainfall was determined by the Thunderstorm Project. In FACE, it also exceeded .60 in nearly all categories shown in Table 2. Both total area and weighted divergence showed high relationships for the 38 August events with rainfall.

The impact on total area divergence of varying the basic wind data was calculated in two ways. First, the smaller the station separation, the better the field describes the actual mesoscale circulations, although changing the FACE 6.4-km grid to 12.9 km was not very important for total area divergence. Second, the smaller the convective system, the smaller the network needed to describe the system adequately. New statistical relations between area-average convergence and rainfall need to be calculated for each network area.

The manner in which visible clouds respond to convergence in the same location was examined for nine clouds in August 1975. An average of 25 minutes (range of 10 to 55 minutes) elapsed from the time of first convergence to first cumulus response, and it was another 35 minutes (range of 20 to 100 minutes) until the rapid upward growth stage was reached. (For details, see Holle and Watson, 1982.) This high variability could be accommodated by taking into account the duration of the storm. When this is done, duration is correlated with time of cloud response to convergence at the .72 to .96 level. Other milestones during the cloud's lifetime, such as radar, convergence, and rain gage parameters, were also highly correlated with duration.

Radar echo merger over several convergence areas was also studied (Cunning et al., 1982) and found to occur from new towers growing upward from cloud base. In all cases, echo merger at the 1.0 or 2.5 mm hr⁻¹ rain rate took place at the same time (to the nearest 5 minutes) as merger of visible clouds at the 9 to 12 km cirrus level. The predecessor radar echoes, and the spaces between them, were found over common convergence areas during the merger process, as measured by the 6.4-km station spacing.

Once convection forms over a boundary-layer convergence area, the further evolution of a storm may be dependent on the storm-induced surface pressure perturbation. Doppler radar and surface pressure data on August 25, 1975, indicated that when surface low pressure formed under the accelerating up-draft, surface convergence was increased in response to this pressure deficit, and was not due to the forcing by the originating convergence (see Watson et al., 1981). Further research with FACE data is in progress to investigate such feedback mechanisms between storm and environment.

Illinois Area Convergence-Rainfall Research

A similar study to that of FACE convection was made of area convergence related to precipitation with data from the VIN project in central Illinois in the summer of 1979. The wind network for this study consisted of 42 stations

analyzed at 6.4-km intervals for 5-minute periods. Details of this data collection are provided in Technical Report 1 (Ackerman et al., 1982) of the VIN series. The analysis details are given in Technical Report 7 (Watson and Holle, 1982) of the VIN series. From the two-month program, 33 days were chosen based on meteorological conditions, availability of data, and overlapping objectives for case studies by other VIN agencies. Rainfall data were analyzed by the Illinois State Water Survey from 260 rain gages which were deployed at a dense 4.8-km spacing over the entire surface network. The rainfall used in this study was an area depth which accumulated in 5 minutes over the VIN mesonet network. The identical definitions of total area divergence, weighted convergence, and weighted divergence were applied to the VIN data as those given earlier for FACE.

A typical convergence event from VIN is shown in Figure 9. The classic sinusoidal pattern was seen again on this day, as shown for FACE in Figure 8. The top panel shows that total area divergence experienced a rapid increase to convergence around 1500 CDT, then it changed to divergence at 1600 CDT. The rainfall (bottom panel) showed a sharp rainfall peak at 1600 CDT. Weighted convergence and weighted divergence also indicate distinct patterns in the time series associated with the rainfall event. The relation between the magnitude of convergence, divergence, and precipitation was considered for the other 32 days in VIN with similar time series.

A total of 106 events was considered with the same event definition from FACE (Table 3). Less than half of the convergence events had associated rainfall, and the correlation was $-.50$. Rain events occurred 28 times without a convergence signal but were usually light in precipitation. When the events were subdivided by other criteria, Table 3 shows widely varying correlations. What is particularly important, though, is the low correlation in categories with light rainfall per event. On the other hand, correlations were better and rainfall was in the heavier portion of the range when 1) humidity aloft had intermediate values, 2) the Showalter Index (SI) was moderate or low, 3) the K-index was high, and 4) the wind speeds were light. It is apparent that under stable and dry conditions, an essentially no-rain forecast can be made, so that low correlations at those times are not especially critical. The larger rain events, then, occurred with events which had better correlations between rain and convergence.

Weighted convergence was calculated for the same categories as shown in Table 3, and typically had somewhat better correlations in each category than total area divergence.

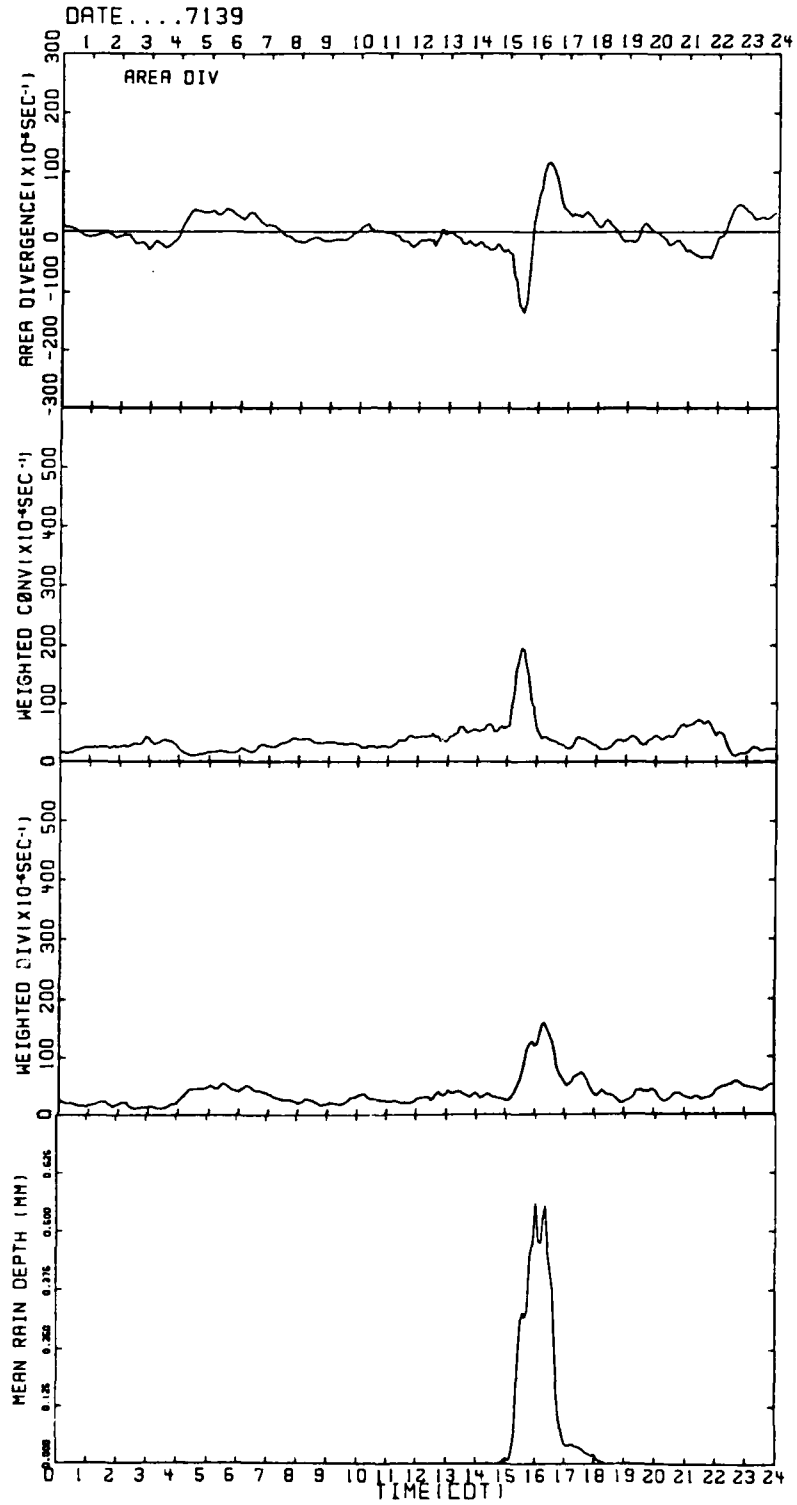


Figure 9. See text for explanation.

Table 3. Total area divergence versus rainfall based upon VIN 1979 mesonetwork data.

Criteria	No. of cases	Rain events	$\overline{\text{Rain}}$ (mm)	Rain misses	$\overline{\text{Rain miss}}$ (mm)	r	F ratio	Sig
All	106	44	1.53	28	.97	-.50	34	<.001
RH < 50%	23	4	.01	3	.84	.06	.07	.79
50% < RH < 65%	45	19	1.52	14	.57	-.57	20	<.001
RH \geq 65%	38	21	2.45	11	1.52	-.39	7	.02
SI > 2	35	9	.39	5	.51	-.04	.05	.83
-1 < SI < 2	49	18	.81	16	1.12	-.47	13	.001
SI \leq -1	22	17	4.92	7	.97	-.52	7	.01
K < 22	28	5	.02	7	.44	.15	.56	.46
22 < K < 29	21	8	1.54	0	.0	-.11	.25	.62
K \geq 29	57	31	2.26	21	1.15	-.50	19	<.001
$V_{1-10} > 5 \text{ m s}^{-1}$	67	31	2.15	19	1.29	-.46	18	<.001
$V_{1-10} \leq 5 \text{ m s}^{-1}$	39	13	.45	9	.31	-.73	42	<.001

Additional Convergence-Related VIN Research

The average time lag between beginning convergence and initial rainfall was only 5 minutes; between maximum convergence and rain maximum the lag was 23 minutes. While the time between the start of the event and first rain is nearly coincident, on the average, as mature convective systems move into the VIN network, there is some predictability in the period until area-average rainfall is at its peak.

Convective outflow was related to precipitation for the 29 events with area rainfall more than 0.5 mm. The correlation coefficients were usually .15 better for divergence-rainfall than the convergence-rainfall statistics shown in Table 3. The more moist and unstable the atmosphere, the more divergence and precipitation was seen. An exception to this trend was during the wettest situations, when the correlation was less for the outflow stage than Table 3 indicates for the convergent stage of the storm's evolution (Watson and Holle, 1982).

Since the correlations between convergence and rainfall in Illinois were not as high as in Florida, and the forcing mechanisms for convection in Illinois may be less reliant on differential surface heating than in Florida, pibal data from 3 stations forming a triangle around the periphery of the VIN network were examined to consider the representativeness of surface divergence with boundary-layer divergence. Data on 30 days were stratified by categories related to 1) the nature of the boundary-layer mixing, and 2) the influence of

outflows on the boundary layer (details in Watson and Holle, 1982). In nearly all types of boundary layers, the correlation was best between the surface and the level closest to the surface (150 m AGL). A correlation of only .26 between the surface divergence and the mean boundary-layer divergence indicates that mean divergence aloft would not be helpful as a predictive tool. During undisturbed conditions, there was a lack of persistence in divergence aloft, both in time and in the vertical. But under disturbed conditions, persistent organization of divergence aloft was always found.

Comparisons of Florida and Illinois Results

Very similar analysis methods and data were used to develop a relationship between area convergence and rainfall in Florida and Illinois. The first test was made in the relatively simple environment of south Florida. Then the hypothesis was developed further in the more complex environment of the mid-west. In south Florida, the correlation coefficient between total area divergence and rainfall was .60, while the analogous figure dropped to .50 in central Illinois (details are given in Watson and Holle, 1982).

It was apparent in both locations that divergence alone was not sufficient and other meteorological factors from the larger-scale environment should be included. There was a different combination of factors producing different relations in Florida compared to Illinois. In south Florida, when convective systems were slow-moving, there was 3 times as much rainfall per event for nearly the same amount of convergence compared to faster-moving systems. In Illinois, there was less precipitation under weak wind regimes compared to strong winds. Moist middle-level conditions produced more rainfall in Florida for the same amount of convergence compared to dry conditions. In Illinois, little rain fell in dry conditions, but under very moist conditions there was heavy precipitation with very little convergence. Stability in Florida did not play a significant part in the rain response to convergence, but in Illinois, larger amounts of rain were recorded when stability was low. It is apparent from this study that each location needs to have a separate determination of larger-scale influences on the rainfall responses to convergence.

Some other interesting comparisons can be made between the two sets of data. Total area divergence was weaker in Illinois than in Florida, principally because the VIN network was twice the size of the FACE mesonet. In Illinois, most systems were organized into squall lines or convective complexes where the associated convergence was along the gust front. For this reason, there was much less time between first detection of convergence and rainfall in Illinois than in Florida. The reduction in correlation between convergence and rain from Florida to Illinois was investigated by comparing surface divergence with divergence aloft in VIN. The correlation between surface and boundary-layer divergence was marginal. However, there was usually more organization of divergence aloft in VIN in time and space under disturbed conditions than in undisturbed situations. Future research with better and more frequent vertical wind profiling systems could be useful for clarification of these questions.

The statistical methods developed from these studies can be applied to approximately 3000 km² areas and smaller by employing only a series of wind stations around the perimeter of a forecast area. A threshold for significant

rain would be predetermined for the area by studies similar to those given here, since each area was found to be rather different in its rainfall response to convergence. On the basis of synoptic-scale, upper-air, and surface reports in the area, a forecast would then be made for each 12-hour period, for example, of the possibility of significant rain. The nowcast of actual times and amounts of rainfall could then be given on the basis of the real-time development of total area divergence in the subject area with lead times of up to 60 minutes. Application of this technique should be useful for forecasting precipitation over a metropolitan area, watershed, or agricultural region.

References

- Ackerman, B., R. W. Scott, and N. E. Westcott, 1982: Summary of Field Program, Summer 1979. Tech. Rpt. 1, NSF grant ATM78-08865, IL Water Survey, Champaign, IL.
- Achtemeier, G. L., 1980: Boundary Layer Structure and Its Relation to Precipitation Over the St. Louis Area. Tech. Rpt. 2, NSF grant ATM78-08865, IL Water Survey, Champaign, IL.
- Achtemeier, G. L., 1982: The relationship between the surface wind field and convective precipitation over the St. Louis area. Submitted to J. Appl. Meteor.
- Brock, F. V., and P. I. Govind, 1977: Portable automated Mesonet in operation. J. Appl. Meteor., 16, 229-310.
- Byers, H. R., and R. R. Braham, Jr., 1949: The Thunderstorm. U.S. Goot Printing Office, 282pp. (Out of print; available through NTIS).
- Changnon, S. A., Jr., and J. L. Vogel, 1981: Hydroclimatological characteristics of isolated severe rainstorms. Water Resources Res. 17, 1694-1700.
- Charba, J., 1974: Application of gravity current model to analysis of squall-line gust front. Mon. Wea. Rev., 102, 140-156.
- Cooper, H. J., and M. Garstang, 1982: The Behavior of Surface Wind and Thermodynamic Fields in the Presence of Deep Convection. Tech. Rpt. 5, NSF grant 78-08865, Champaign, IL.
- Cooper, H. J., M. Garstang, and J. Simpson, 1982: The diurnal interaction between convection and peninsular scale forcing over south Florida. Mon. Wea. Rev., 110, 486-503.
- Cunning, J. B., R. L. Holle, P. T. Gannon, and A. I. Watson, 1982: Convective evolution and merger in the FACE experimental area: Mesoscale convection and boundary layer interactions. J. Appl. Meteor., 21, 953-977.
- Garstang, M., and H. J. Cooper, 1981: The role of near surface outflow in maintaining convective activity. Proc. I.A.M.A.P. Symposium, Hamburg, West Germany, 25-38 August 1981, 161-167.
- Holle, R. L., and A. I. Watson, 1982: Duration of convective events related to visible cloud, convergence, radar and rain gage parameters in south Florida. Submitted to Mon. Wea. Rev.

- Huff, F. A., 1979: Hydrometeorological Characteristics of Severe Rainstorms in Illinois. Rep. Invest. 90, IL State Water Survey, Champaign.
- Matsumoto, S., K. Ninomiya and T. Akiyama, 1967: Cumulus activities in relation to the mesoscale convergence field. J. Meteor. Soc. of Japan. 45, 292-304.
- Pielke, R. A., 1974: A three-dimensional numerical model of the sea breezes over south Florida. Mon. Wea. Rev., 102, 115-134.
- Purdum, J.F.W., 1979: The development and evolution of deep convection. Preprints, 11th Conf. Severe Local Storms, Kansas City, Amer. Meteor. Soc., 143-150.
- Scott, R. W., 1980: Outflow from a Nocturnal Thunderstorm. Tech. Rpt. 3, NSF grant ATM78-08865, IL Water Survey, Champaign, IL.
- Scott, R. W. and B. Ackerman, 1983: Surface signatures of a dry nocturnal gust front. Mon. Wea. Rev. 111, (January issue).
- Ulanski, S. L. and M. Garstang, 1978: The role of surface divergence and vorticity in the life cycle of convective rainfall. Part I. Observation and analysis. J. Atmos. Sci. 35, 1047-1069.
- Vogel, J. L., 1982: Sub-Cloud Layer Kinematics and Convective Rainfall in Central Illinois. Tech. Rpt. 8, NSF grant ATM78-08865, IL Water Survey, Champaign, IL.
- Watson, A. I., R. L. Holle, J. B. Cunning, P. T. Gannon, and D. O. Blanchard, 1981: Low-Level Convergence and the Prediction of Convective Precipitation in South Florida. Tech. Rpt. 4, NSF grant ATM-78-08865, IL Water Survey, Champaign, IL.
- Watson, A. I., and R. L. Holle, 1982: The Relationship Between Low-Level Convergence and Convective Precipitation in Illinois and South Florida. Tech. Rpt. 7, NSF grant ATM78-08865, IL Water Survey, Champaign, IL.

APPENDIX A

PROJECT REPORTS AND PUBLICATIONS

I. Technical Reports

1. Ackerman, B., R. W. Scott, and N. E. Westcott: Summary of Field Program, Summer 1979.
2. Achtemeier, G. L.: Boundary Layer Structure and Its Relation to Precipitation Over the St. Louis Area.
3. Scott, R. W.: Outflow from a Nocturnal Thunderstorm.
4. Watson, A. I., R. L. Holle, J. B. Cuning, P. T. Gannon, and D. O. Blanchard: Low-Level Convergence and the Prediction of Convective Precipitation in South Florida.
5. Cooper, H. J., and M. Garstang: The Behavior of Surface Wind and Thermodynamic Fields in the Presence of Deep Convection.
6. Beven, K. J., and G. M. Hornberger: The Effect of Spatial Variability in Precipitation on Streamflow.
7. Watson, A. I., and R. L. Holle: The Relationship Between Low-Level Convergence and Convective Precipitation in Illinois and South Florida.
8. Vogel, J. L.: Sub-Cloud Layer Kinematics and Convective Rainfall in Central Illinois.

II. Journal Articles

A. Published

- Changnon, S. A., Jr., and J. L. Vogel, 1981: Hydroclimatological characteristics of isolated severe rainstorms, Water Resources Res., 17, 1694-1700.
- Cooper, H. J., M. Garstang, and J. Simpson, 1982: The diurnal interaction between convection and peninsular scale forcing over south Florida. Mon. Wea. Rev., 110, 486-503.
- Cuning, J. B., R. L. Holle, P. T. Gannon, and A. I. Watson, 1982: Convective evolution and merger in the FACE experimental area: Mesoscale convection and boundary layer interactions. J. Appl. Meteor., 21, 953-977.

Holle, R. L., and M. W. Maier, 1980: Tornado formation from downdraft interaction in the FACE mesonet network. Mon. Wea. Rev., 108, 1010-1028.

Scott, R. W., and B. Ackerman, 1983: Surface signatures of a dry nocturnal gust front. Mon. Wea. Rev., 110, No. 1.

B. Submitted for Publication

Achtemeier, G. L., : The relationship between the surface wind field and convective precipitation over the St. Louis area. Submitted to J. Appl. Meteor.

Beven, K. J., and G. M. Hornberger, : Assessing the effect of spatial pattern of precipitation in modelling streamflow hydrographs. Submitted to Water Resources Bull.

Holle, R. L., and A. I. Watson, : Duration of convective events related to visible cloud, convergence, radar and rain gage parameters in south Florida. Submitted to Mon. Wea. Rev.

Watson, A. I., and D. O. Blanchard, : The relationship between low-level convergence and convective precipitation in south Florida. Submitted to Mon. Wea. Rev.

C. In Preparation for Submittal to Referred Journals

Ackerman, B., N. E. Westcott, and I. Conroy, : Development of a warm-sector squall line: A case study. To be submitted to Mon. Wea. Rev. for publication.

Cooper, H. J., and M. Garstang, : A composite Florida storm. To be submitted to Mon. Wea. Rev.

Watson, A. I., : The association between total area divergence at the surface and convective rainfall in Illinois. To be submitted to Mon. Wea. Rev.

Watson, A. I., : Mesoscale divergence in the boundary layer using VIN 1979 pibal data. To be submitted to Mon. Wea. Rev.

III. Conference Proceedings and Presentations

Achtemeier, G. L., 1982: Predicting rainfall over the St. Louis area with mesoscale windfield data, Preprints, 9th Conf. on Weather Forecasting and Analysis, Seattle, 28 Jan. - 1 Jul. 1982.

Ackerman, B., 1979: METROMEX revisited. Preprints, Seventh Conf. on Inadvertent and Planned Wea. Mod., Banff, Oct. 8-12, 1979, 26-27.

Ackerman, B., 1980: Aggregation of small convective rain centers. Proceedings, Eighth Int. Conf. on Cloud Physics, Clermont-Ferrand France, 15-19 July 1980, 371.

- Ackerman, B., and N. E. Westcott, 1982: Evolution of thunderstorm lines: Two case studies. 12th Conf. on Sev. Storms, San Antonio, Jan. 12-15.
- Changnon, S. A., Jr., and J. L. Vogel, 1980: The morphology of an isolated severe rainstorm and hydroclimatological characteristics of such storms. Preprints, Second Conf. on Flash Floods, Atlanta, March 18-20, 1980, 5-10.
- Cunning, J. B., R. I. Sax, and R. L. Holle, 1979: Morphology of seeded clouds as determined from triple-Doppler radar - a case study. Preprints, Seventh Conf. on Inadvertent and Planned Wea. Mod., Banff, Oct. 8-12, 1979, 142-143.
- Garstang, M., and H. J. Cooper, 1981: The role of near surface outflow in maintaining convective activity. Proc. I.A.M.A.P. Symposium, Hamburg, West Germany, 25-28 August 1981, 161-167.
- Holle, R. L., and A. I. Watson, 1980: Evolution of visible clouds, surface convergence, and rainfall in the FACE mesonetwork normalized to cloud duration. 13th Conf. on Hurricanes and Tropical Met., Miami Beach, 1-5 Dec.
- Watson, A. I., and D. O. Blanchard, 1980: The relationship between area-averaged divergence and convective rainfall in south Florida. 13th Conf. on Hurricane and Tropical Met., Miami Beach, 1-5 Dec.
- Vogel, J. L., and I. C. Conroy, 1982: Boundary layer dynamics and convection. Preprint, 12th Conf. Severe Storms, San Antonio, Jan. 12-15, 589-590.

IV. Thesis

- Cooper, H. J., 1981: The Behavior of Surface Wind and Thermodynamic Fields in the Presence of Deep Convection, Ph.D. Dissertation. Univ. of Va., Dept. of Env. Studies, May 1981.

APPENDIX B

CASE STUDY: JULY 30, 1979

PREFACE

The research carried out by the three groups involved in this project was most closely coordinated on the intensive analysis of the storm occurring in central Illinois on 30 July, 1979. In planning for this case study, each organization accepted responsibility for some specific component of the analysis. There was also some planned overlap in the research, primarily in the analysis of the surface kinematic and precipitation fields. Although working from a common data base, each group used their own analysis techniques and approaches, which produced a synergistic result and a minimum of true redundancy.

Time and financial resources have not permitted a complete integration and synthesis of the analyses during the course of this grant. The contributions to this case study are presented in this Appendix as provided by each organization, except for a few minor editorial changes to delete redundant material covered in earlier parts of the report. A summary discussion at the end of the Appendix points out some of the most salient findings of the analyses.

Sections 1 through 3 of the Appendix and the summary at the end were provided by the Illinois State Water Survey. Organizational authorship of the various segments of Section 4, which presents analyses of the VIN network data, is indicated at the beginning of each sub-section.

1. INTRODUCTION

On the afternoon of 30 July, a major convective cloud system developed slowly from a few scattered showers oriented east-west across central Illinois. A long line of widely-spaced clouds at 1500 CDT gradually filled in and evolved into a solid line by about 1830 CDT. The line along which the storm developed was nearly stationary across central Illinois although individual clouds moved east-southeast or southeast during the earlier parts of the development period. As the cloud line became increasingly dense, the motion of the individual elements decreased and the cloud mass was stationary during the final stages of development. It was not until the system had become a fully mature, solid squall that it started moving south-southeastward across the state, decaying shortly before midnight just north of the southern border of Illinois. The stratiform "remains" and occasional small convective cells continued to give light rain over central Illinois into the early morning hours (Fig. B-1b).

The rainfall was generally heavy prior to midnight, although over a limited area (Fig. B-1a). Most of the precipitation came from individual convective clouds during the developmental period and from convective cells embedded in the solid squall line. (Rains in Missouri were from the prefrontal squall line described later.) Locally heavy rains up to 12-13 cm were detected in the VIN network (Fig. B-2), primarily from sequential rains due to the generation and southeastward movement of individual shower clouds developing along the line of convection, and from individual cells in the solid squall (see Fig. 7, Section III of the main body of this report).

This storm developed in the warm sector of an open-wave cyclone. The orientations of the cloud line and of the mature squall cloud were at sharp angles to that of the cold front associated with the cyclone (Fig. B-3). The storm was not part of the line which formed along and just ahead of that front during the day. However, outflow and subsidence associated with a major convective storm which moved across southern Wisconsin and northern Illinois very early that morning introduced sub-synoptic gradients at the surface and in the lower troposphere which were favorable for convective development in central Illinois.

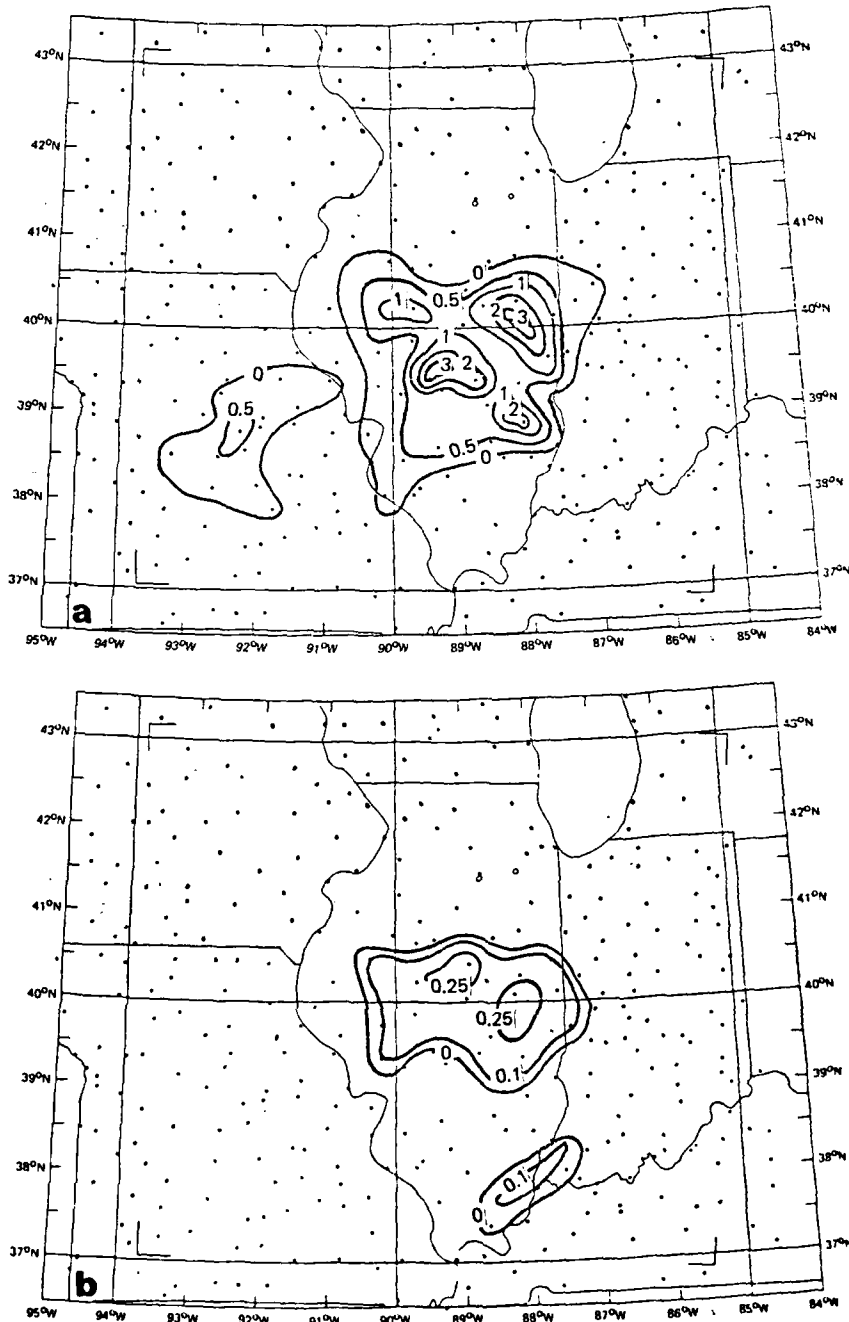
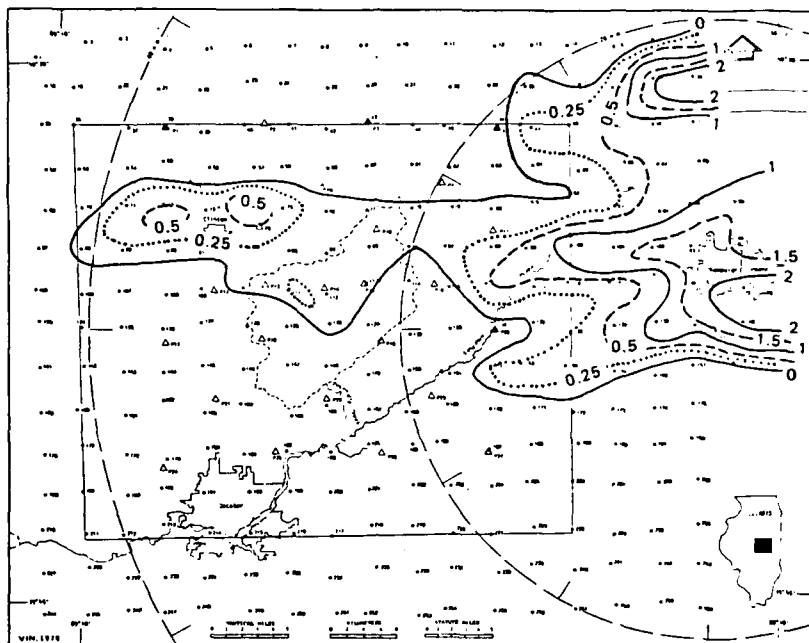
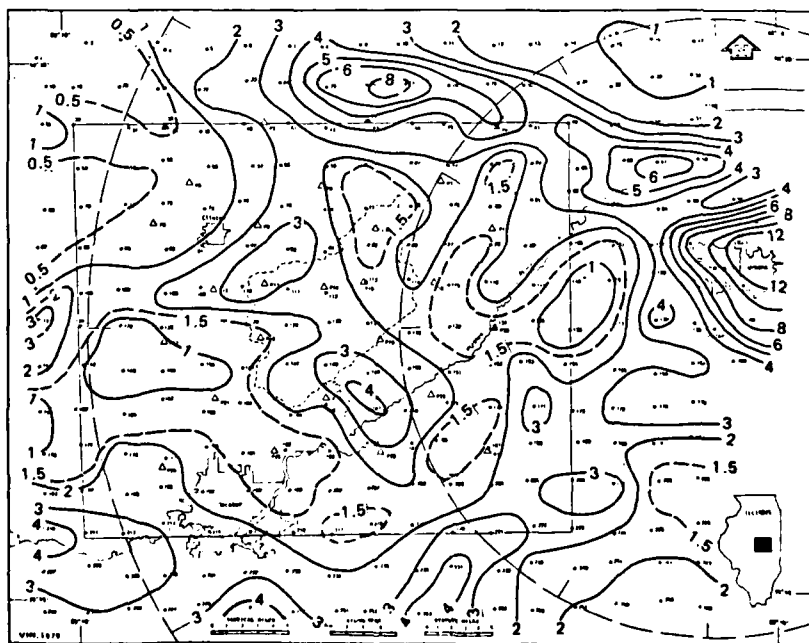


Figure B-1. Isohyets (inches) for rains on 30 July from (a) main convective areas of Illinois storm, and (b) from stratiform "remains" after midnight. These charts are based on published hourly measurements from NWS network. Dots indicate station locations. The rain in Missouri was from a pre-cold frontal squall line.



a. First storm period



b. Second storm period

Figure B-2. Storm rainfall (in cm) in the VIN Network on 30 July, 1979. Solid lines are isohyets at 1-cm intervals (2-cm above 6); dashed and dotted lines are intermediate contours of 0.5 and 0.25 cm, resp.

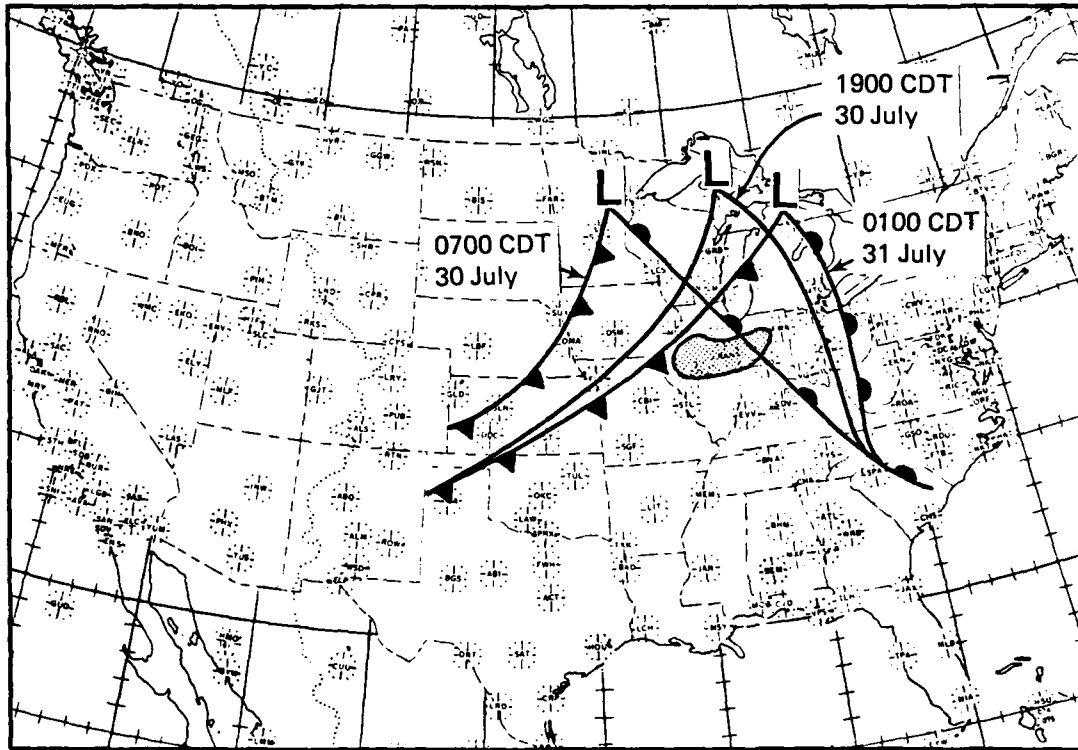


Figure B-3. Surface frontal positions on 30 and 31 July and location of storm in Illinois (shaded) at 1900 CDT on 30 July.

2. SYNOPTIC-SCALE CONDITIONS

Thermodynamic and Kinematic States

East Central Illinois was embedded in a warm, tropical airmass throughout the day. Between 0700 CDT, 30 July and 0100 the next morning, a major cyclone moved east from north-central Minnesota to the Straits of Mackinac with central pressure falling from 1007 to 1003 mb (Fig. B-3). The warm front associated with the cyclone moved rapidly to the east from central Wisconsin and central Illinois at 0700 CDT (12 GMT) to eastern Michigan and eastern Ohio by 0100 CDT (06 GMT) on 31 July. The cold front, which extended southwest from the low pressure center across Iowa to western Kansas, moved more slowly during the day and by 0100 CDT was just entering the northwest corner of Illinois. It was 500 km to the west when the convection started developing in central Illinois in mid-afternoon and did not pass through the VIN network until 1000 CDT the following morning.

Surface temperatures over east central Illinois ranged from the lower 20's (°C) at 0700 CDT to the lower 30's at 1600 CDT. Throughout the day the surface dewpoint temperatures were 22-24°C, 4-6°C above the July normal. Mixing ratios were 17-19 gm/kg, 5-7 g/kg above normal.

Upper air soundings from Salem in southern Illinois indicated precipitable water of 4.0 cm at 0700 CDT on 30 July, increasing to 4.8 cm at 1300 CDT, well above the July average of 3 cm. The lifted index was -5 at 0700 CDT and -8 at 1900 CDT. A midday sounding at Champaign indicated precipitable water of 3.9 cm and lifted index of -5, while the 1900 CDT Peoria sounding in western Illinois (none were available for earlier times) indicated 4.3 cm and -3, respectively. Thus, the airmass over central Illinois was moist throughout the lower troposphere and thermodynamically favorable for intense thunderstorm activity.

The 850-mb dewpoint temperatures were 10C or greater within the warm sector of the synoptic-scale system throughout the day. At 0700 CDT the highest dewpoint temperatures below 3 or 4 km occurred over Missouri, Illinois, and southern Wisconsin. By 1900 CDT the humid air had spread to southern Michigan, Indiana, and western Kentucky, providing a large pool of moisture in the lower troposphere over the middle Mississippi and Ohio valleys. Precipitable water in this region was generally 4 cm or greater, 30 to 50% above normal. Moreover, some warm air advection was indicated in the lower troposphere over this same region at both 0700 and 1900 CDT (Fig. B-4).

The flow at 500 mb was mostly zonal across the northern tier of states, while the southern half of the United States was dominated by a relatively flat gradient and light winds (Fig. B-4). The frontal trough was shallow at 500 mb but a split in the flow was evident by 1900 CDT, as the southern trough lagged behind the northern section. A strong jet at 200 mb, with wind speeds to 40-50 mps, curved anticyclonically northeast from the lee-of-the-Rockies to Lake Superior. Cold air advection was indicated at 500 mb and above over much of the upper Midwest at 0700 CDT. This cold air advection, coupled with warm air advection in the lower troposphere, served to increased the thermodynamic

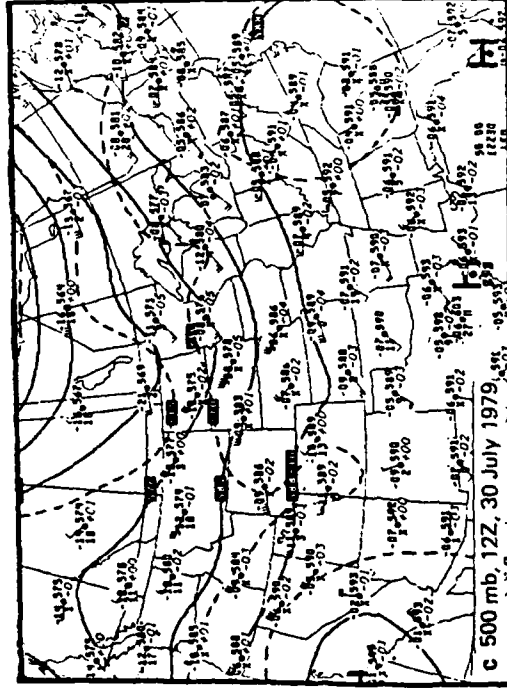
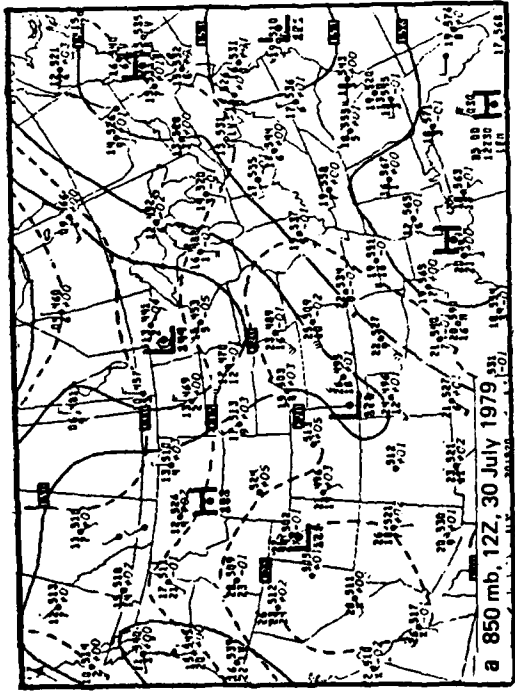
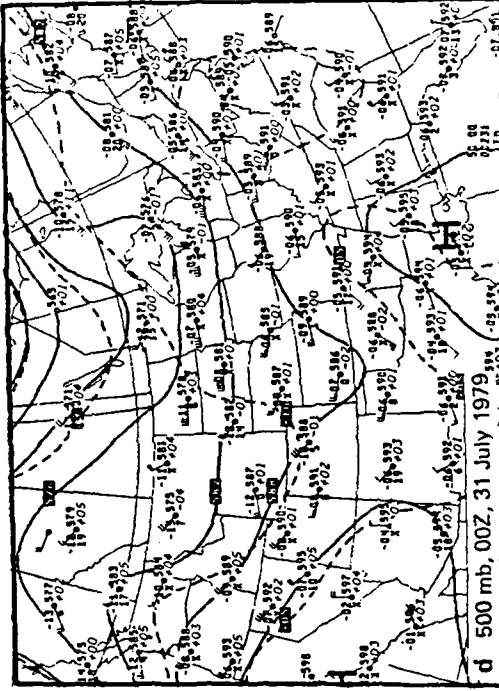
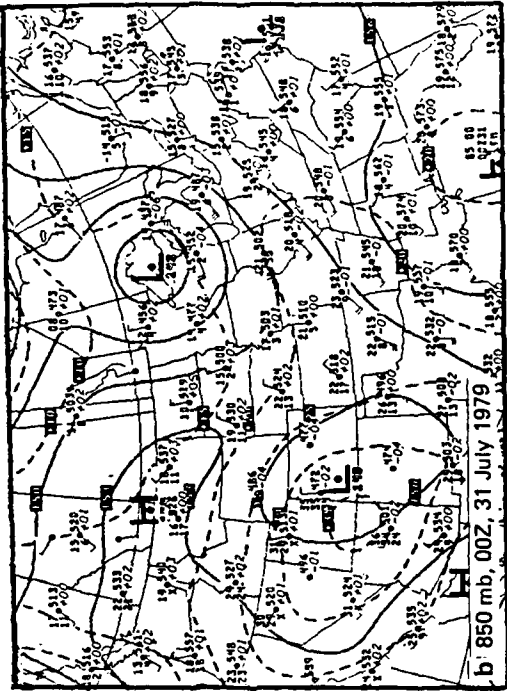


Figure B-4. Upper air charts (NWS analyses).

instability in the region. All that was required to release this instability was a favorable dynamic "trigger." In the west, the convergence associated with the cold front led to the development of the frontal squall line. Sub-synoptic (regional) factors which could have provided the necessary trigger for the development of the warm-sector squall line will be discussed in a later section.

Cloud Systems

A large convective complex which was centered over the eastern borders of South Dakota and Nebraska at midnight on 29 July moved rapidly eastward and by 0930 CDT the next morning the enhanced IR satellite photographs indicated that the convective center was over southern Lake Michigan, northeast Illinois and northwest Indiana. The cloud shield associated with the storm was large and extended west to eastern Minnesota and Iowa and southward into central Illinois. The tallest radar echoes indicated by the NWS radar network for this storm were 13-15 km in height.

This mesoscale convective complex (MCC) continued to move eastward during the morning. The areal coverage of the coldest cloud tops decreased, as did the area of precipitation. By 1100 CDT, the highest (coldest) part of the MCC was located over north central Indiana and southeastern Michigan with (relatively) lower clouds extending north into Canada (Fig. B-5a). A narrow zone of "cloud free" air (as seen on visual satellite photographs) started to "intrude" into the cloud mass on the north and west sides of the deepest convection by 1000 CDT. This clearing intensified in the next couple of hours. Shortly after noon the MCC separated into two areas with the coldest tops still located along the Indiana-Michigan border. The northern section of cloud was associated with the surface low and the southern with the remnants of the main convective area of the MCC.

A "line" of scattered low clouds extended west from southeast Michigan across central Illinois and northern Missouri at 1300 CDT (Fig. B-5b). A cloud "band" (possibly stratocumuli) in the same area at 1430 CDT (Fig. B-5c) was also very low cloud since it is clearly seen in the visible channel satellite photograph but was not detectable in the infrared at this time. This band appears to mark the leading edge of the intrusion of dry and/or cool air suggested by the cloud-free zone mentioned above. It was in this area that the warm sector squall line subsequently developed.

A second area of cloudiness in the early morning of 30 July, located over western Kansas and the Oklahoma Panhandle, was associated with the surface cold front and the upper level trough (Fig. B-6). Clouds in this area were shallower than those associated with the MCC, with the tops of radar echoes at 7-9 km. This cloud area continued with little change in cloud top temperature or areal extent from 0930 to 1330 CDT while moving slowly eastward. Isolated thunderstorm activity was reported with maximum tops between 9 and 11 km in the forenoon. New development began along the front at about 1330 CDT in eastern Kansas and northwestern Missouri and then expanded southward. The anvils from this cloud line expanded rapidly between 1330 and 1500 CDT. Radar measurements confirmed the development of the frontal line as the area covered by the stronger echoes expanded and cloud tops increased to nearly 17 km between 1430 and 1530 CDT.



Figure B-5. Photographs from the GOES satellite (visible channel) on 30 July

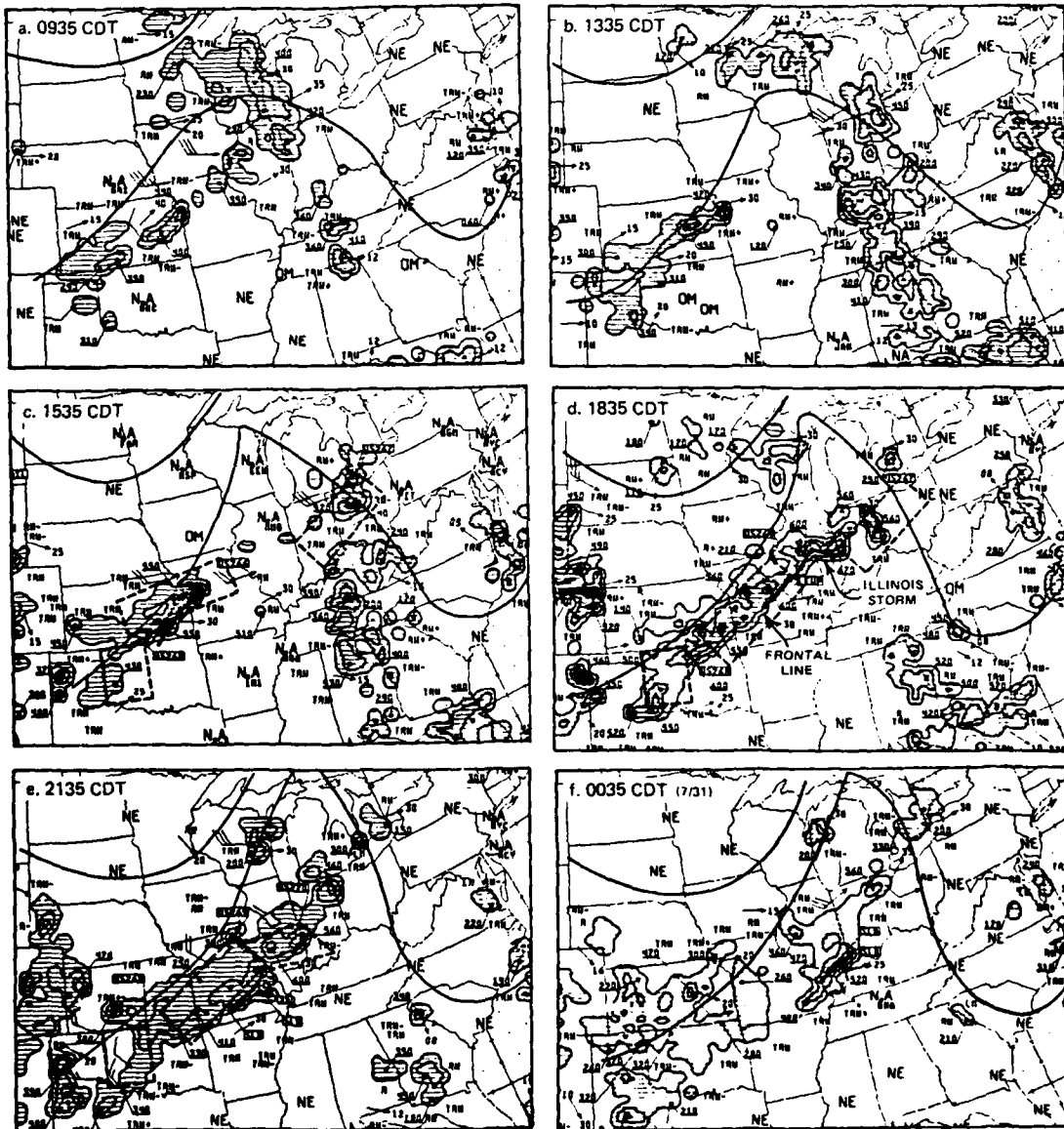


Figure B-6. National Weather Service radar summaries for 30 July with frontal positions superimposed.

Although the frontal cloud region and the warm sector line were to come into very close proximity, and on the radar summaries appear to merge, they developed as two entirely separate entities. Interaction between the two cloud systems is likely. However a careful examination of the radar and surface data confirms a relative independence in development, location and movement. This can be seen even in the transmitted radar summaries. Even though the echo masses appear to be joined, the heaviest echoes are well separated (e.g., Fig. B-6d, e), the line of strong echoes move at different speeds, and the separation is well defined again at dissipation (Fig. B-6d).

Central Illinois Clouds

Around 1500 CDT, well-defined convective clouds started to appear along the fore mentioned tenuous band of low level cloudiness extending across central Illinois. The earliest convection occurred at the east and west ends of this band, with the eastern cloud initially the more intense (Fig. B-5d). By 1700 CDT these two cloud masses dominated the convection in central Illinois and by 1830 CDT had developed extensive cirrus shields. Subsequent cloud development along the line anchored by these two clouds is hidden in the satellite photographs by these cirrus shields but is well documented in the radar records which will be discussed below. As will be seen, the line filled in, with continued growth at either end, until a little after 1730 CDT, when explosive growth near the center resulted in the solid squall.

After 2000 CDT this squall line which developed just north of the VIN network, moved south, with the most intense part of the storm passing through the network by 2100 CDT. Cloud development subsided in the late evening and no new cloud regions were observed in the infra-red satellite imagery anywhere in the Midwest after about 2200 CDT.

Summary

The main synoptic scale factors which favored the development of the warm sector squall line over central Illinois on 30 July were:

- 1) Central Illinois was embedded in a warm tropical airmass throughout the day.
- 2) Moisture advection occurred at 850 mb and at the surface during the day over Illinois, as well as at 700 mb to a lesser degree.
- 3) Warm air advection was indicated over central Illinois below 700 mb while a cold band of air was advected over central Illinois from Kansas and western Missouri at higher elevations. The low-level warming (1-2°C at 850 mb) and upper-level cooling (2-3°C at 500 mb) resulted in an increase in instability during the forenoon and early afternoon.
- 4) An intrusion of cool and/or dry air appeared to occur on the west and south sides of an MCC over Lake Michigan during the forenoon. By early afternoon in northern/central Illinois a narrow band of low clouds marked its southern extent. Convective cells began to develop along this band around 1500 CDT.

3. REGIONAL-SCALE PROCESSES

Data Base and Analysis Methods

Surface data for Illinois and parts of the 6 surrounding states were carefully analyzed to investigate regional-scale processes that may have contributed to the storm development over central Illinois. Hourly thermodynamic and kinematic surface data from 37 National Weather Service stations, covering a 700 km x 650 km area (Fig. B-7) were objectively analyzed for this study. The average station spacing was 110 km and data were interpolated to a uniform grid with about 47.5 km spacing. The objective analysis scheme that was used adjusts the weighting to reflect variable station spacing (Achtemeier et al., 1978). Nevertheless, the large data gap in the southern third of Illinois is unfortunate and tends to cause aliasing of scale in this region. In addition, when data were not available from a station (an occasional occurrence) the contoured fields would change somewhat - primarily in a shift in the center or axis of a "cell" of maximum or minimum value. Despite the limitations of the hourly weather network, the analysis of these data reveals that regional-scale surface processes had significant influence on storm development.

Storm development was traced through the microfilm records from the NWS WSR-57 radar at Marseilles (MMO) in north central Illinois. (The microfilm records from the WSR-57 radar at St. Louis, MO on this day were of very poor quality and essentially unusable.) Surface rainfall amounts were analyzed hourly using the National Weather Service summaries. These summaries include about 220 stations, with an average station spacing of 45 km in the region covered by the analysis. The hourly values were summed for the storm rainfall shown in Fig. B-1.

The study covered the period from several hours before the start of measurable rain from the cloud system and continued for several hours beyond the time the squall line reached its mature stage. The surface fields are described below for the following periods: the pre-storm phase, the growth stage, and the mature-storm stage.

Pre-Storm Phase: 0900-1400 CDT

The surface meteorological fields were generally non-uniform over most of the region during the morning and early afternoon. At 1000 CDT the mixing ratios in northern Illinois varied from 14 to 17 g kg⁻¹, whereas they were in the range of 17 to 20 g kg⁻¹ in the south, with a band of high humidity (19 to 22 g kg⁻¹) over central Illinois (Fig. B-8a). By 1400 CDT, the perturbation in the moisture field had decreased somewhat (Fig. B-8b), but the band of high moisture still extended across central Illinois, with a 4 g kg⁻¹ difference between Peoria (PIA) and Springfield, IL, (SPI), a distance of about 90 km.

The temperature field also was perturbed (Fig. B-8c, d) and reflected the effects of convective activity associated with the MCC. Relatively cool temperatures covered the northern part of the network at 1000 CDT, with

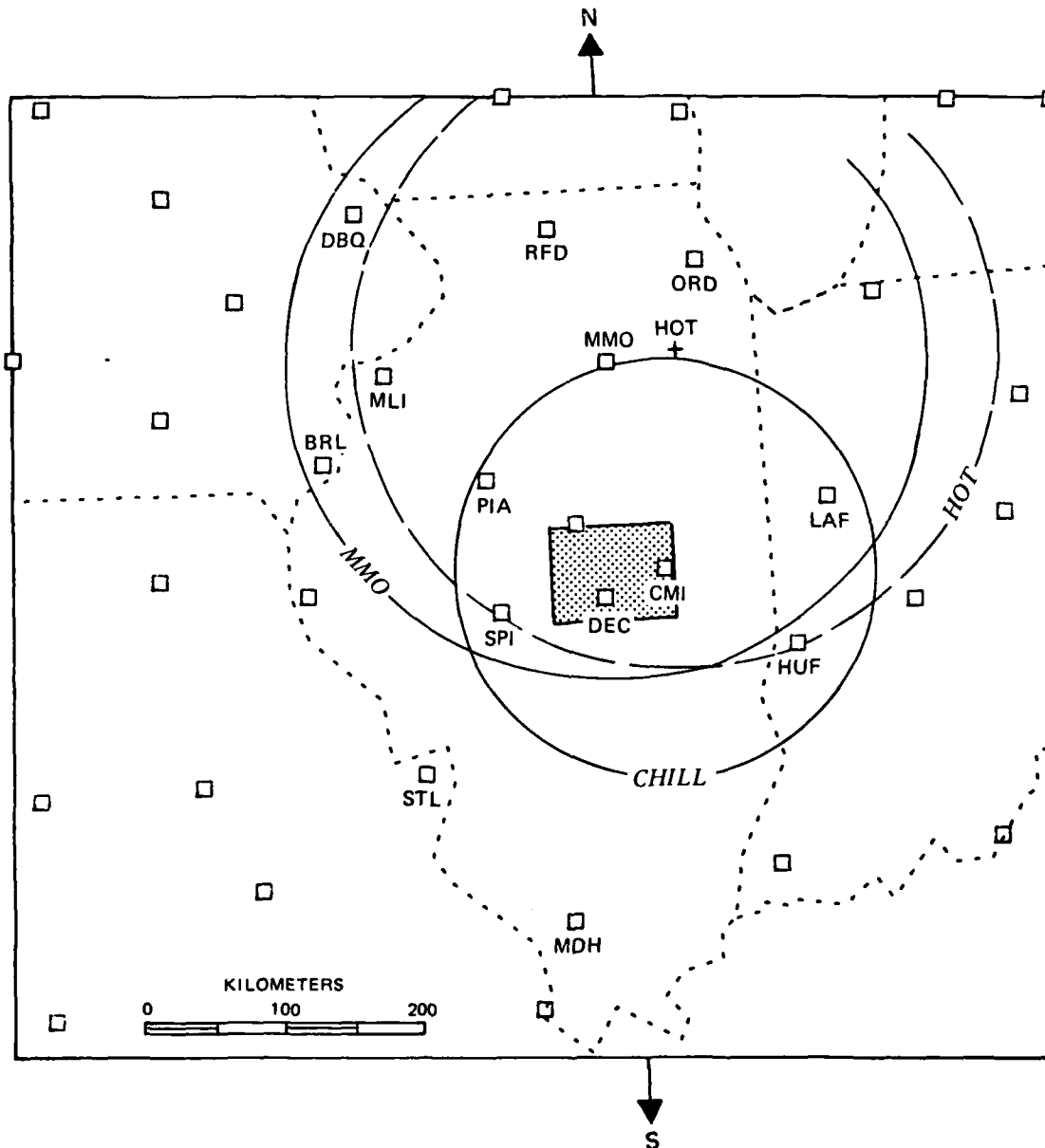


Figure B-7. Region for which hourly surface data were objective analyzed. Box symbols locate stations reporting on 30 July. Circles delineate the ranges of the 3 radars for which data were available (MMO: NWS WSR-57 at Marseilles, HOT: SWS 10-cm radar near Joliet; CHILL: SWS 10-cm radar at CMI). The shaded area delineates the high density VIN network. (Projection: Lambert conformal conic.)

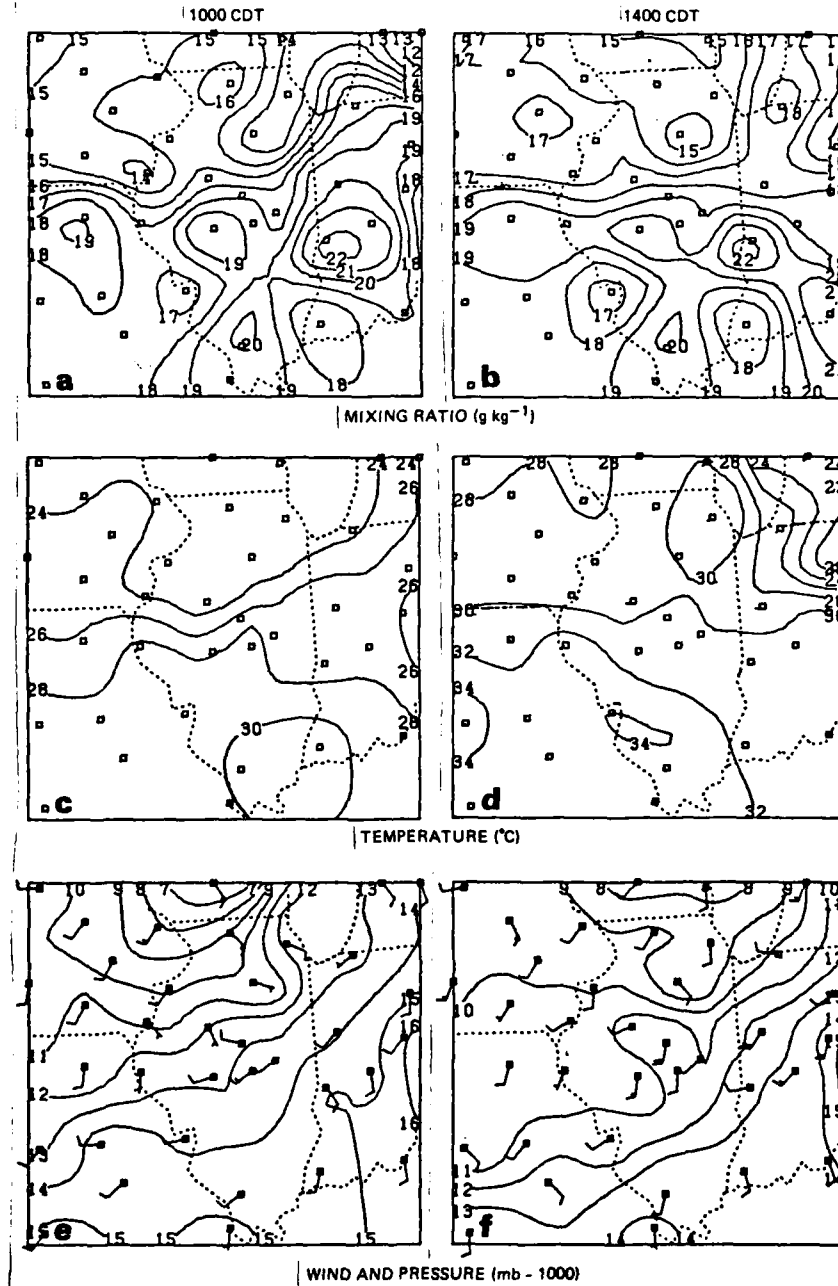


Figure B-8. Surface fields at 1000 and 1400 CDT (left and right columns, resp.) for mixing ratio (a,b), temperature (c,d), and pressure and wind (e,f). Wind speed is shown by the feathers on the wind barbs; one full feather equals 5 ms^{-1} . States are outlined by dots.

temperatures approximately 7°C higher in southern Illinois than in the north. Most of the change occurred in central Illinois, where the temperature gradient was about 5°C per 100 km. The cool pool of air in the northern portion of the region is probably a consequence of both cold outflow from the MCC and reduced early morning insolation because of cloud cover. In addition, as has been noted, there is evidence of dry air advection along the west side of the MCC (Fig. B-5a). By 1400 CDT, the temperature variation across the state had decreased to about 4°C as solar heating increased the temperatures 5-7°C over the region as a whole. There was still evidence of cloud outflow air from the MCC in the northeast corner of the region.

Winds were generally south to southwest at about 4 mps across the analysis network throughout the morning and early afternoon (Fig. B-8e, f). A shift to westerly in northern Iowa, in the far northwestern corner of the region at about 1400 CDT, may have been associated with the leading edge of the frontal zone. The pressure field was dominated by the synoptic gradient but mesoscale perturbations on the macroscale pressure fields are very evident. Local winds were moderately consistent with the perturbed pressure field.

In Figure B-9 are shown the streamlines and divergence fields for each hour between 0900 and 1400 CDT. Convergent flow persisted over east-central Illinois throughout this pre-storm period, with grid point values at the centers of convergence cells ranging between 4 and $8.8 * 10^{-5} s^{-1}$. By 1100 CDT, a region of convergence was developing over extreme west-central Illinois as well. This area expanded eastward over the next two hours and by 1300 CDT this second convergence in western Illinois was "joined" to the center in the east, while clearly separated from it by nearly non-divergent flow. The maximum grid point value in the western "cell" was $5.1 * 10^{-5} s^{-1}$ at 1300 CDT, increasing to over $6 * 10^{-5} s^{-1}$ by 1400.

The continual small cloud development trailing to the southwest of the MCC, which was noted in the satellite photographs in the forenoon (Fig. B-5a), lay just on the north edge of the convergence zone extending from the Illinois-Indiana border, southwest to St. Louis at 1000 and 1100 CDT (Fig. B-9b, c). However, this cloud band rapidly decayed and only scattered remnants remained by 1230 CDT. Shortly after, scattered cumulus clouds started to develop in a roughly east-west line (Fig. B-5b) on the north (downwind) side of the convergence zones in Illinois (Fig. B-9e) and also downwind of the band of moisture extending across Illinois, 1200 CDT, et seq., (Fig. B-8b). By 1430 CDT a narrow cloud band extended across the State. The largest convective element in this band was located on the downwind side of the area of convergence in east central Illinois which had persisted since morning. This band of small clouds was to shortly evolve into a line of rapidly developing convection.

Development Stage: 1500-1900 CDT

The transformation of the cloud band to a line of active convective clouds started at about 1500 CDT. By 1530 CDT, two precipitation echoes appeared on the NWS radar summary, one in east central Illinois and one in west central Illinois (Fig. B-6c). (Illinois was clear of radar echoes an hour earlier.) Very light rain occurred at Rantoul, just north of Champaign (CMI) between 1400 and 1500 CDT but no precipitation was reported elsewhere in the State.

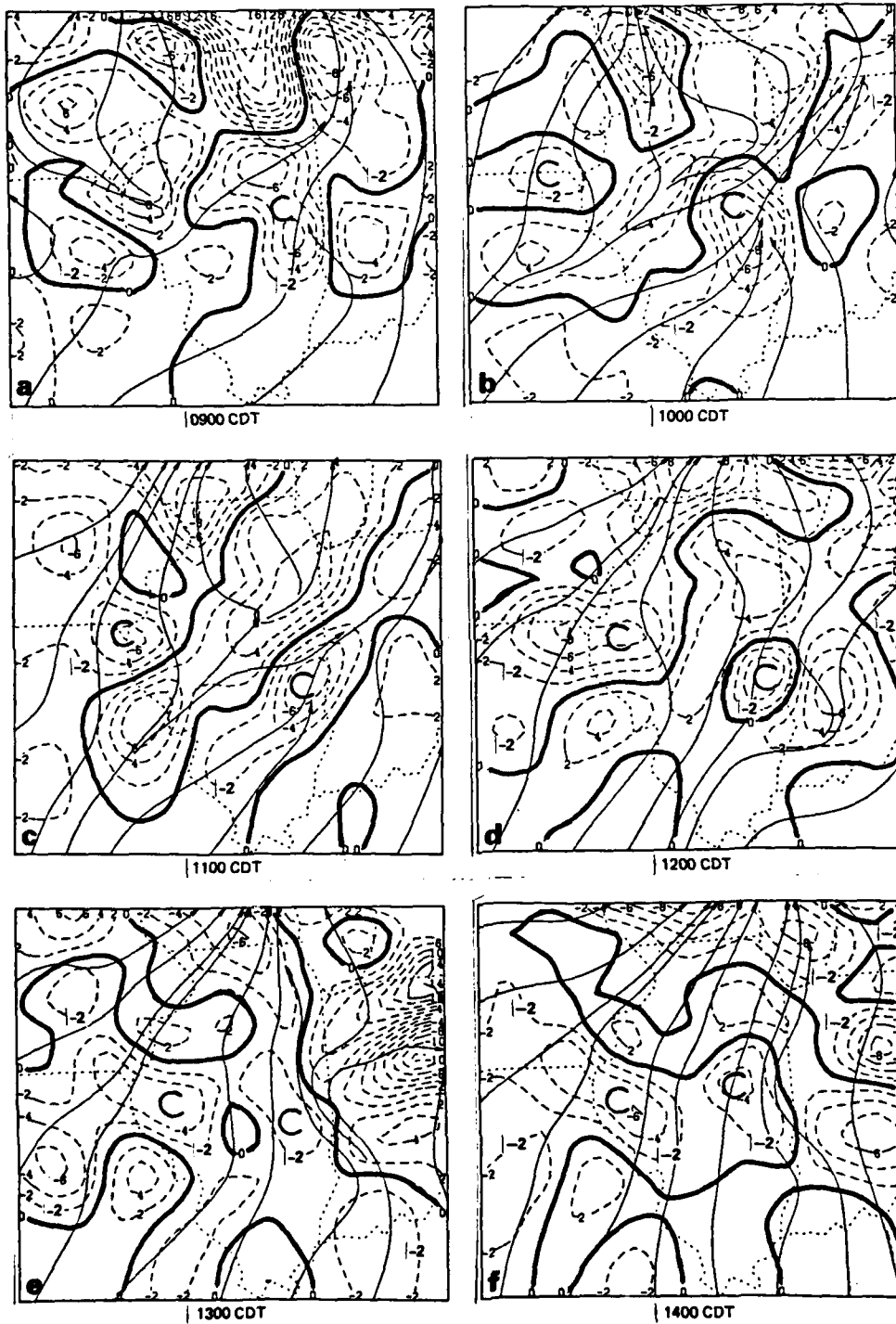


Figure B-9. Streamlines (solid lines) and divergence contours (dashed) for each hour from 0900 CDT to 1400 CDT. Contours of divergence are labeled in units of 10^{-5} s^{-1} , with negative values indicating convergent flow. Heavy contours are for divergence equal to zero, thus separating convergent from divergent flow. The "C" symbol identifies persistent areas of convergence discussed in text.

Clouds continued to develop along an east-west line joining these two echoes, with increasing size and areal density. By 1800 CDT, a nearly solid squall line extended east-west across the State, from western Indiana to northeastern Missouri. Individual precipitating clouds and cells in this line moved slowly to the east-southeast, but the line along which the development occurred was essentially stationary throughout most of the 4-hour period of development. This is best seen in the sequence of photographs from the NWS WSR-57 radar at Marseilles, IL (MMO) shown in Figure B-10 since the expanding cirrus shields obscured the lower cloud development in the satellite photographs.

In Figure B-11, the MMO radar echoes are superimposed on the concurrent streamline and divergence fields. As can be seen, the two areas of convergent flow in east-central and west-central Illinois which formed during the pre-storm period, persisted throughout the afternoon and early evening. The first precipitation echoes in the line developed downwind of the convergence zone in eastern Illinois at about 1445 CDT to be followed shortly after by a few small echoes on the north side of the area of convergent flow in western Illinois (Fig. B-11a). The very light rain (<0.25 cm) at Rantoul, IL, just north of CMI between 1400 and 1500 CDT, mentioned above was followed by 1.5 cm in the subsequent hour.

The number of echoes and the sizes of the individuals increased rapidly between 1500 and 1600 CDT. However, at the end of that hour the main echoes in the line still remained as two clusters, each developing fairly independently of the other. Both clusters were on the north sides of regions of convergence in central Illinois (Figs. B-10b, c; B-11b). As the convection developed between 1400 and 1600 CDT, the rate of mass inflow* into the area defined by convergent flow in eastern Illinois, increased significantly, by 60% between 1400 and 1500 and 85% between 1500 and 1600 CDT. In the west the mass inflow for the convergence "cell" did not change in the first hour but increased by 60% between 1500 and 1600.

As indicated by the development of the precipitation echoes, the rainfall was more extensive in the east than in the west during the hour following 1600 with an additional 3.3 cm rainfall at Rantoul between 1600 and 1700 CDT. Rain was also measured for the first time in the west, with a single station reporting slightly less than 1 cm for the hour. (The heaviest rain may not have been measured because of the small size of the precipitating cloud and the location of stations in the NWS network.) The two echo clusters continued to expand and intensify between 1600 and 1700 CDT, both still anchored to the two regions of convergent flow. The precipitating cloud areas also became increasingly solid, due both to "merging" of echoes and to new development between individuals.

The two convergent zones still persisted at 1700 CDT (Fig. B-11c) with the net rate of inflow in the east remaining at the same level as at 1600 CDT. The

*Inflow in this instance was calculated for the areas over which grid point values of convergence were $\geq 2.5 * 10^{-5} \text{ s}^{-1}$.

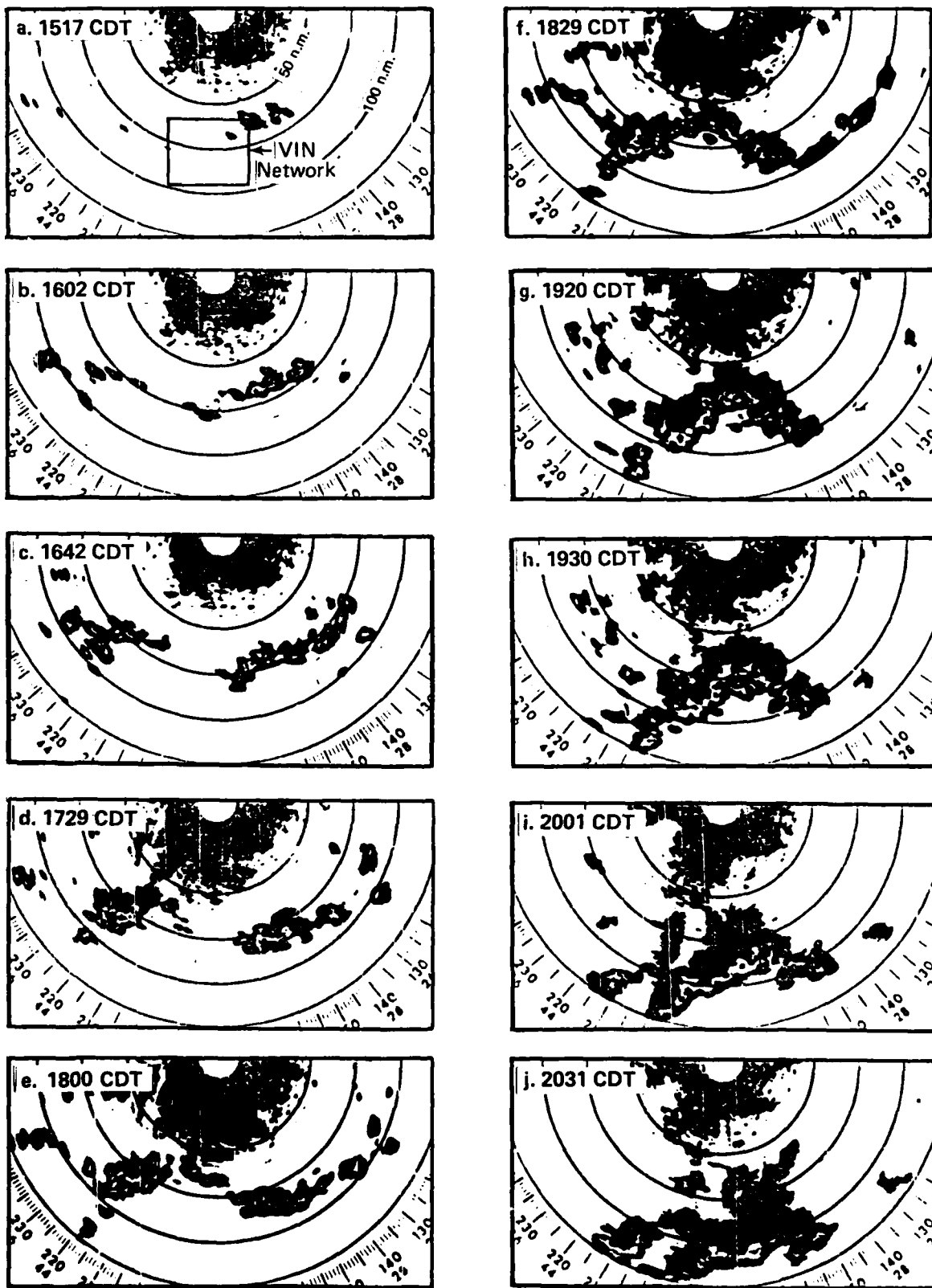


Figure B-10. Precipitation echo development as recorded by NWS WSR-57 radar at Marseilles

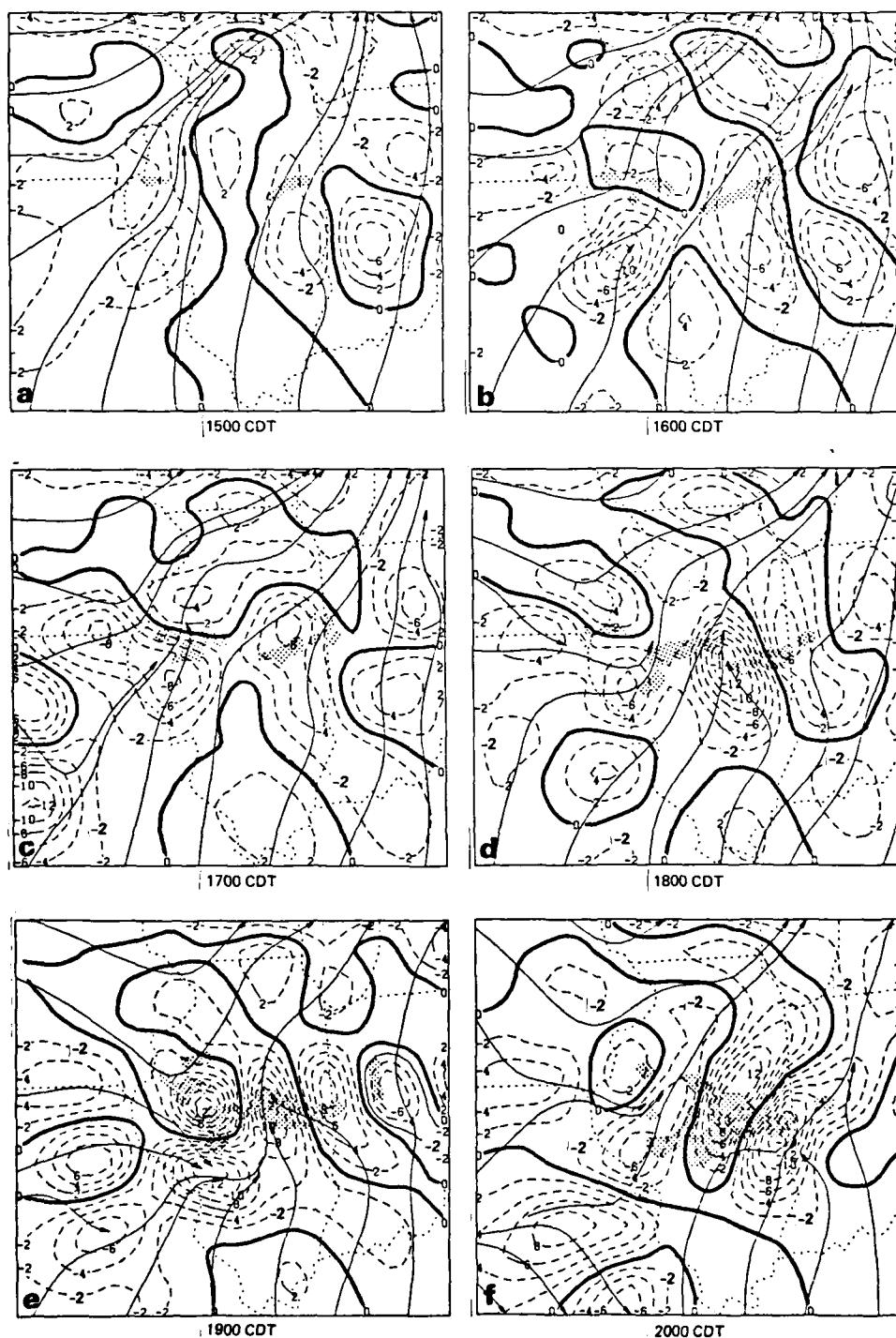


Figure B-11. Streamlines and divergence field, as in Figure B-9, for each hour from 1500 to 2000 CDT. The locations of echoes recorded in the MNO WSR-57 photographs are shown by shading. In the hours prior to 1700, the echo areas shown are "envelopes," i.e., not completely filled with echo; in the hours after 2200, they were essentially solid (see Figure B-10).

seeming expansion of convergent flow on the Missouri, Iowa border at 1700 CDT was a harbinger of new cloud development along the front, not part of the warm sector squall (see Figs. B-6d, e). By 1800 CDT the two areas in the west were clearly definable at convergence values above $2.5 * 10^{-5} \text{ s}^{-1}$, whereas earlier they appeared as one at that level, probably because of the low spatial resolution in the data.

The convergence in east central Illinois increased greatly in intensity at 1800 CDT (Fig. B-11d) with maximum grid point value of $14.3 * 10^{-5} \text{ s}^{-1}$. This large increase, as well as a shift of the center westward, was probably related to the arrival of cool outflow from heavy showers just to the east of Champaign (CMI), where the wind shifted from SSW to E and the temperature fell from 28 to 23°C. A companion zone of divergence with maximum grid point value of $7.3 * 10^{-5} \text{ s}^{-1}$ appeared on the Illinois-Indiana border at about the same time, replacing generally non-divergent flow in this location.

The westward shift of the axis of convergent flow in east central Illinois was accompanied by a merging of the two zones of convergence at the $2 * 10^{-5} \text{ s}^{-1}$ level. At about the same time there was nearly explosive cumulus development to the north and the gap between the two cloud clusters was "bridged" in less than 30-minutes (Fig. B-10d, e). This very rapid increase in the convergence and accompanying cloud growth in central Illinois suggests that circulations on the scale of the cloud systems were now beginning to significantly alter the surface wind field, modifying the regional scale kinematics.

In the hour following the appearance of this area of strong convergence at 1800, CMI and Farmer City (FAR), both located near the center of the convergence, recorded rainfalls of 4.2 cm and 2.7 cm, respectively, and 2.6 and 1.6 cm, respectively, in the hour from 1900 to 2000 CDT.

By 1900 CDT, the squall line was rapidly reaching a mature stage. It was a nearly solid cloud with a wave-like form, extending across most of the width of Illinois (Fig. B-10f, g), although the heaviest rainfall still tended to be in the eastern part of the State. In central Illinois the surface wind and its derivative fields were dominated by this major rain storm, completely overwhelming the pre-storm regional wind field. The winds were variable as a consequence of the outflows from several individual rain centers. Within the resolution of the regional network, two main areas of strongly convergent flow continued, both with maximum point convergence in excess of $12 * 10^{-5} \text{ s}^{-1}$, but with decreasing areal extent (Fig. B-11e). These were accompanied by two areas of divergent flow of nearly equal size and magnitude. The more intense divergence occurred beneath and to the north of the western part of the squall line.

Reference back to Figure B-8 reveals that the echo line developed in the area of strongest temperature gradient, i.e., just on the downwind side of the warm temperatures, and on the downwind side of the region of high moisture content. Thus, cloud development was in an area favored by persistent temperature and moisture advection as well as by mass convergence.

The transport of heat into the area due to advection was much less than that brought by mass inflow, and thus the patterns of heat divergence are essentially identical to those shown in Figures B-9 and B-11, although the contour values are, of course, different. Moisture advection, on the other hand,

was not always insignificant, as would be suspected from the gradients. Nevertheless, the fields of moisture divergence are sufficiently similar to those shown in Figures B-9 and B-11, that it is not necessary to show them here. Suffice it to say that the regions of mass inflow indicated in the figures by the divergence field were also regions of heat and moisture inflow. More quantitative discussion of the heat and moisture inflow will be given later in this section.

The regional temperature field was not seriously affected by the convection until shortly after 1700 CDT, although there was evidence of cold storm outflow at one station in east central Illinois at 1700 CDT (Fig. B-12c, d). By 1800 CDT, however, the influence of the thunderstorm outflow was obvious in the temperature field, with cool pools of air below and to the north (downstream) of the line, and decreases in individual station temperatures of 4 to 6°C.

The alteration in the moisture field was similar (Fig. B-12a, b). Moist air continued to hover in an E-W band across central Illinois until 1700 CDT. Within the next hour the regional field began to reflect the effect of the thunderstorm outflow as the moisture as well as the temperature dropped dramatically beneath the clouds on the eastern end of the line. By 1900 the surface air beneath and downwind of the storm was characterized by relatively low moisture content and low temperatures.

Evidence of a pressure perturbation began to evidence itself as early as 1200 CDT. The "disturbance" was unsteady, but, over time, a flat pressure gradient (i.e., nearly uniform pressure) became established over central Illinois and northwest Missouri, rather than the increasingly strong gradient one would expect with the advancing cold front. This flat pressure gradient was sustained for several hours, with occasional small centers of relatively low (or high) pressure developing due to local conditions. By 1700 the winds in the extreme northwest of the region had shifted to the west, indicating a frontal passage, and by 1900 CDT, they were westerly throughout Iowa (Fig. B-12e, f).

Mature Stage: 2000-0100 CDT

By 1900 CDT the storm had a solid wavelike shape with a wavelength of about 270 km and full amplitude (i.e., displacement from southern extremity to peak) of about 50 km. The area enclosed by this wave form, and in particular that region close to the apex, was one of strongly convergent flow in which convergence reached $12 * 10^{-5} \text{ s}^{-1}$. Within this area small feeder cells developed and tended to increase the width of the cloud at the apex of the wave. This culminated shortly after 1900 with a small line of clouds reaching across the two limbs of the wave and the almost instantaneous filling of the area in between with new cloud matter (Fig. B-10g, h). As the upper half of the wave echo filled, the eastern edge of the convection decreased in areal extent and intensity. This was the final stage of development and by 2000 CDT the storm had lost its wavelike form and had become a mature and solid rain mass oriented approximately ENE-WSW (Fig. B-10j). There was continual development of new rain cells on the upwind (south) side of the echo and a broad

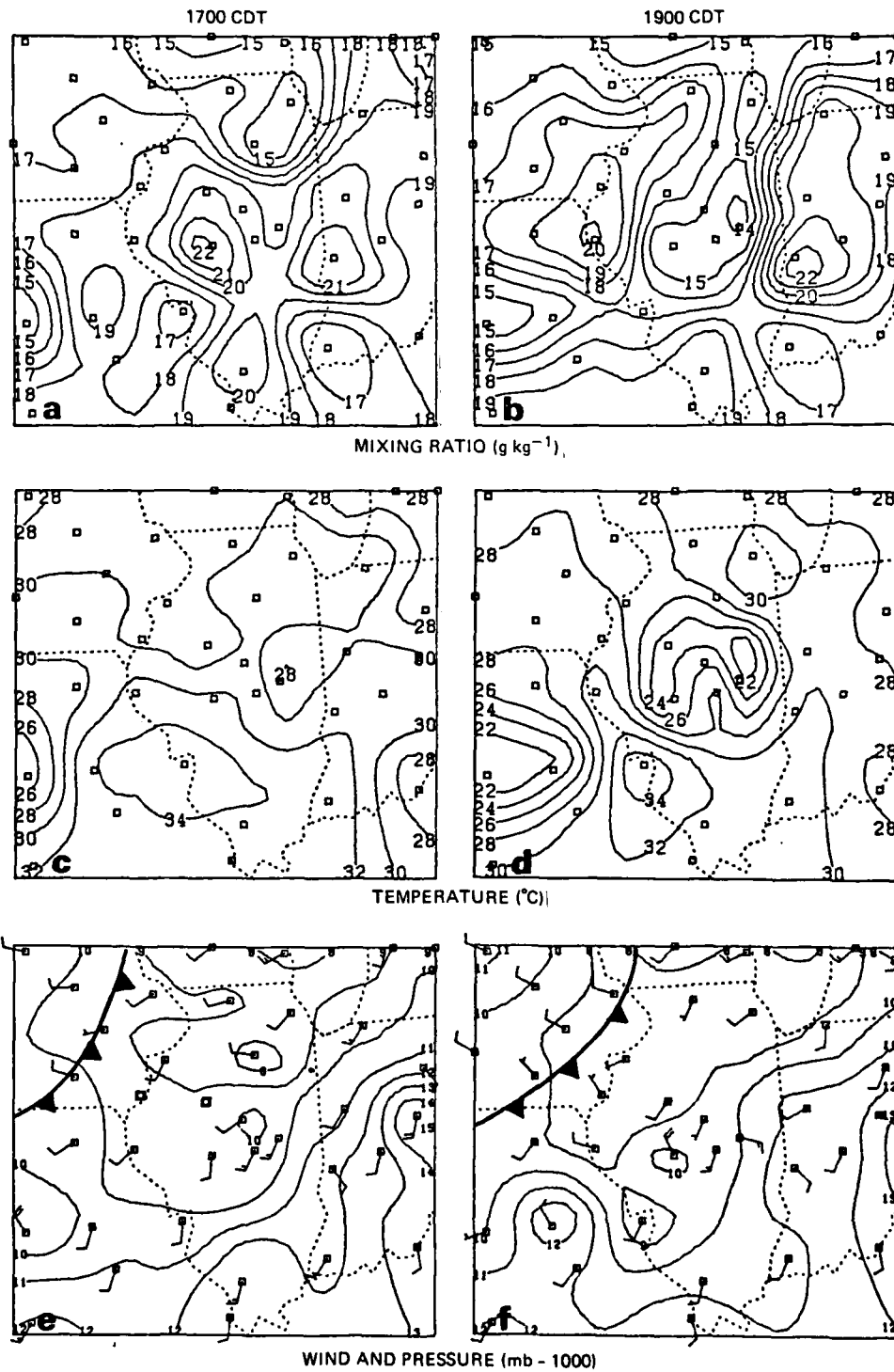


Figure B-12. Surface fields of mixing ratio (a,b), temperature (c,d), pressure and wind (e,f), for 1700 and 1900 CDT (left and right columns, resp.), plotted as in Figure B-8. The front is indicated by the "toothed" line.

region of more-or-less uniform, weaker, stratiform echo on the downwind side. As the storm took on its new character it also started a steady movement southward, after 5 hours of nearly stationary development.

When the storm reached maturity around 2000, the storm outflow dominated the surface wind field, (Fig. B-11f). At this hour there was strongly divergent flow due to the storm outflow in east central Illinois, an area that an hour earlier had strongly convergent flow. Strongly convergent flow still existed on the eastern end of the line, with mass inflow into the storm system indicated on the southwest as well. By 2200 CDT a single doublet of strong divergence/convergence, with central values greater than $10 * 10^{-5}$ and $8 * 10^{-5} \text{ s}^{-1}$, respectively, dominated the regional surface field. This general pattern of divergence continued for the next 3 hours shifting SE as the squall moved SE (Fig. B-13a, b). By 0100 the squall line which we had been following since midday lay just to the north of the Kentucky-Illinois border (Fig. B-6f) and by 0200 the wind field was readjusting to the synoptic scale forces in responses to the arrival of the front in northwest Illinois.

The precipitation area shown in Figure B-13a (2200 CDT) is truncated on the south because of the range limits of the Marseilles radar. However, the NWS radar summary (Fig. B-6e), indicates that the echo did not extend very much farther south at this hour and shows considerable echo development to the northeast, as suggested by the convergence in northeast Indiana. The radar echo shown in Fig. B-13b is not, on the other hand, at all representative since most of the storm, and particularly the active regions, had moved out of range of the MMO radar.

During the hour from 2000 to 2100 CDT the heaviest rainfall still occurred as two "storms", one in east central and the other in west central IL, both with maximum station values of 3.3 cm for the hour. However, as the eastern cloud area decreased in intensity and the cloud mass became more unified, it was the western part of the cloud mass that dominated, with station rainfall reaching a high of 4.8 cm in the hour from 2100 to 2200 CDT. The rainfall on the leading edge remained heavy for about another hour, as the storm moved southeast. It still tended to be localized, with the largest station amounts of about 3 to 4 cm for the hour between 2200 and 2300. The rain intensity then decreased, and despite the indication of some strong precipitation echoes in the radar summaries, rainfall recorded for any station after midnight was less than 5 mm. This was accompanied by decrease in the magnitude of both the divergence and convergence related to the storm outflow.

The incursion of the new airmass behind the cold front into the northwestern part of the area covered in the analysis is clearly seen in the moisture and temperature fields by 2200 CDT (Fig. B-13). However, the influence of the storm outflow remained dominant over most of the region as a large pool of cool air with relatively low moisture content covered central Illinois. The perturbation in the synoptic field gradually weakened, but continued to be well-defined in both the temperature and moisture fields for at least an additional 4 hours (when the analysis was terminated), with temperatures 1 to 3°C lower and mixing ratios approximately 3 g kg^{-1} lower than elsewhere in the region.

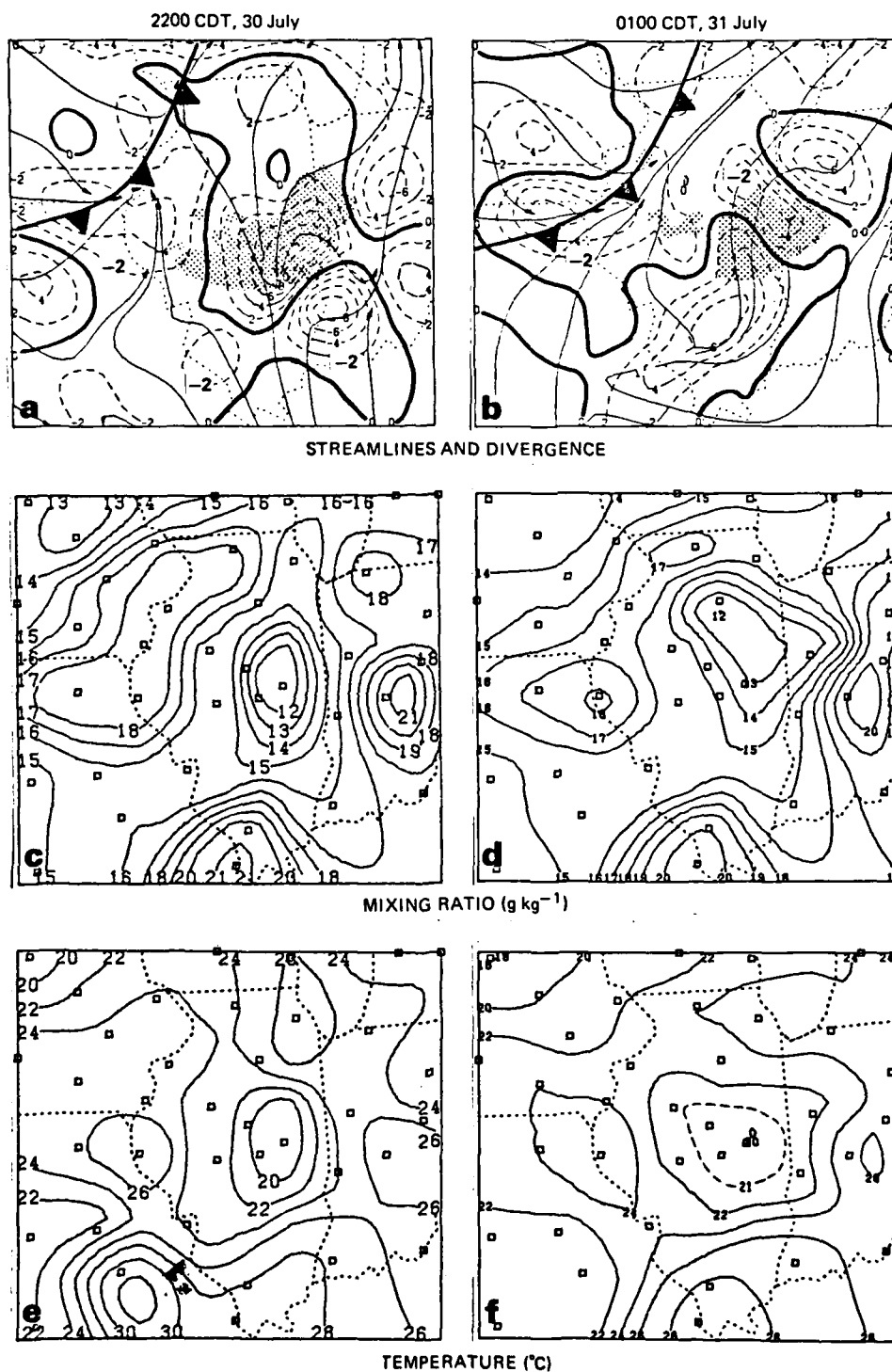


Figure B-13. Streamlines, divergence field, and echo areas, (a,b), as in Figure B-11, and the surface fields of mixing ratio (c,d), and temperature (e,f), as in Figure B-8, for 2200 CDT on 30 July and 0100 CDT on 31 July (left and right columns, resp.). The location of the front is indicated by the toothed line in a,b.

Vertical Fluxes and Rainfall

The association between the locations of persistent convergence at the surface and the storm development is clear in the above discussion. Unfortunately the NWS upper air network is inadequate in resolution, in both space and time, to determine the depth through which the convergence "cells" may have extended. It was, however, possible to estimate the flux of heat and moisture through the top of the surface layer, and then, based on data from the VINCIPAL network, make an estimate of the net transport into the cloud layer for comparison with the evolution of the water mass represented by the rain. The analysis considered both the net vertical flux for the whole area defined by the storm rainfall as well as the upward flux in the regions of convergent flow spatially related to the area of the storm development. The rain mass was also calculated for each hour and for the total for the Illinois storm, shown in Figure B1. (The early rainfall in Missouri was associated with the generation of the frontal cloud line and was not included in the calculation. This rain was adequately separated spatially from the Illinois storm in the hourly data for the two storms to be resolved easily.)

From Gauss' theorem, the net inflow of quantity B, I(B), into an area of size, A, can be calculated from the grid point values by

$$I(B) = -\sum (\nabla \cdot B\vec{V})_{i,j} \Delta x \Delta y = -\sum d_{i,j} \Delta x \Delta y \quad (1)$$

where i,j are grid point indices, Δx , Δy is grid spacing in the x, y direction, respectively, and sums are taken over all i,j.

In the following discussion, d will be referred to as divergence in the generic sense but actually represents the divergence in the field represented by $B\vec{V}$. Thus, in this discussion it may refer to mass, moisture or heat divergence.

The horizontal inflow and vertical transport were calculated for three quantities:

Mass : $B = \rho$; $d = \nabla \cdot \rho\vec{V}$

Moisture: $B = \rho m$, where m is mixing ratio; $d = \nabla \cdot \rho m\vec{V}$

Heat : $B = \rho C_p T$, where C_p is specific heat of dry air and T in the temperature in degrees Kelvin; $d = \nabla \cdot \rho C_p T\vec{V}$

Since the variation in density was only 3 or 4%, it has been considered a constant in the computations. In expanded form, I(B) for each of these properties is given by

$$\text{Mass} = -\bar{\rho} [\sum (\nabla \cdot \vec{V})_{i,j}] \Delta x \Delta y \quad (2)$$

$$\text{Moisture} = -\bar{\rho} [\sum (m \nabla \cdot \vec{V} + \vec{V} \cdot \nabla m)_{i,j}] \Delta x \Delta y \quad (3)$$

$$\text{Heat} = -\bar{\rho} C_p [\sum (T \nabla \cdot \vec{V} + \vec{V} \cdot \nabla T)_{i,j}] \Delta x \Delta y \quad (4)$$

The first term in parentheses in equations (3) and (4) is inflow of the quantity into the area due to mass convergence, while the second represents inflow due to advection. In the case of heat flux, the advective term was usually 1 to 2 orders of magnitude smaller than the velocity convergence; in the case of moisture convergence, however, the two terms were not infrequently of the same order of magnitude. However, in both instances the fields were so similar to those of the velocity divergence, that the relationships between cloud development and moisture and temperature convergence (divergence) can be inferred from the figures above.

The vertical flux of quantity B through level z, over area A, due to inflow into the area can be expressed as

$$F = \sum B_{i,j} w_{i,j} \Delta x \Delta y \quad (5)$$

where w is the mean vertical velocity due to mass inflow, and the sum is taken over all i,j.

Integrating the continuity equation gives, for B conservative in the layer, at the level z

$$F = [\sum B_{i,j} w_{i,j} \Delta x \Delta y]_z = -\sum \bar{d}_{i,j} \Delta x \Delta y \Delta z + F_{z-\Delta z} \quad (6)$$

where the overbar indicates average over the layer Δz . If $z-\Delta z$ is at the ground, one may assume $w = 0$ and therefore $F_{z-\Delta z} = 0$. Lacking information as to the value of d at the ground, one must estimate an "average" for the layer from the ground to the anemometer level. Virtually nothing is known about the variation in height of divergence in the surface boundary layer and assumptions have ranged from linear to constant, throughout the layer below. For anemometer heights of 10 m, the vertical velocity would vary from .06 to .12 cm s^{-1} under these two assumptions, for even the largest calculated grid values of mass divergence. In the following calculations of vertical transport out of the surface layer the second assumption has been used, with value of d calculated at the anemometer level applied throughout the layer below.

In Fig. B-14a is plotted the vertical mass flux through 8 m, approximately the average anemometer level, for a rectangular area of about 125,000 km^2 encompassing the rainfall from the Illinois storm shown in Fig. B1a, for several hours prior to and during the rains from the active convection. The upward flux from the regions of convergent flow within the area is also shown. Both are plotted at the time of the hourly observation. The rain mass accumulated during an hour and the mean rain depth over the area are plotted, in Fig. B-14b, at the end of the hour during which the rain fell.

A dramatic change from net outflow to inflow for the area as a whole took place at about 1300 CDT, at least 2 hours before precipitation was measured at the surface. However, regions of net upward flux occurred within the storm area even earlier, as indicated by the curve for regions of the convergence.

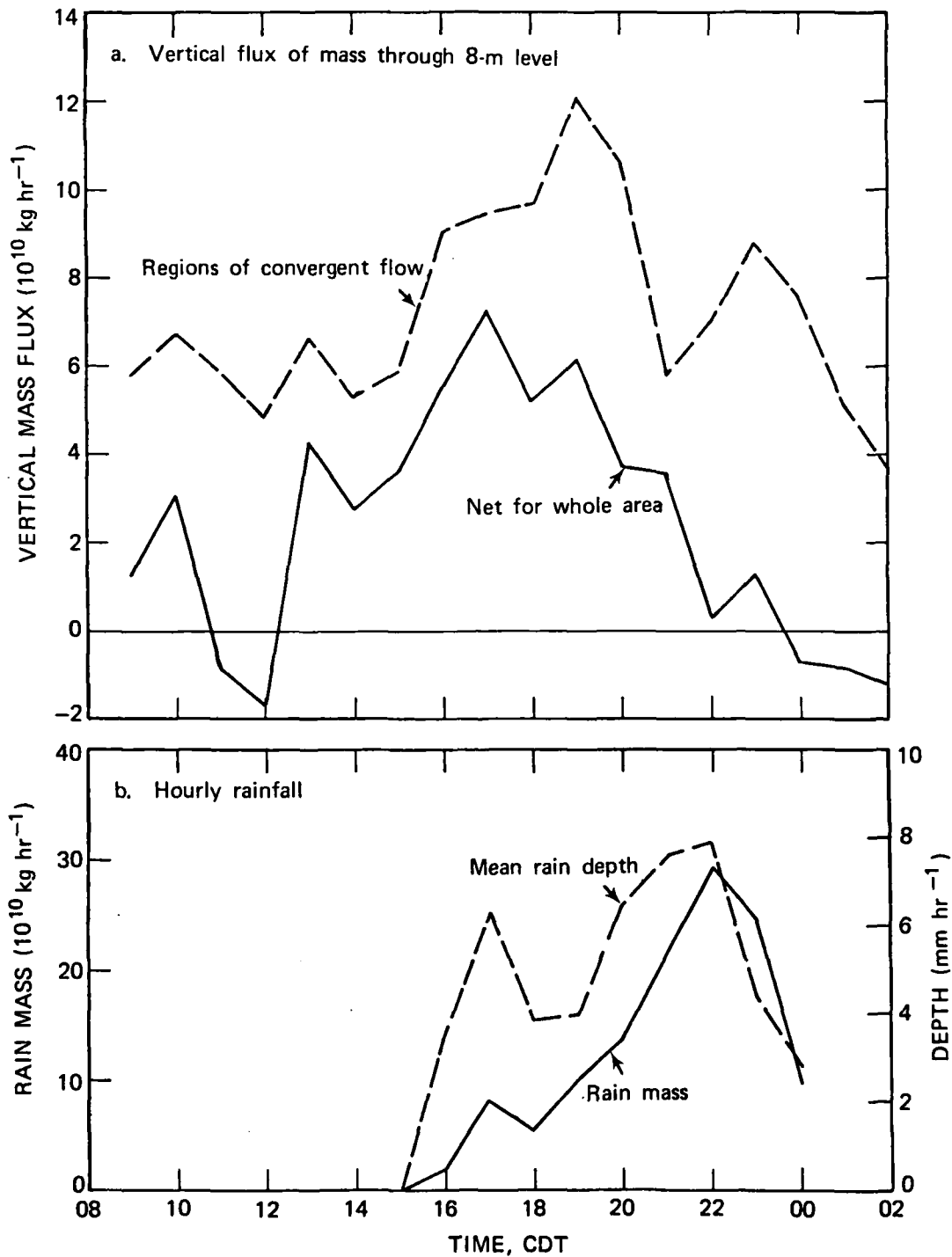


Figure B-14. (a) Time profile of vertical flux of mass through 8-m level based on calculated inflow for area encompassing total storm rainfall (solid) and for regions of convergent flow within that area (dashed).
 (b) Time profile of rainfall.

Significant net inflow into the storm area continued until some time between 2100 and 2200, when the net flux returned to near zero. This sharp decrease occurred as the mean rain rate for the area and the hourly accumulated rain mass neared their peak and was a reflection of the development of regions of strong divergence due to local storm outflows (Fig. B-13). The influence of the outflows from the light rains between 1600 and 1800 are also seen in this figure, although less dramatically. There was a significant increase in the local downward flux between 1700 and 1800, followed immediately by an increase in upward flux between 1800 and 1900. (Downward flux in regions of divergence is given by the difference between the two curves.)

The development of the "bridge" between the cloud clusters in the west and east occurred shortly after 1800. By 1840, the storm had evolved into a solid squall line. After 2000 CDT, the total upward flux in regions of convergent flow decreased greatly. By this time, the squall line was fully mature, with strong convective cells on the leading (south) edge and a large rain shield on the north side. The increase in the local upward flux at 2300 and 2400 provided a source of low level moist air to the convective cells embedded in the rain shield (see shaded area in Fig. B-13a) and for some continued cell development in the south.

A very crude estimate of the efficiency of the storm may be obtained by comparing the total rain mass with the total accumulated inflow and upward transport of moisture in this area surrounding the storm. In order to obtain this estimate, several assumptions have been made. Firstly, it was assumed that moisture transported into the cloud layer from below was available to the storm system and was not advected out of the area. A corollary was that no moisture was imported through advection in the cloud layer (or alternatively that the horizontal flux divergence was zero in the cloud layer). Secondly, it was assumed that the sub-cloud layer was well mixed and the moisture content was essentially uniform. This was probably valid after the late morning hours. Thirdly, it was necessary to assume that the inflow calculated at the anemometer level was valid through some greater depth in the sub-cloud layer. A final assumption was that the inflow measured at the surface on the hour was equal to the average for the hour surrounding it, i.e., for 30-minute before to 30 minutes after measurement.

In Figure B-15, are plotted the accumulated rain mass, and the accumulated vertical transport of moisture for the the whole area and for the regions of convergent flow. The latter two are plotted 30 minutes after measurement time. In calculating the accumulated moisture flux, it was assumed that the surface divergence was a good estimate for the mean through a 800 m depth, a common height for cloud base in central Illinois. (Divergence calculated for the pibal triangle in the network indicated that this assumption is adequate for at least the lower 400 m, Section 4D.)

It is quite evident from Fig. B-15 that a significant amount of moisture had been "fed" into the cloud layer from below, before the rain started. It also can be seen that the rate at which it was being transported upward increased when the rain started but then decreased as the rate of accumulation of rain mass increased around 2000 CDT, for both convergent regions and for the whole area.

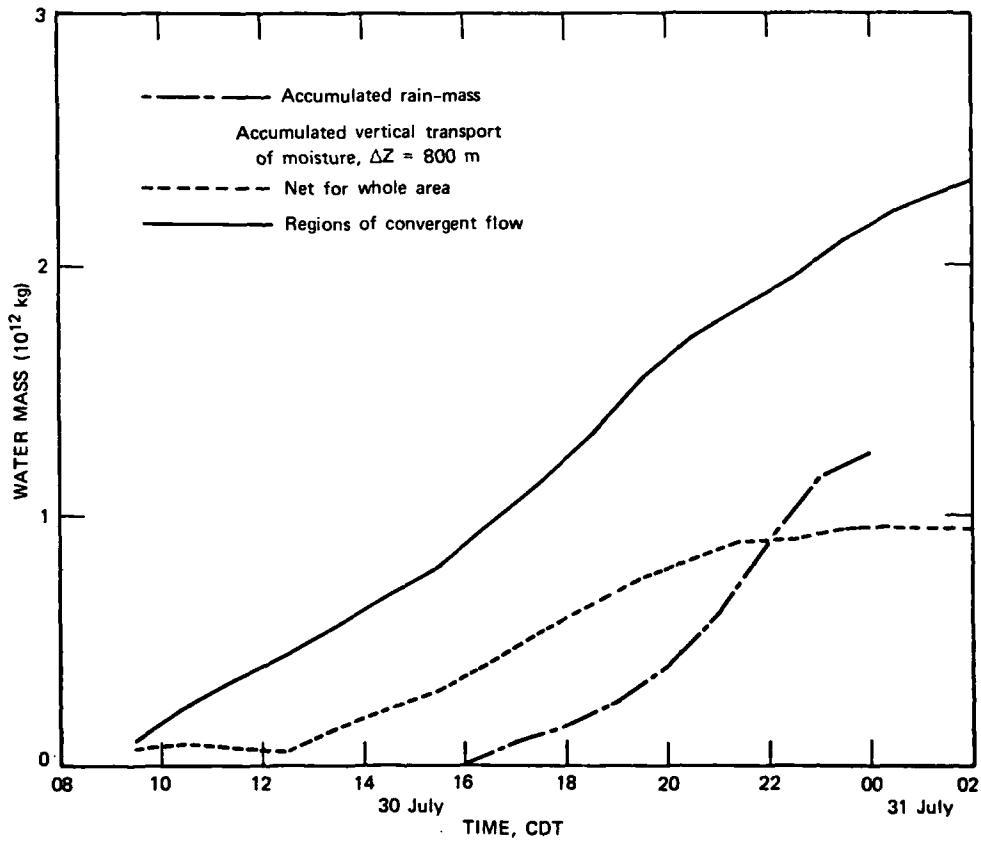


Figure B-15. Time profiles of accumulation of rain mass and of vertical transport of moisture through the 800 m level for area encompassing total storm rainfall (dashed) and for regions of convergent flow within that area (solid).

By midnight, the accumulated net inflow into the surface layer (8 m depth) was $9.5 * 10^9$ kg for the 12500 km^2 area and the accumulated upward transport through the anemometer level in the regions of convergent flow was $21.5 * 10^9$ kg. For a "uniform" source depth of 800 m, these values become $9.5 * 10^{11}$ and $21.5 * 10^{11}$ kg respectively. The accumulation of rain mass reached about $12.4 * 10^{11}$ kg. It is evident that either the storm was an unusually efficient one, converting 57% of the moisture inflow in a sub-cloud layer of 800 m into precipitation, or that the assumptions that have been made are not all valid. There is reason to believe from the regional and network analyses that this was a relatively efficient system. Nevertheless, this is a very high percentage. One possible source of error is an underestimate of the mean inflow for the sub-cloud layer. The calculations from the pibal data indicate that the pre-rain convergence was higher aloft and that the surface convergence underestimates the mean by as much as 50%. If this adjustment is applied, it decreases the efficiency from 57% to a more reasonable 38%. A second likely source of error is the assumption of no moisture inflow in the cloud layer. The synoptic flow is such that advection of moisture into the area is likely; however, the rawinsonde measurements do not indicate significant increase in moisture content over Illinois above 850 mb during the day.

4. MESOSCALE METEOROLOGICAL FIELDS AND PROCESSES

A. Visual Cloud Fields (NOAA)

Two cameras were operating on 30 July 1979 in the VIN mesonet at pilot balloon stations. One was located at station 11 in the northwest portion of the network (Fig. B-16), and was pointed toward the southeast; the other was located at station 13 in the southwest region and was pointed toward the north-east. Because the flow was mainly perpendicular to the viewing angle of the camera at station 11 during most periods, the clouds moved across the view so quickly that less detail was available from this site than from station 13. The Bolex cameras took color photographs on 16mm film at approximately one frame per 7 seconds. The angle of view was from 115° to 170° from station 11, and from 030° to 080° from station 13. A clock was usually visible in all pictures. A 100-foot roll was taken at each site on July 30, and a detailed narrative of events at each site is given below.

Station 13 in the southwest portion of the network began camera operations at 1255 CDT with scattered stratocumulus which became congestus about 1330 CDT. At 1445, new and growing congestus towers began moving in from the left at a large distance to the NNE. At 1520, a large but distant tower in this group of clouds grew substantially. At 1545, new congestus appeared in the NNE in the form of a large tower which moved slowly to the right until it became iced at 1600 CDT. Overshooting tops with well-defined boundaries were visible at 1605, 1613, 1615 and 1617 CDT to the ENE, then the cloud top became mainly ice. Between 1600 and 1605 CDT, other towers became visible between NNE and NE, but the clouds were mainly ice on top and not growing much. From 1622 to 1627 CDT, a separate but major tower was apparent to the NE, as well as another tower to the NNE from 1622 to 1638 CDT. During the next hour, there were no major clouds visible and only multi-level scattered clouds were apparent while a major cirrus layer was visible in the distance to the ENE.

At 1737 CDT, an overshooting top grew out of the anvil mass to the ENE. Major congestus began to grow in the medium distance to the NNE at 1750 CDT, then it moved to the right and swelled horizontally until it was obscured at 1810. Another major cloud with an anvil first became visible to the ENE at 1755 and an overshooting top at 1800 CDT to the ENE came from what was an extremely large cumulonimbus mass extending from the NE to E. This cloud became obscured at 1815 by thin stratocumulus overcast. Further events to the end of the roll at 2030 were not visible due to darkness during heavy convection.

Station 11, in the northwest portion of the network, began camera operations at 1200 CDT with scattered altocumulus; flat cumulus formed by 1330. These cumuli became congestus at about 1400, then the bases became darker starting at 1430 as they deepened and haze became quite thick. From 1515 to 1600, numerous small, non-raining congestus started to grow between ESE and S at an estimated 10-15 km distance. At 1545, rain was visible near the station to the SE. From 1600 to 1730 there was a continued growth of large congestus

which moved across the view of the camera; little rain was visible from these clouds. At 1730, a light shower was observed at the camera site. From 1730 to the end of the roll at 1940, there were disturbed multi-layer clouds with embedded congestus and cumulonimbi which became impossible to distinguish as darkness and a broken layer of stratocumulus prevailed during heavy convection. Five lightning flashes are visible on the film during the period of the storm.

B. Mesoscale Weather Fields and Precipitation (NOAA)

Introduction

In this section, the mesoscale characteristics of the events on 30 July 1979, are discussed in detail. The larger-scale influences, such as instability due to low-level warming and upper air cooling, and increased moisture advection, provided the necessary conditions for deep convection across central Illinois, as discussed earlier. The VIN surface mesonet network furnished a platform to describe in detail and possibly shed some light on the convective events that occurred on this day. Two periods of interest are emphasized here. The early period (1500-1700 CDT) consisted mainly of weak showery precipitation. The later period (1730-2030 CDT) contained an extremely intense and organized squall line which provided 20 mm area-averaged rainfall across the VIN network in a 3-hr period.

Mesonetwork Data Collection and Analysis Methods

A dense inner inner weather network encompassing 1500 km² (dashed line in Fig. B-16), composed of 49 sites separated by 8.4 km, was used to study the relationship between surface convergence and convective rainfall. Twenty-seven of these sites were a part of the NCAR PAM (Portable Automated Mesonet) network (Brock and Govind, 1977). Meteorological quantities such as pressure, temperature, moisture, rainfall, and winds were recorded in 1-min increments at these stations. The remainder of the sites in the inner network had only analog wind-recording devices. An outer ring of 17 analog wind stations surrounded the inner network on three sides by 9.6 km (solid line in Fig. B-16). A dense, rectangular grid of 160 rain gages, 4.8 km apart, covered the entire 2800 km² surface network. Figure B-16 also shows 11 other sites beyond the outer wind network which measured temperature and moisture only.

Because of the extensive data reduction effort, only wind data from the 27 PAM sites of the inner network and 15 outer network stations were combined to provide the wind and divergence information used in this study. The surface divergence fields were calculated from 5-min averaged PAM and outer network analog data. A 9 x 11 grid of equally spaced (6.4 km) points was superimposed upon the original network. Through the use of an objective analysis scheme (Cressman, 1959), the mesonet wind data were transformed into a uniform grid of u- and v-components. The values of the wind components at each grid point were then used to compute the divergence quantities.

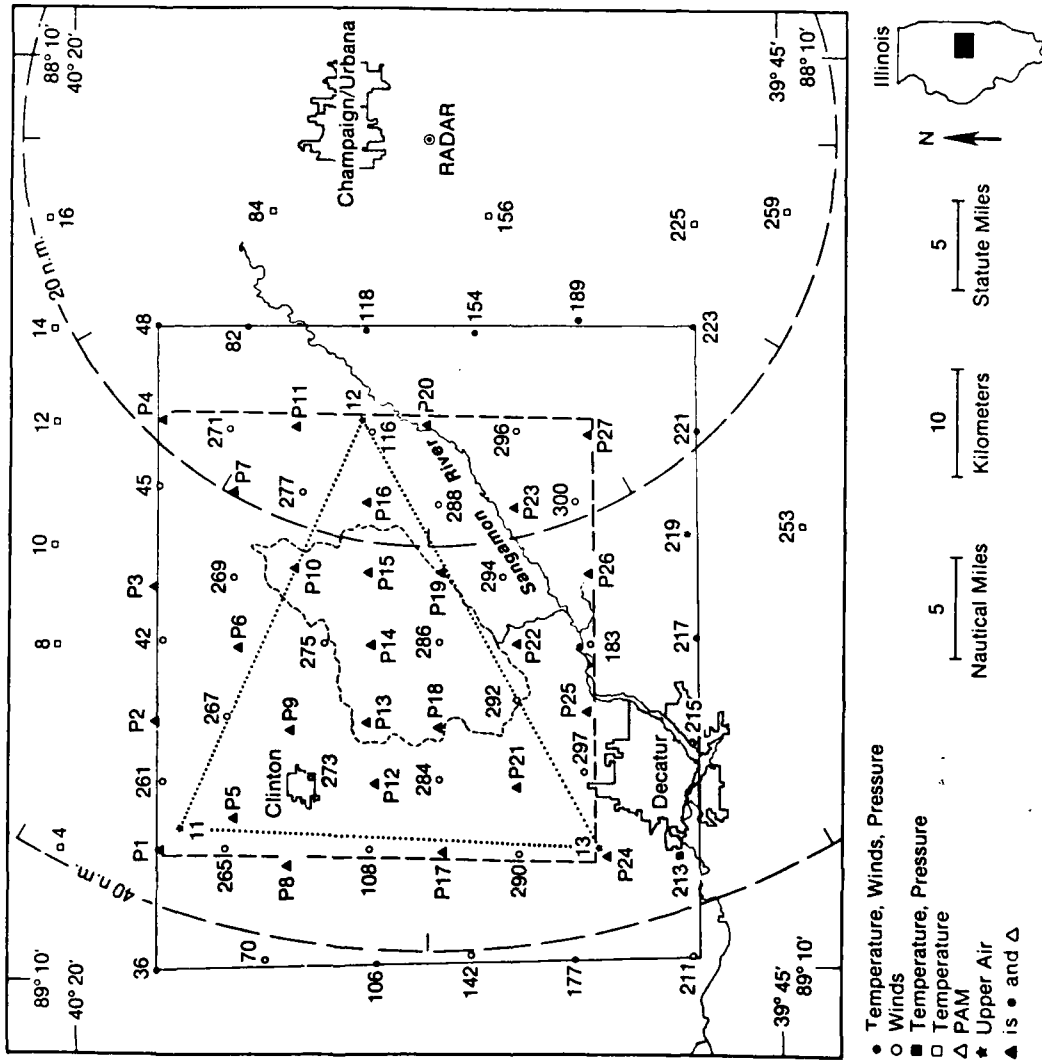


Figure B-16. VIN 1979 mesonet network. The dashed line encloses the inner network, the solid line shows the outer network boundary, and the dotted line, the pibal area.

One-minute analyses of meteorological quantities such as temperature, wet-bulb temperature, wind, divergence, and equivalent potential temperature (θ_e) were also performed using only PAM network data. The analysis technique employed here is similar to that used on the 5-min wind data. Rainfall data have been analyzed for each rain gage in the VIN mesonetwork in 5-min increments.

Overview

The surface meteorological conditions leading to, during, and following the convective events on 30 July 1970 are shown in Figures B-17 and B-18. Figure B-17 includes time profiles of averaged meteorological quantities from all 27 PAM sites located within the inner network. Figure B-18 depicts area-averaged divergence calculated, as described above, and area precipitation from the total 2800-km² network.

During the early morning hours on the 30th, the averaged VIN network temperature (not shown) reached a minimum of 22°C. Maximum temperature reached 30.5°C between 1300 and 1500 CDT. Relative humidities (Fig. B-17) were 100% until 0730 CDT, then decreased slowly due to surface heating to a rather moist minimum of 73% around 1300 CDT. A gradual increase in relative humidity is noted to a maximum of 83% at 1830 CDT just prior to the entire network being engulfed with heavy precipitation. Following the heavy rain, the temperature dropped to 19°C and the relative humidity increased to 94%.

The mixing ratio profile (Fig. B-17) shows the extent of low-level moisture which became available for the development of deep convection. From that time forward, a rapid increase in moisture occurred. An area-averaged maximum of 21.8 gm km⁻¹ was recorded at 1720 CDT. As cool convective downdrafts spread across the network, the mixing ratio decreased to 13.2 gm km⁻¹ at 2000 CDT.

The θ_e profile (Fig. B-17) vividly depicts the effects of the massive convective activity on this day. A gradual decrease is shown from 350°K at midnight to 340°K at 0500 CDT. At 0500 CDT, the θ_e profile slowly increased to a maximum network value of 370°K at 1720 CDT. A striking 40°K drop was recorded due to the intense convection and precipitation which reduced θ_e to 330°K after the passage of the squall line at 2000 CDT.

It has been shown by Watson *et al.* (1981), Cooper *et al.* (1982), and Watson and Holle (1982) that a sinusoidal pattern in the time series of the total area divergence is related to precipitation. Convergence followed by divergence is a signal generated by the inflow and outflow patterns of major convective entities. Three distinct sinusoidal patterns (Fig. B-18) were detected in the total area divergence profile on this day. A weak event was shown beginning around 0100 CDT. Very light precipitation accompanied the event. A second event occurred between 0800 and 1230 CDT; however, no rainfall was recorded. This event was a result of a small north-south line of clouds passing just to the north of the mesonetwork. The third event of the day, and the strongest convergence and precipitation event of the VIN 1979 experimental

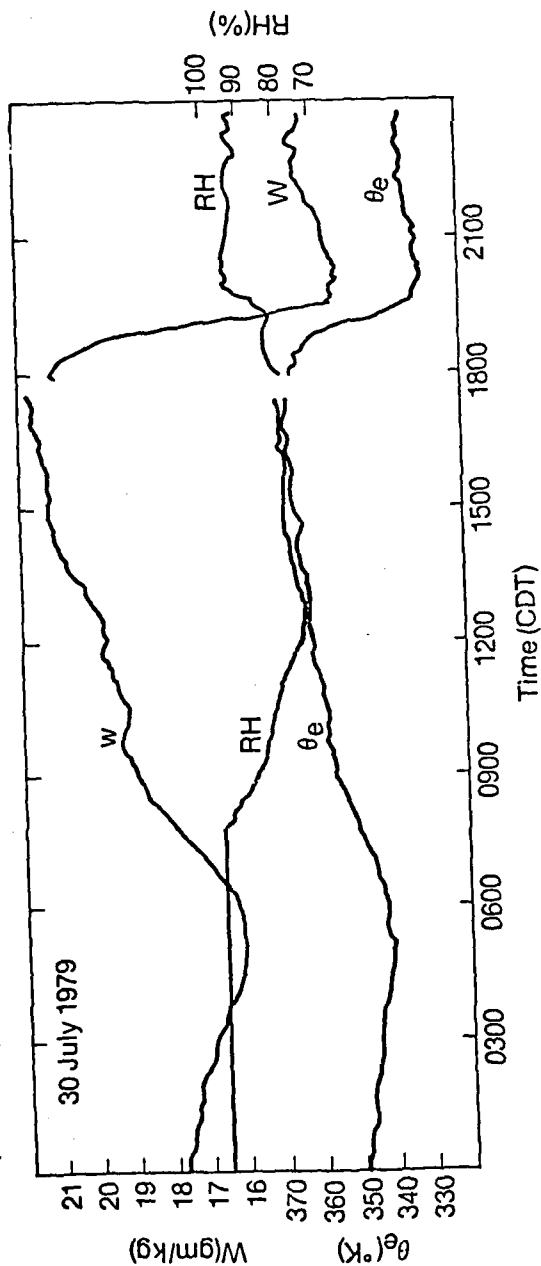


Figure B-17. Time profiles of area-averaged mixing ratio (w), relative humidity (RH) and equivalent potential temperature, θ_e , based on one minute measurements at the 27 PAM stations.

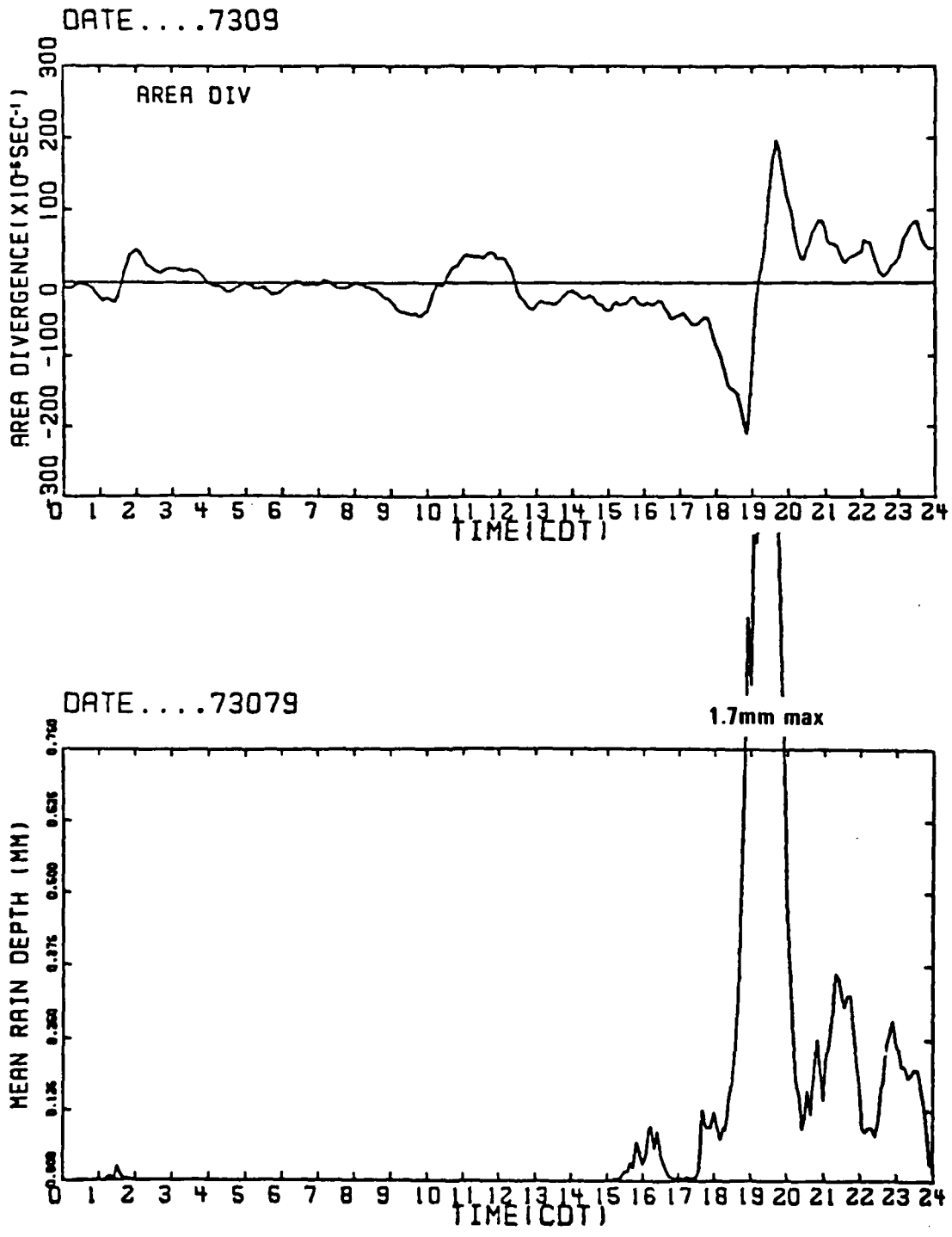


Figure B-18. Time profiles of total area divergence (10^{-6} s^{-1}) and area precipitation for 30 July 1979, using five-minute averaged quantities.

season, began at 1745 CDT. A rapid increase in network convergence attained a peak of $-2.1 \times 10^{-4} \text{ s}^{-1}$ at 1855 CDT. Significant rainfall began just after 1800 CDT. Area rainfall reached a maximum of 1.7 mm in 5 min at 1920 CDT. Area divergence associated with precipitation and outflow attained a maximum of $2.0 \times 10^{-4} \text{ s}^{-1}$ at 1945 CDT. Several other pulses of divergence and precipitation occurred until after midnight. Light precipitation is also recorded throughout the early morning hours on 31 July.

There was one precipitation event that was not detected in the convergence field. During the "early period" on 30 July, between 1500 and 1700 CDT, there was very little change in the total area divergence profile (Fig. B-18). A slight decrease in divergence began at 1400 CDT, and reached a minimum at 1500 CDT. No divergence outflow was measured with the VIN station separation (avg. = 7.4 km) from the disorganized group of cells in the total area divergence field. However, there was background convergence but conditions aloft were probably not yet favorable for intense convection to take place.

Early Period: 1500-1700 CDT

The early period on the network scale was characterized at the surface by weak to moderate south-southwesterly flow with fairly weak divergence and vorticity. Temperatures recorded by the 27 PAM stations remained between 28 and 31°C for the entire period. Wet-bulb temperatures were quite high with a range between 25 and 27°C.

Figures B-19 to 21 show a composite of surface events which took place during this period. The analyses of wind, divergence, and vorticity describe an area encompassing both the inner and outer network wind stations (see Fig. B-16). The rainfall analysis depicts a somewhat larger region in which the rain gages were located. The locations of the inner network (small square) and outer network (intermediate rectangle) are shown in upper right of Figures B-19-21.

Figure B-19 describes the surface wind and rainfall at 1500 CDT. Weak convergence is occurring in an east-west line which splits in the center of the network toward the northwest and southwest corners. This zone appears to be the spawning ground for much of the convective activity that takes place during this period. Vorticity is presented but it is weak and does not vary more than $200 \times 10^{-6} \text{ s}^{-1}$ (contour interval) from zero. No rain is being reported at this time.

First rain occurs at 1515 CDT along the western border of the inner network and on the northeast corner of the outer network. For the next 35 min, both areas intensify slowly. The westernmost precipitation area grows eastward along the convergence line.

Figure B-20 presents the wind and rainfall data for 1550 CDT. Precipitation has increased in the center of the network. The northwest cell has a 25 mm hr^{-1} rainfall rate, and the northeast cell has 41 mm hr^{-1} . One wind site, PAM-5, near the northwest corner has a northwest wind showing the effects of precipitation in the vicinity. Brief rain (5 min) began at PAM-5 at 1556 CDT. Convergence is still being maintained in the center of the network.

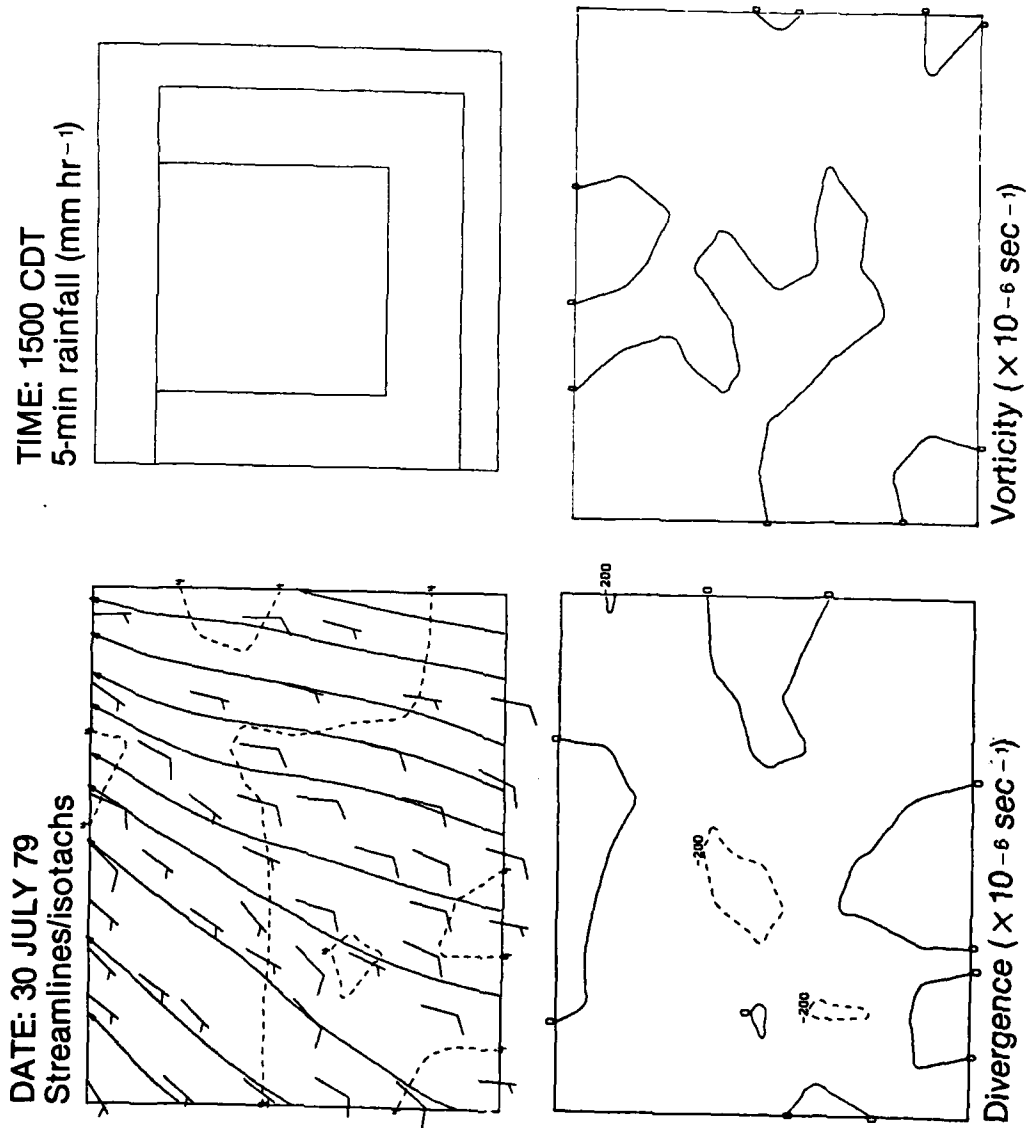


Figure B-19. Surface winds, divergence, vorticity, and rainfall analyses for the 5-min period beginning at 1500 CDT. Divergence and vorticity contour intervals are $200 \times 10^{-6} \text{ s}^{-1}$; rainfall presented as a rate, with contour interval of 4 mm hr^{-1} , with first contour of 1 mm hr^{-1} .

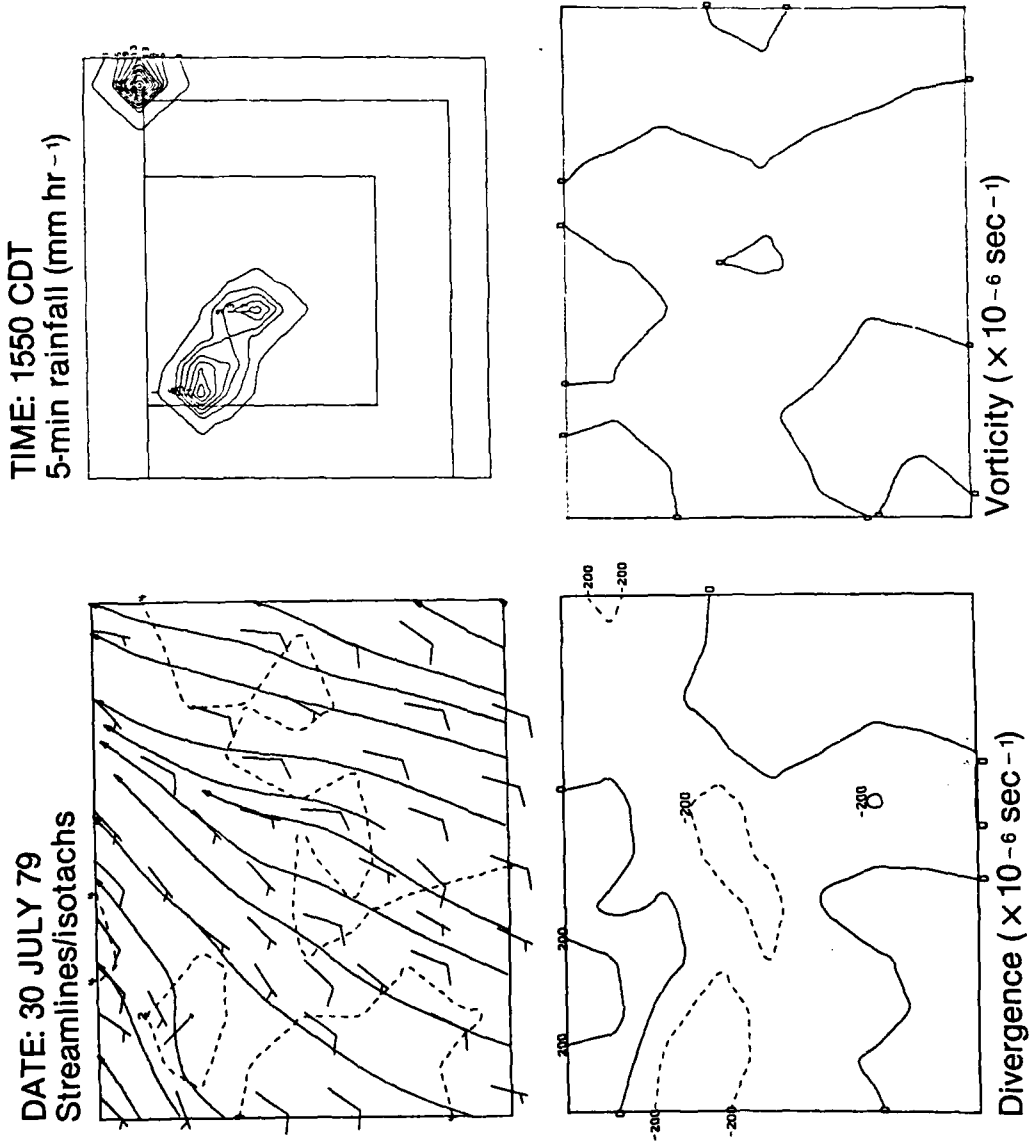


Figure B-20. Surface winds, divergence, vorticity, and rainfall analyses for the 5-min period beginning at 1550 CDT. Presentation as in B-17.

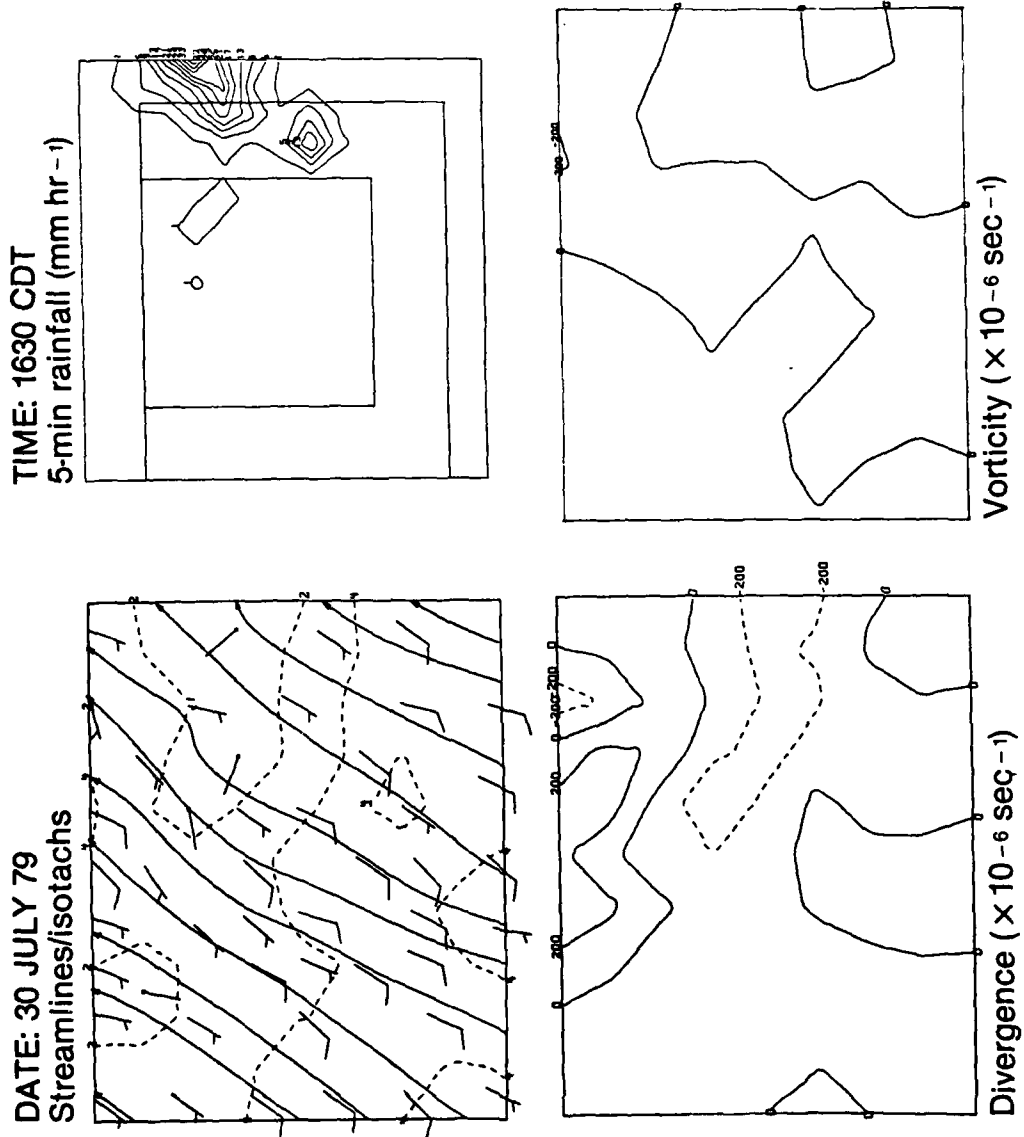


Figure B-21. Surface winds, divergence, vorticity, and rainfall analyses for the 5-min period beginning at 1630 CDT. Presentation as in B-17.

Light showery precipitation continues across the center of the network in an east-west line until 1620 CDT. At 1605 CDT, a north-south linear structure becomes apparent on the east side between the inner and the outer network borders. These cells possibly extend from the heavier convection occurring in the northeast corner and outside the network.

The surface events at 1630 CDT are illustrated in Figure B-21. Southwesterly flow is being altered slightly in the northeastern portion of the network by precipitation. The convergence pattern is also being modified by precipitation, and is now orientated in a more northwest-southeast line. A divergence maximum associated with the precipitation outflow lies in an arc across the northern border. Since 1615 CDT, the northeastern PAM stations have been under the influence of outflow and/or light precipitation. θ_e values in the vicinity have dropped as much as 8°K.

After 1630 CDT, the activity weakens for the next hour before setting the stage for the occurrence of organized deep convection. Much of the convection during the early period developed along a weak convergence zone lying across the north-central portion of the mesonet. It was quite stationary throughout the period in spite of the southwesterly surface flow. Area precipitation total for the period was .83 mm.

Late Period: 1730-2030 CDT

Events described in this section occurred between the times of 1730 and 2030 CDT on 30 July 1979. The heaviest rainfall and strongest convergence of the VIN 1979 project were measured during this time. Area-averaged rainfall for the mesonet totaled 20 mm. The maximum point rainfall during the storm was 203 mm measured at a site along the eastern border of the ISWS raingage array just east of the VIN mesonet. Divergence cells, on a 6.4-km grid, peaked at $-1.2 \times 10^{-3} \text{ s}^{-1}$ and $+1.4 \times 10^{-3} \text{ s}^{-1}$. Two areas of strong convective development, one to the east of the mesonet and the other to the west, filled across the northern border of the VIN network. The western portion then moved across the network as an intense squall line.

The development period had begun by 1745 CDT. Two intense mature systems had formed over an hour earlier to the east and west of the project area. By 1745 CDT, a line of convection was bridging the gap between the two systems across the northern border. Figure B-22 presents selected surface quantities for this time. θ_e is analyzed for the inner network (PAM sites) only. Weak convergence is shown in a northwest-southeast line beginning in the northwest corner of the network. The convergence pattern is very similar to the configuration in Figure B-19, one hour and 15 min earlier. Divergence and θ_e illustrate the effects of precipitation along the northern border. One cell has a rainfall rate of 53 mm hr^{-1} . Development continues over the next 30 min. The surface meteorological variables at 1815 CDT are shown in Fig. B-23. The east-west gust front is quite visible as it drifts deeper into the network. Distinct northerly flow is occurring on one side and southerly flow on the other. Moderate convergence is taking place across the northern third of the network along and in front of the gust front. An unbroken line of precipitation now extends across the northern border; the maximum rainfall rate is about

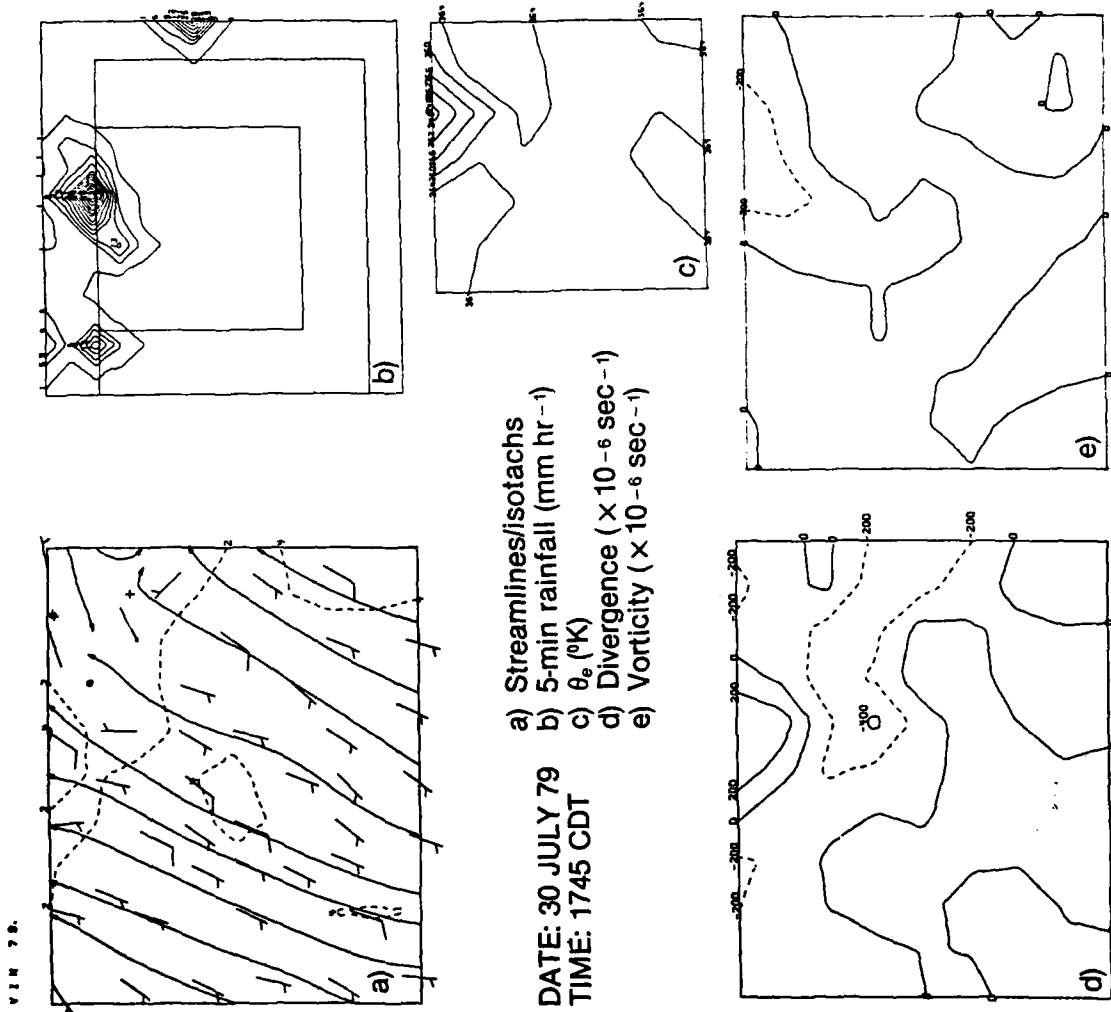


Figure B-22. Surface winds, divergence, vorticity, rainfall, and equivalent potential temperature for the 5-min period beginning at 1745 CDT. θ_e contour intervals are 4K, others as in Fig. B-17.

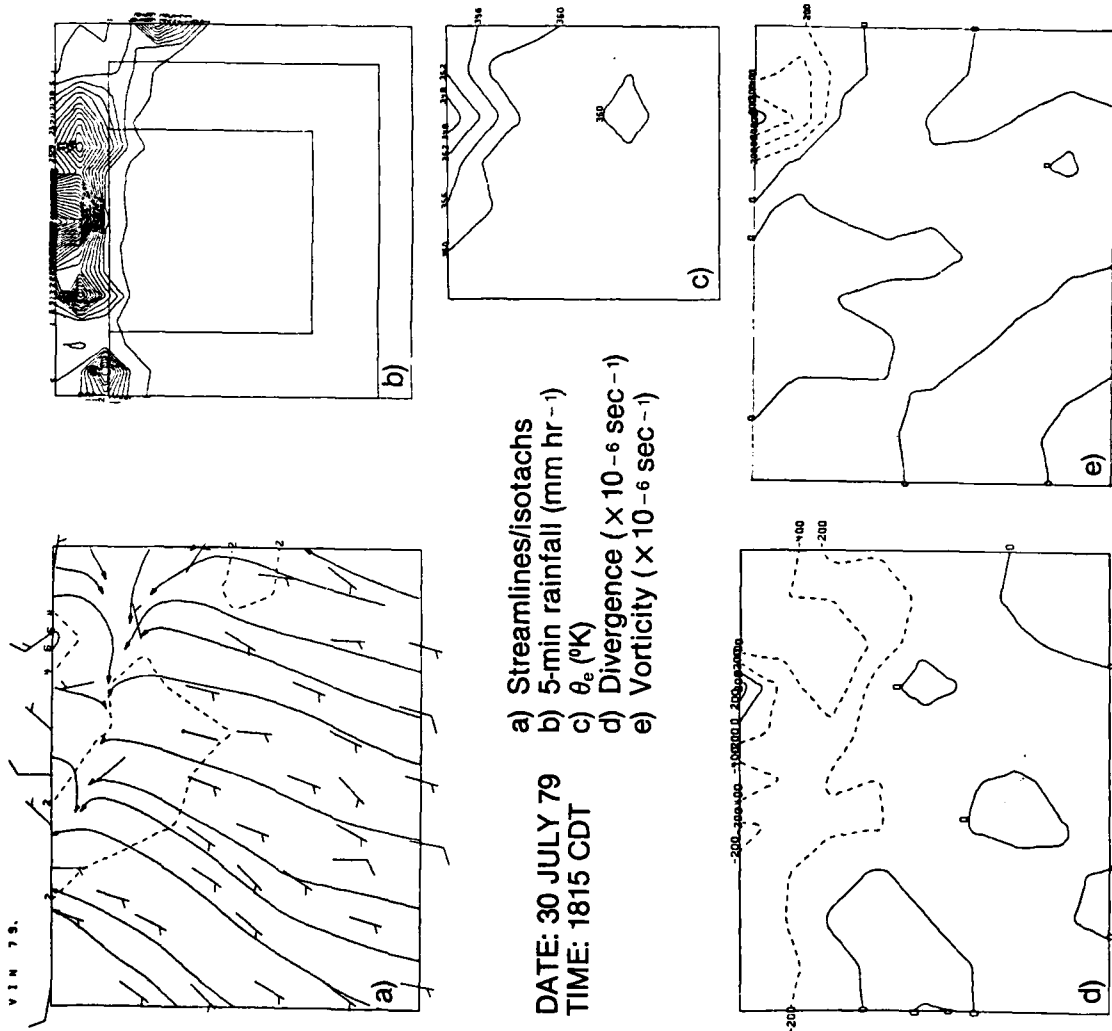


Figure B-23. Surface fields as in Fig. B-20, for the 5-min period beginning at 1815 CDT.

100 mm hr⁻¹. The 360K isoline of θ_e is slipping farther southward. The first indication that convection is entering the network from the west happens at this time; the wind site at the northwest corner has switched to the northwest.

Figure B-24 describes the events at 1830 CDT. The north-south gust front is progressing rapidly eastward with a well-defined convergence zone. The east-west gust front has remained almost stationary during the last 15 minutes. The maximum convergence ($-1 \times 10^{-3} \text{ s}^{-1}$) occurs at the intersection of the two gust fronts near the northern border. Precipitation has entered the outer network from the west but rainfall rates are still light when compared to the activity along the northern border. The lowering of θ_e temperatures in the inner network continues slowly, moving south-southwestward in advance of the rapidly approaching weather from the north.

At 1845 CDT (Fig. B-25), the northwest quarter of the network is under the influence of the advancing north-south squall line. The northern gust front remains stationary approximately 6-10 km into the northern part of the network. A positive vorticity maximum ($>600 \times 10^{-1} \text{ s}^{-1}$) has formed to the north of the strong shear coupled with curvature caused by a strong center of outflow ($>10 \text{ m s}^{-1}$). Anticyclonic shear and curvature form the vorticity minimum along the northern border. Rainfall continues to spread eastward; however, the precipitation maximum (73 mm hr⁻¹) continues to be along the northern border. θ_e temperatures began to drop along the western border of the inner network as the area is affected by the advancing precipitation.

The total area divergence time profile (Fig. B-18) reaches peak convergence at 1850 CDT. The horizontal analysis (not shown) shows two convergence peaks ($-1 \times 10^{-3} \text{ s}^{-1}$) near the intersection of the two gust fronts at this time.

During the next ten minutes, very strong downdrafts were initiated near the apex of the two gust fronts. They produced a strong surge southward of the east-west gust front. Three separate precipitation centers with rain rates greater than 65 mm hr⁻¹ may have caused this surge. Figure B-26 presents the θ_e time profile for PAM-6 (see Fig. B-16) located in the north-central portion of the inner network. The profile graphically illustrates the effects of the two occurrences of precipitation; the southward drift of the east-west line after 1815 CDT and intense surge associated with the passage of the north-south squall line just before 1900 CDT.

Figure B-27 depicts the progress of the storm across the network at 1910 CDT. Several important features are found in the wind field. Now, only one predominant northeast-southwest gust front is shown nearing the southeast corner. Strong outflow ($>10 \text{ m s}^{-1}$) is occurring with a diffluent center in the northwest part of the network. A dipole structure is apparent in the divergence field. The total area divergence profile (Fig. B-18) is approximately zero at this time because convergence is exactly balanced by divergence. Maximum convergence is centered along the gust front. Maximum divergence is in the center of the network coincident with the rainfall maximum ($>70 \text{ mm hr}^{-1}$). The northeast-southwest line of precipitation is entirely within

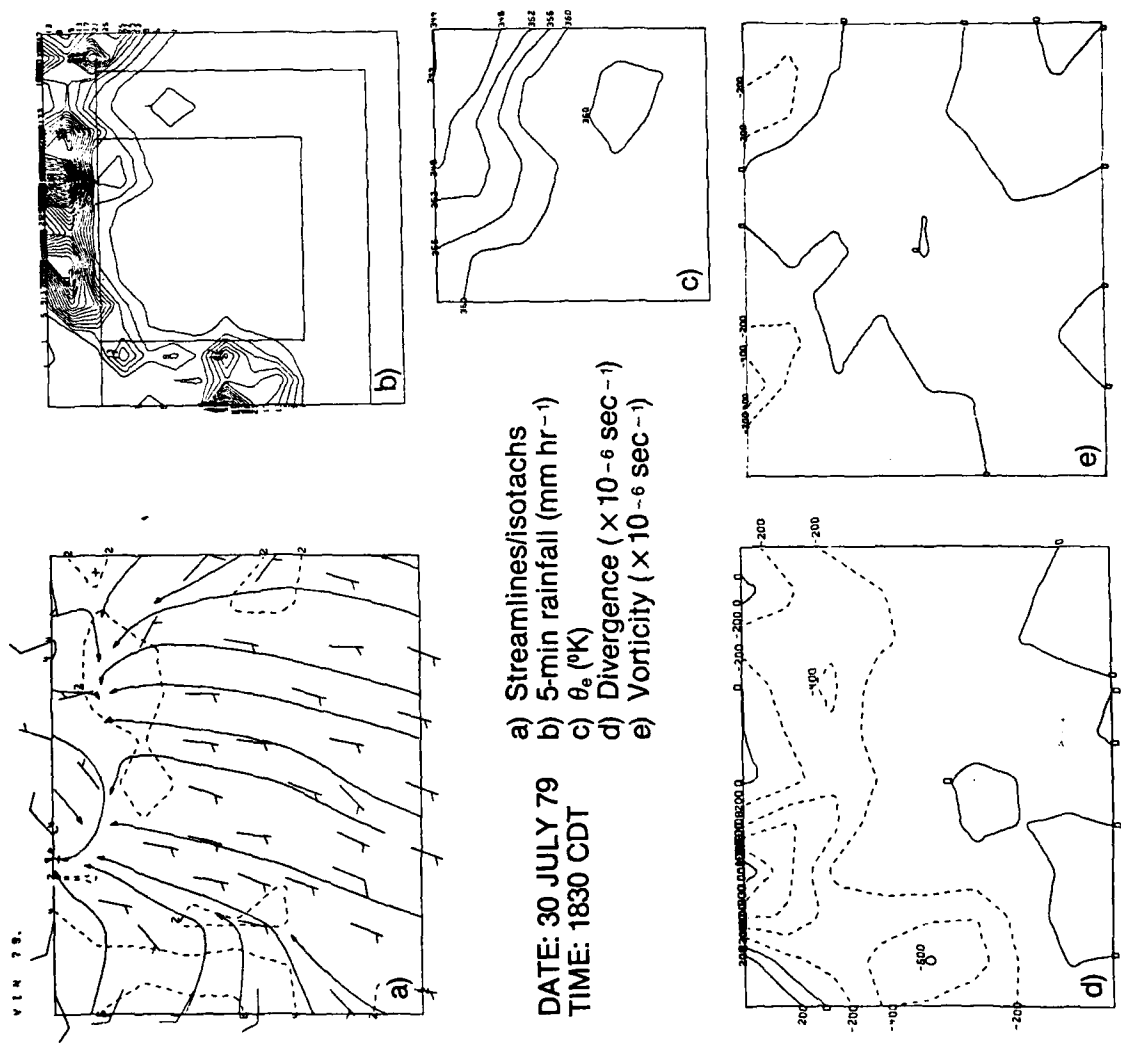


Figure B-24. Surface fields as in Fig. B-20, for the 5-min period beginning at 1830 CDT.

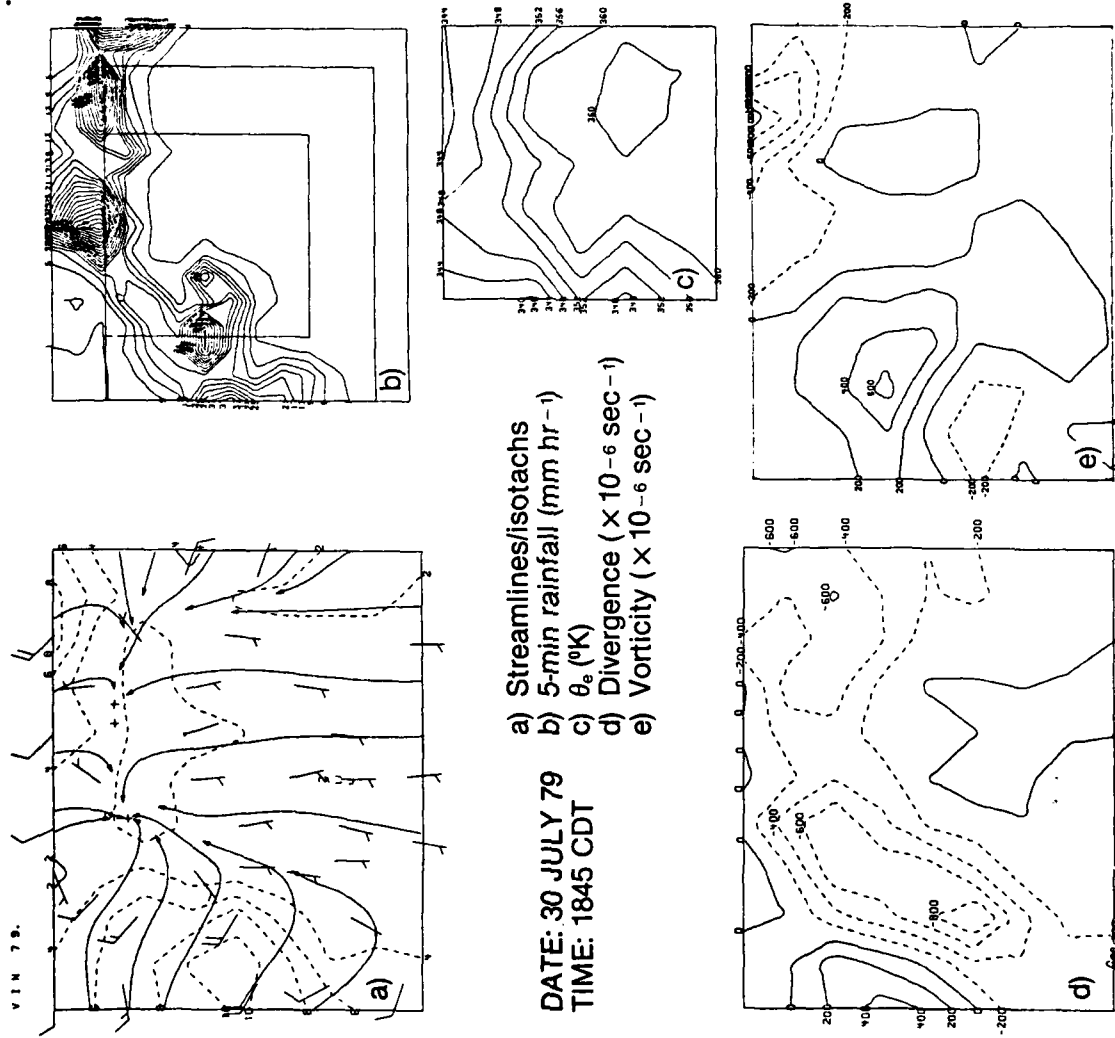


Figure B-25. Surface fields as in Fig. B-20, for the 5-min period beginning at 1845 CDT.

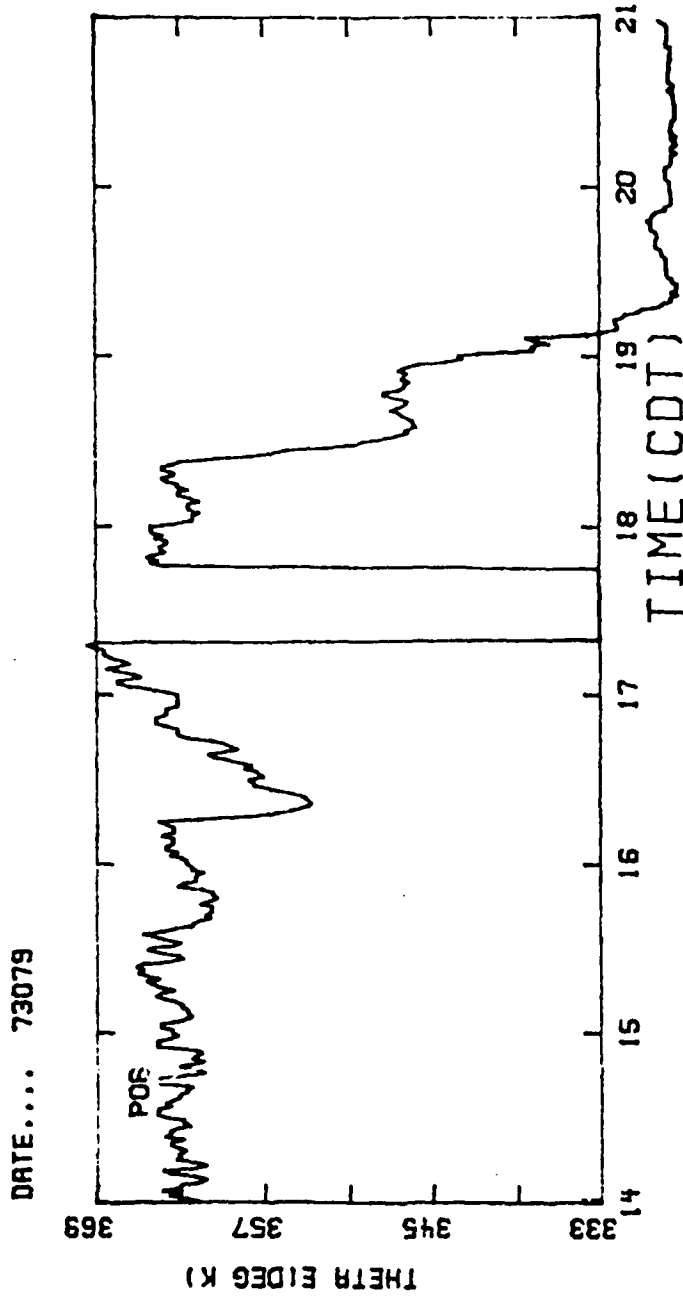


Figure B-26. Time profile of equivalent potential temperature at PAM-6 for the period 1400-2100 CDT, 30 July 1979. (Data missing between 1720 and 1745)

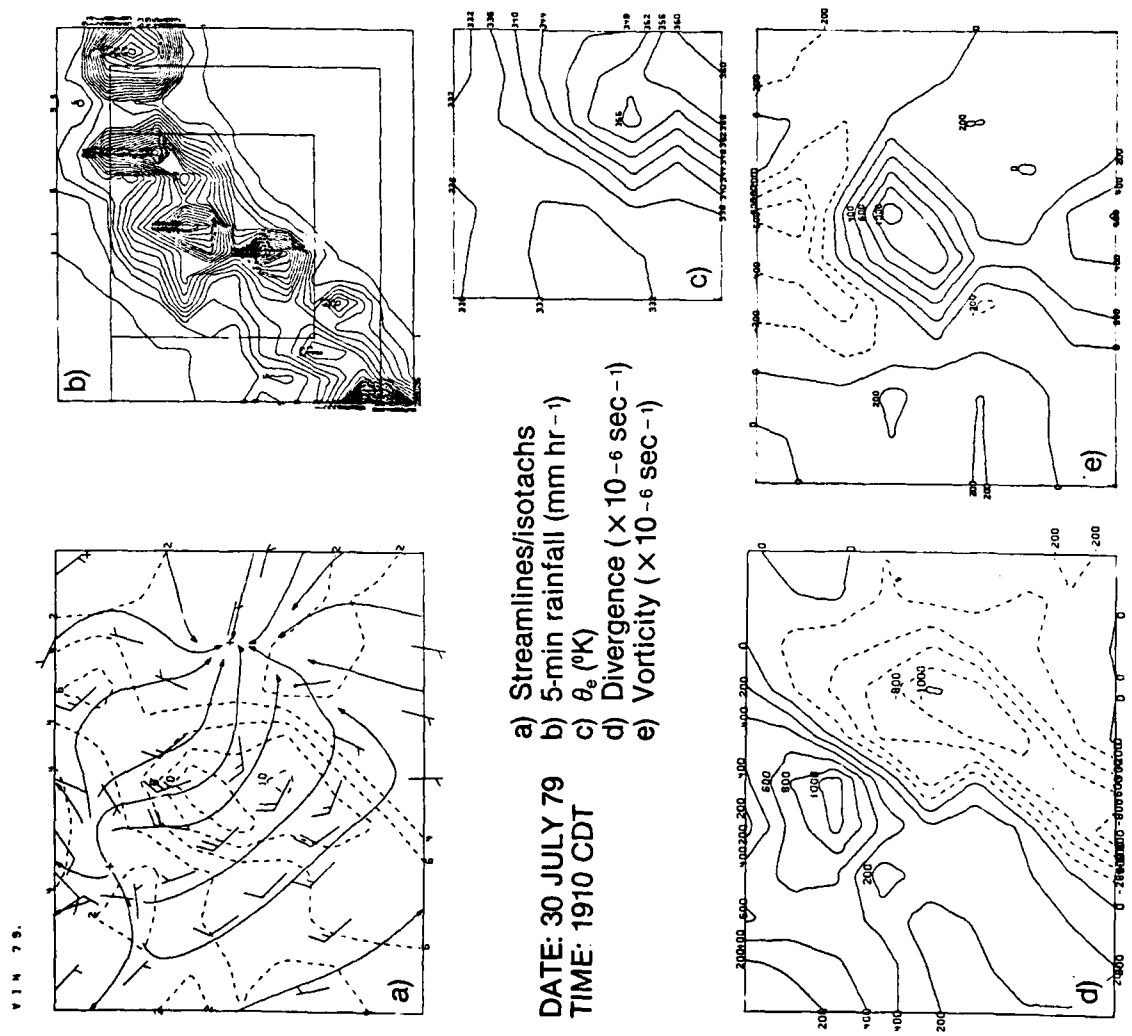
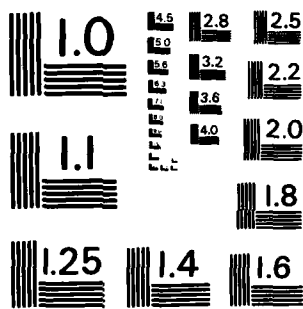


Figure B-27. Surface fields for the 5-min period beginning at 1910 CDT.



MICROCOPY RESOLUTION TEST CHART
NATIONAL BUREAU OF STANDARDS-1963-A

the inner network; the width being about 35 km. At 1710 CDT, the area-averaged value of θ_e had been 368°K (see Fig. B-17). Now, θ_e has dropped to less than 332°K in the rain area. Strong shear associated with the outflow continues to produce a large value of positive vorticity.

The next series of figures (B-28 and B-29) shows the progress of the squall line across the center of the mesonet using several PAM stations. PAM-12 through 16 are presented because they are situated in an east-west line across the center of the inner network separated by 6.4 km. Figure B-28 gives the time profiles of θ_e and wind speed. The θ_e profile illustrates the dramatic 35°K drop associated with the passage of the downdrafts and precipitation. The peak in the wind field vividly describes the strength of this system. The rainfall records for each PAM site are shown in Fig. B-29. (The PAM instruments are tipping bucket rain gages with one tip being equal to .25 mm (.01 in).) Movement of the system toward the east is noticeable in both figures. Speed of the system is approximately 65 km hr⁻¹.

At 1930 CDT (Fig. B-30), the gust front is about to exit the network. There is a diffluent zone extending from the northeast corner of the mesonet to the middle of the western border coincident with the rear of the rain shield. Maximum area rainfall (1.7 mm in 5 min) is occurring at this time. θ_e has reached its minimum of 328 K coincident with the precipitation maximum. Peak total area divergence (Fig. B-18) occurs 10 min later at 1940 CDT.

By 2000 CDT (Fig. B-31), the storm has passed. The winds are diffluent and the divergence analysis confirms it. The entire network is under easterly winds coming from the outflow center which has moved to the east out of the project area. A fairly uniform precipitation region is exiting the southeast corner of the network.

C. Surface Fields and Subnetwork Scale Processes, Preliminary Description (University of Virginia)

Synopsis of the Convective Activity

On July 30, 1979 strong convective activity took place over the PAM network in Illinois due to the passage of a squall line. Satellite pictures (Fig. B-5) indicate a WSW-ENE line of confluence over Illinois, that can be traced back to 1300 CDT (all times are expressed in local time unless otherwise specified). At 1430 (Fig. B-5c) the pictures show invigorated cumulus activity over the line of confluence. The cloud line had a sharp northern border. Toward the north of the cloud line over Illinois an extensive area almost without convective clouds is observed. By 1530 the satellite photographs indicated the presence of an anvil over the ENE extreme end of the cloud line close to the Illinois-Indiana border. Half an hour later, at 1600, (Fig. B-5d) several anvils can be observed over the cloud line across Illinois indicating the generation of the squall line. The simultaneous development of local storms

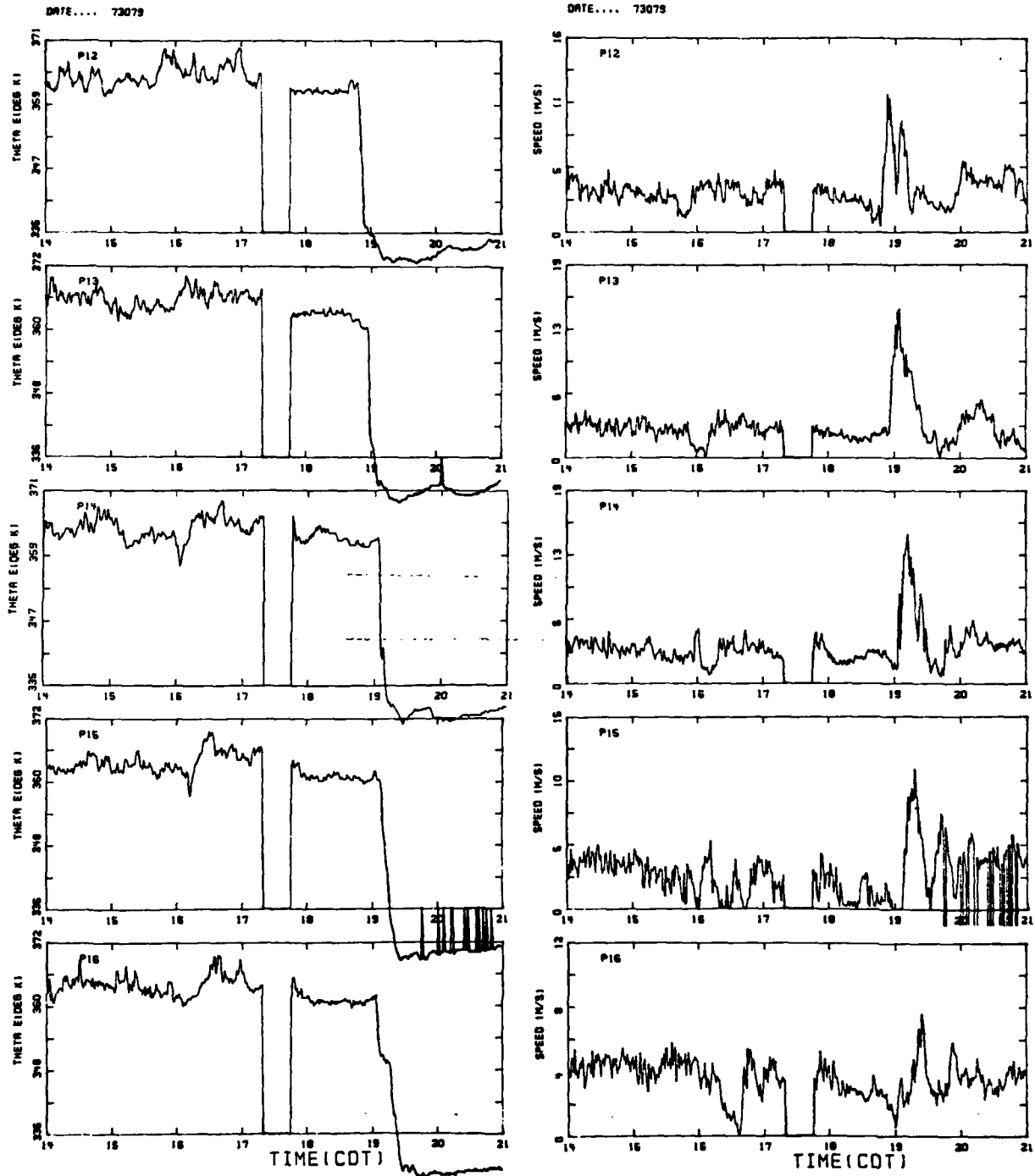


Figure B-28. Time profiles of equivalent potential temperature and wind speed along the east-west line between PAM-12 and PAM-16 for the period 1400-2100 CDT, 30 July 1979. (Data missing from 1720 to 1745)

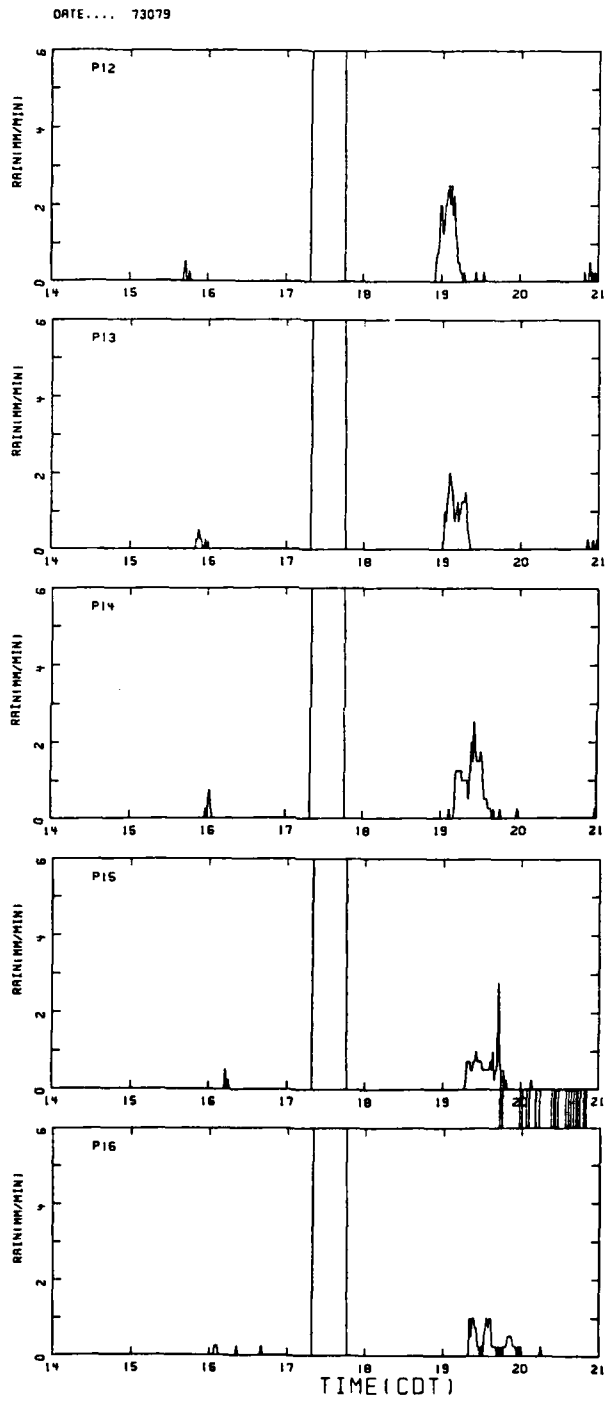


Figure B-29. Rainfall along the east-west line between PAM-12 and PAM-16 for the period 1400-2100 CDT, 30 July 1979.

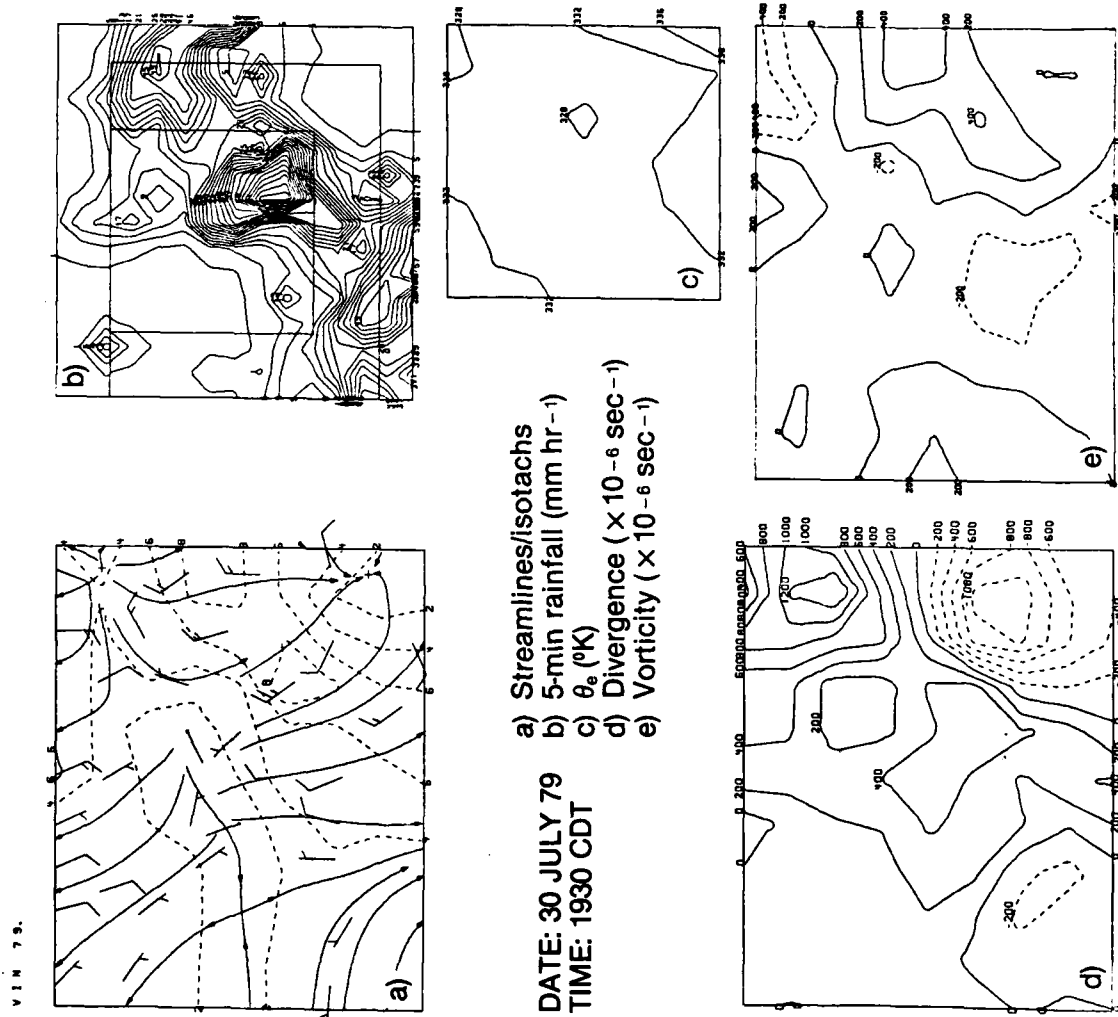


Figure B-30. Surface fields as in Fig. B-20, for the 5-min period beginning at 1930 CDT.

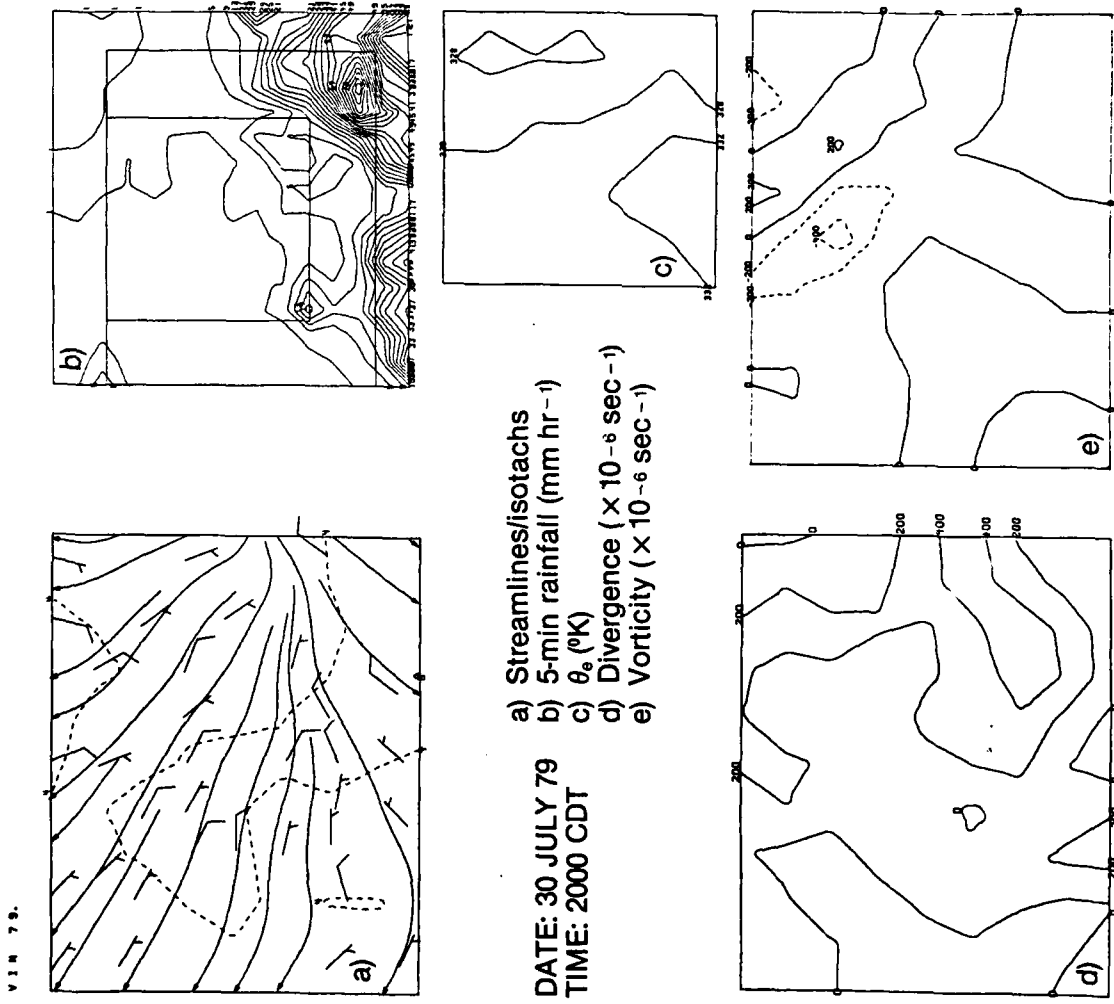


Figure B-31. Surface fields as in Fig. B-20, for the 5-min period beginning at 2000 CDT.

along the cloud line suggests an external forcing mechanism in the development of the squall line. At about 1745 satellite pictures showed the northeastward propagation of the squall line by the generation of five convective storms along an arc oriented in a N-S direction and located over the northeastern sector of Indiana.

About 1720, lightning knocked out the radar and the PAM system. The PAM system was back on line at 1745. At this time, heavy rainfall was measured at PAM station No. P3, on the northeastern boundary of the PAM network. (See Fig. B-16 for locations of stations).

At the time the squall line arrived over the network, the mesoscale flow was southerly (Figs. B22a, 23a) with high mixing ratio, close to 22°g/kg , a high relative humidity (RH) of 86%, an equivalent potential temperature, θ_e , of about 370°K . This value contrasted with the 5 min-averaged θ_e value of 341°K measured at station P3, representing a dramatic fall of 29°K in 10 min (1741-1750); outside of the storm outflow area the rest of the network exhibits a homogeneous θ_e field. Rain in excess of 6 mm was measured at that station during the 5 min interval beginning at 1746. Associated with the detection of low θ_e value, there was a decrease in RH, to 70%, suggesting a downdraft originating in the mid-troposphere (Barnes, 1978), although Lemmon and Doswell (1979) have suggested that non-hydrostatic pressure perturbations arising from blocking of middle level air flow could play a role in downdraft generation. The special sounding taken at 1800 Z (1300 CDT) from Salem indicates that a dry layer, with minimum relative humidity of 26%, was present between 760 mb and 700 mb. The equivalent potential temperature ranged from 326°K to 330°K . The minimum θ_e value registered at the surface in the network was 327°K , a further indication of the presence of undiluted downdrafts originating from the layer.

By 1805 the only surface signals in the velocity field indicating the presence of convection were located in the northeastern part of the network, where a zone of peak convergence of $-0.4 \times 10^{-3} \text{ s}^{-1}$ was present. An annular pattern of stronger convergence emanating from the northeast corner is evident in the divergence field at 1805. (See also divergence field at 1815, Fig. B-23d). Most of the network at this time is covered by a weakly convergent wind field.

Between 1800 and 1830 convective signals in the surface thermodynamic and kinematic fields continued to be present over the northeastern part of the network. Storm outflow air built up during this period but progressed only slowly to the south. This pool of air, reinforced over the next half an hour, interacts later with the outflow produced by the westerly advancing storm embedded in that part of the squall line.

The contoured echo from the SWS HOT radar at 1840 CDT (Fig. B-32a) shows the oncoming squall line and an outline of the VIN network. At 1840 the arch-shaped squall line is just moving into the PAM network. The central part of the squall line is narrow in the N-S direction compared to the width at both eastern and western ends, a consequence of convection developing at a later time in the center of the squall line. By 1840 the squall line has been in

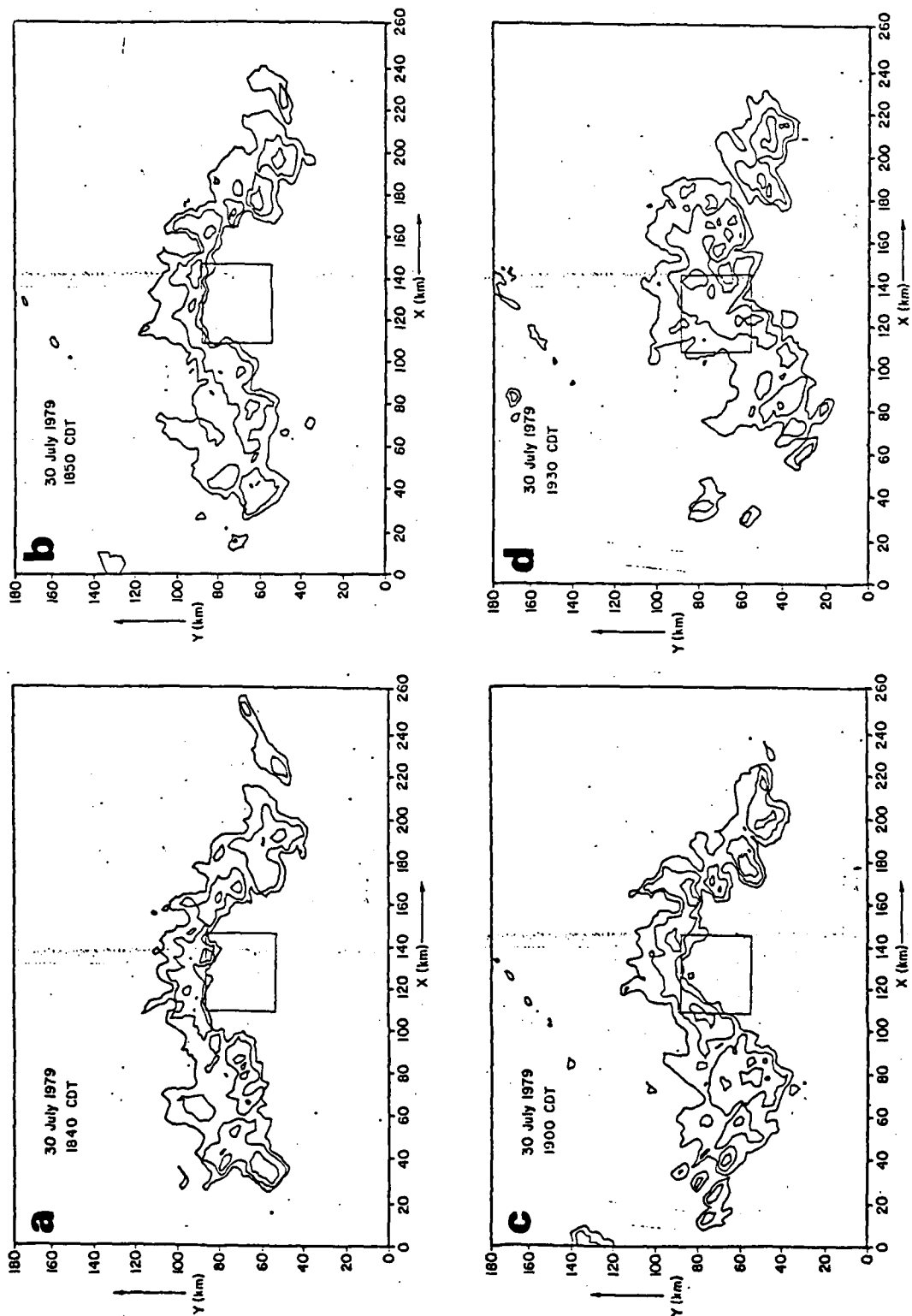


Figure B-32. Contoured echoes detected by SWS H0T radar at Joliet. Box indicates location of the VIN network.

existence for 3 hours and has developed a wide trailing area but still retains strong reflectivity gradients at its leading edge. At 1831, station P1 (on the northwestern corner of the inner wind network) registers the entrance of strong westerly outflow. Rapid development of convective activity takes place over the network, as shown by a comparison of the radar echoes at 1840 and 1850 (Fig. B-32a, b) and the surface thermodynamic and kinematic fields at these times (Figs. B-33-35). This convective activity is associated with a storm that will be called W.

About 10 min after the detection of storm W in the PAM network, strong surface signals were detected at the northern part of the network that indicated a renewal of the convective activity in that area. This northern convective activity, labelled storm N, produced a chain of outflows advancing over the network with large northerly component.

Radar echo contours at 1900 (Fig. B-32c) show the presence of two clearly defined radar cores, one on the western side of the network and the other in the far NE corner of the network. These two reflectivity cores correspond to storm W and N respectively. Storms W and N developed distinctive kinematic features and evolved in very different ways, as seen by the PAM network.

Both the surface signals and radar echoes detected from storm N during the period 1845 to 1900 indicate that it was a multicell storm, with two centers of strong convective activity. At 1900 a small isolated radar echo formed over the north-central part of the network just ahead of the main body of radar reflectivity of the squall line. It is very likely that this small radar reflectivity echo was produced by the interaction of the southeasterly and southwesterly propagating outflows, as indicated by the isochrones of main wind shift lines (Fig. B-37). Notice the complexity of the pattern of wind shift lines in this sector due to the peculiar arch-shape of the squall line.

At 1845 the wind field analysis over the PAM network shows that storm W, advancing over the network, had a cyclonic circulation (Fig. B-33b). The sequence of wind field graphs (5 min-averaged) up to 1915 show very clearly the advance of the mesocyclonic circulation over the network. The wind field analysis at 1925 shows that the mesocyclone was about to leave the mesonet network at that time. The size of the mesocyclone was large, about 25 km in diameter.

Simultaneously with the traverse of the mesocyclone across the network, outflow from storms W and N were colliding and general intensification of the surface kinematic field was taking place. A comparison of the wind field analysis of 1905 and at 1910 (Figs. B-33d,e) show the invigoration of the circulation. The strengthening of the cyclonic circulation is corroborated by the increase of vorticity from 1830 to 1915. The collision of outflows is supported by the equivalent potential temperature field, the location of wind shift lines and the wind field itself. The line of collision presents a zone of strong convergence moving at the same speed of the leading intersection point of outflow W and the northerly outflows. The occurrence of strong convergence and strong downdraft shows a general intensification of storm W during the time of collision over the network. The mesocyclone travels on a line parallel to the collision line.

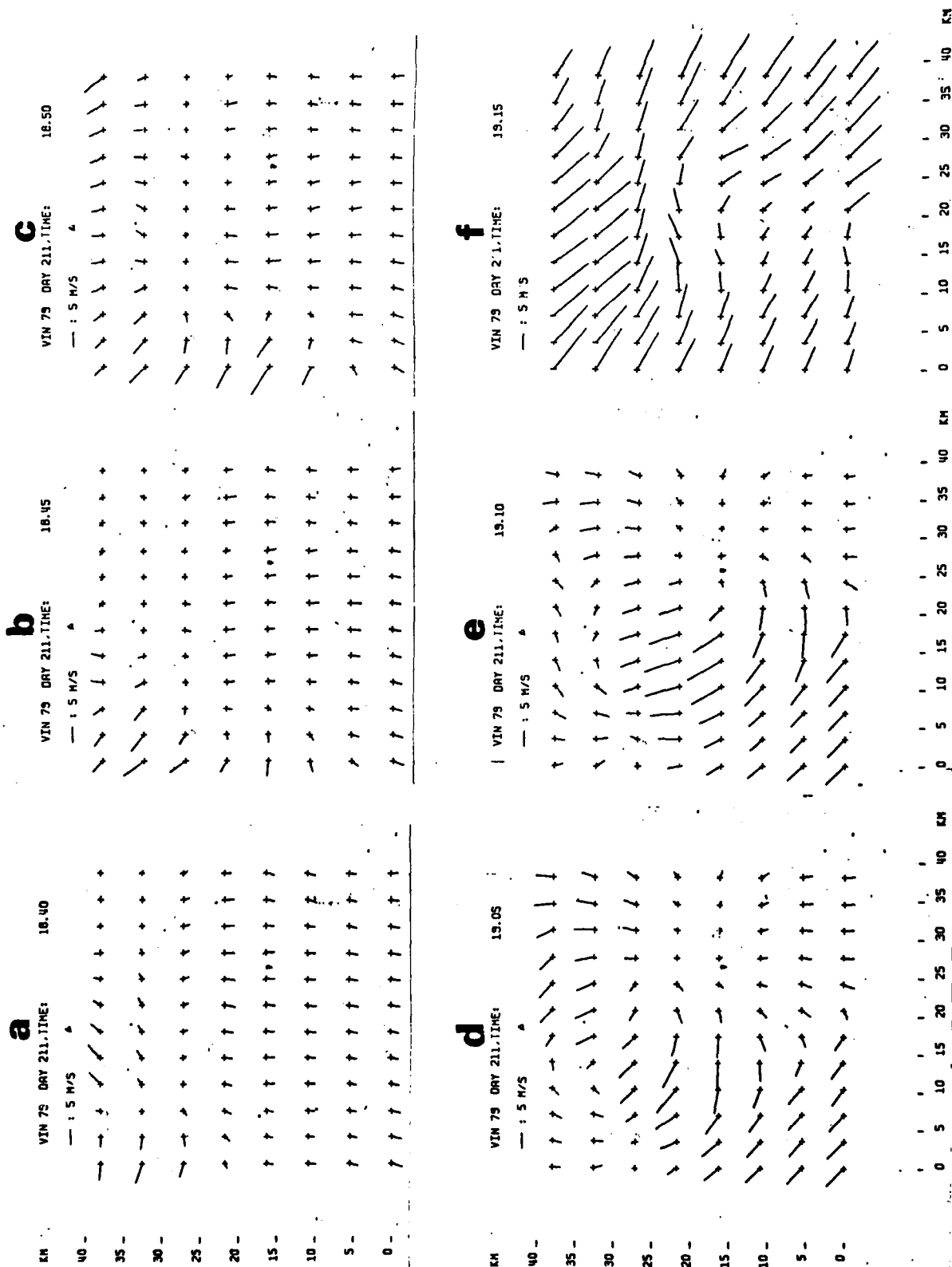


Figure B-33. Wind fields in the inner network.

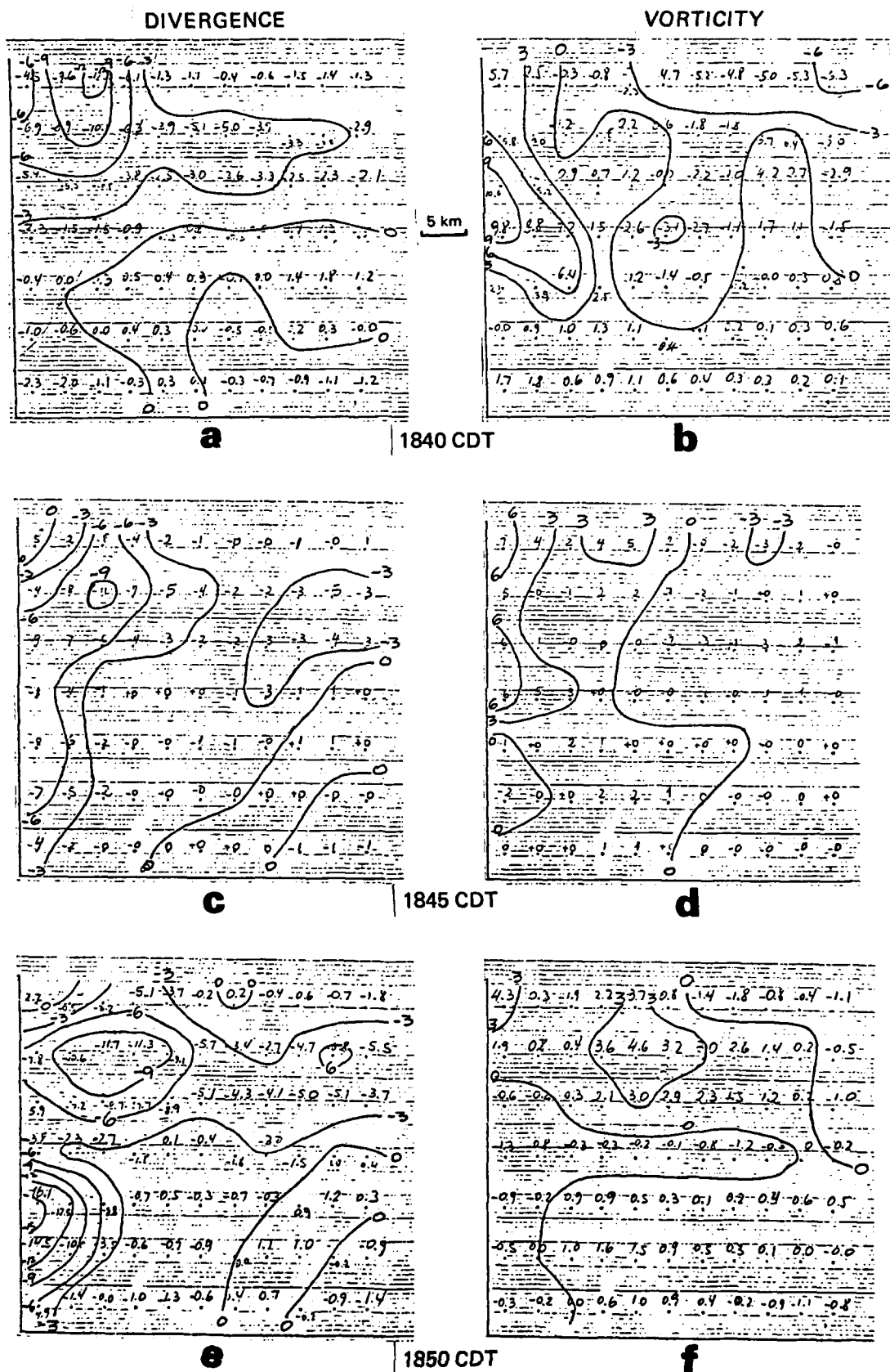
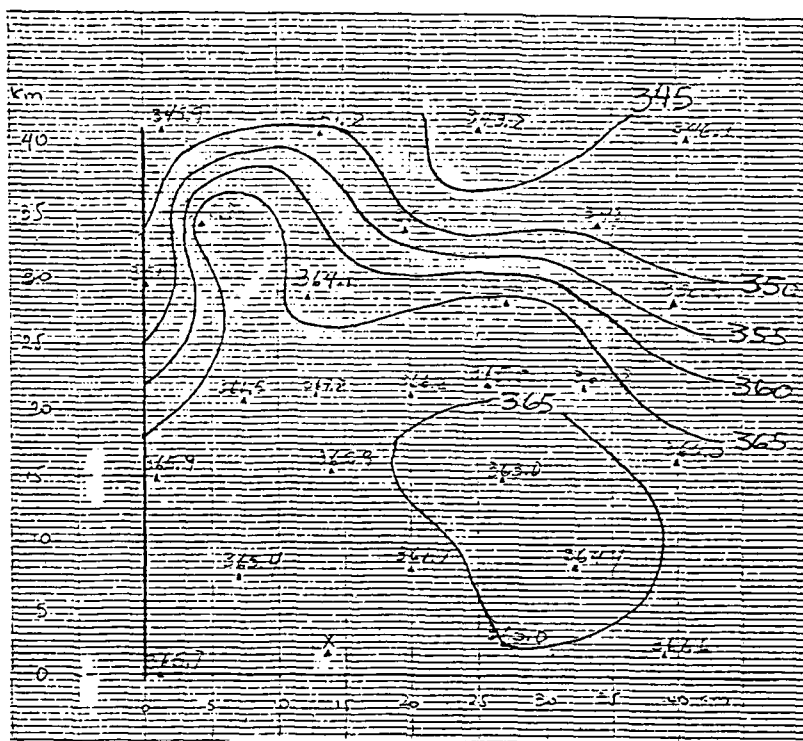
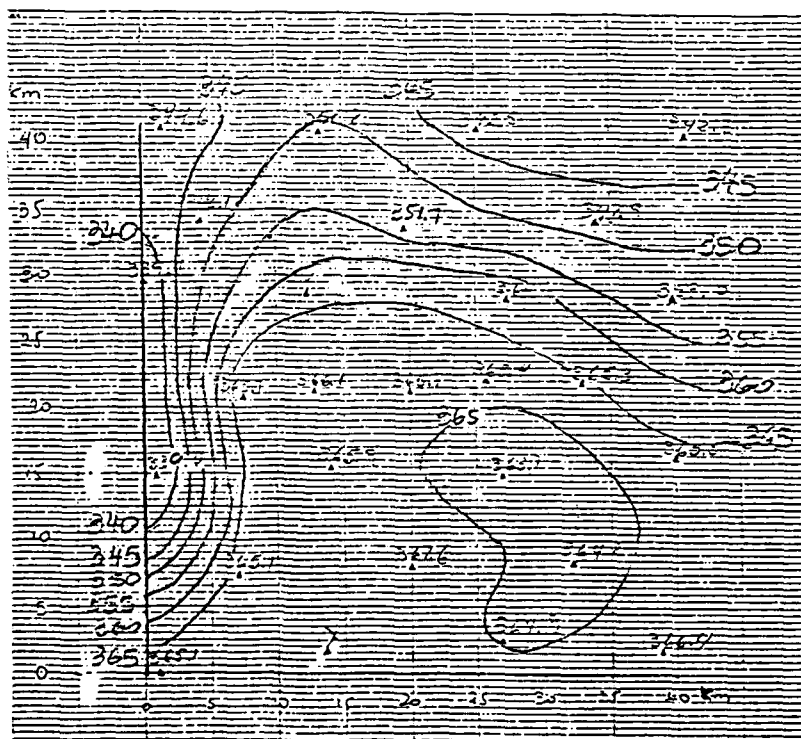


Fig. B-3' Divergence and vorticity (10^{-4} s^{-1}) over inner network, 1840-1850 CDT.



a. 1840 CDT



b. 1850 CDT

Figure B-35. Fields of equivalent potential temperature ($^{\circ}\text{K}$) in the inner weather network.

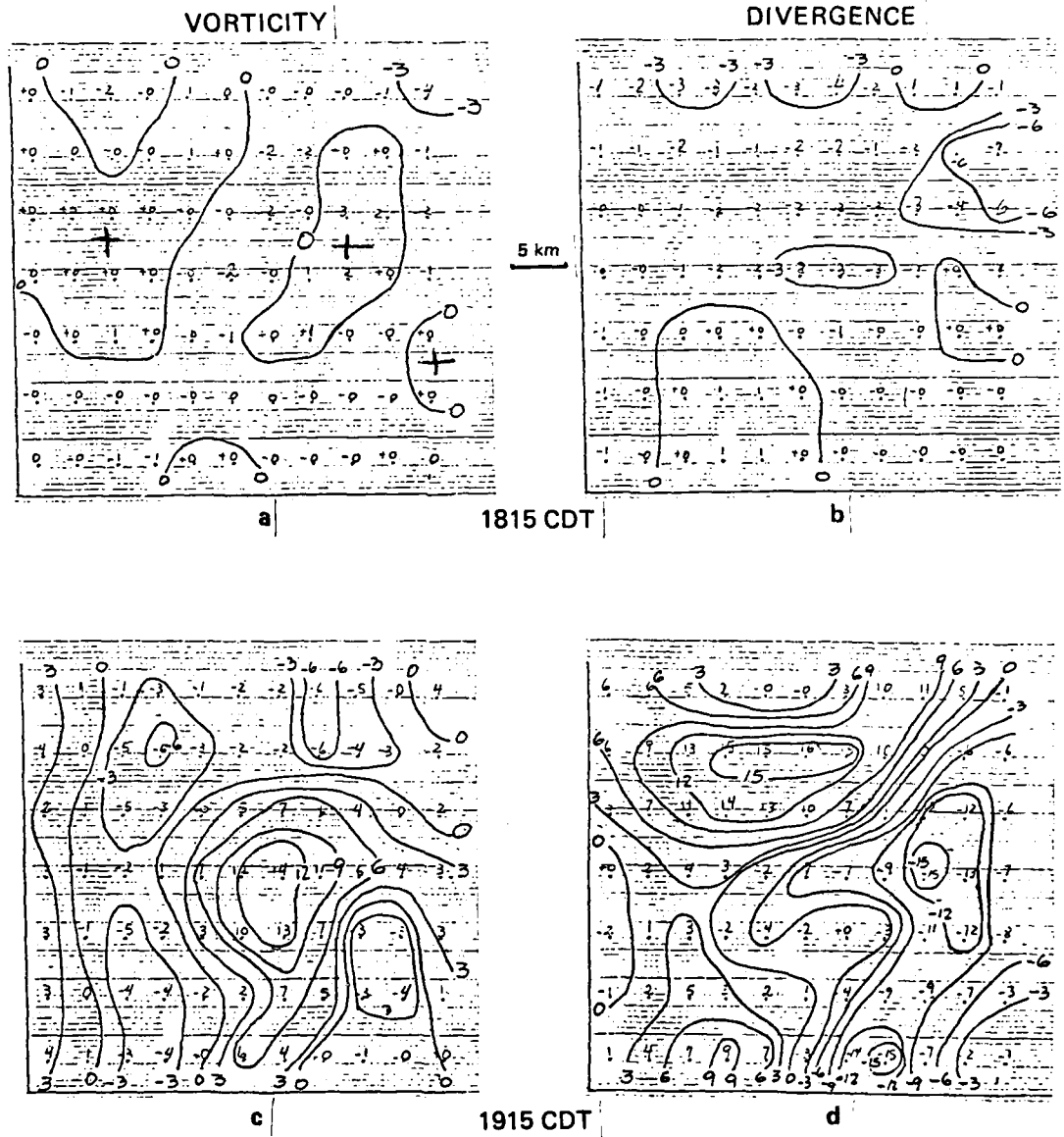


Figure B-36. Vorticity and divergence in inner weather network at 1815 CDT (a,b) and 1915 CDT (c,d). Units are 10^{-4} s^{-1} .

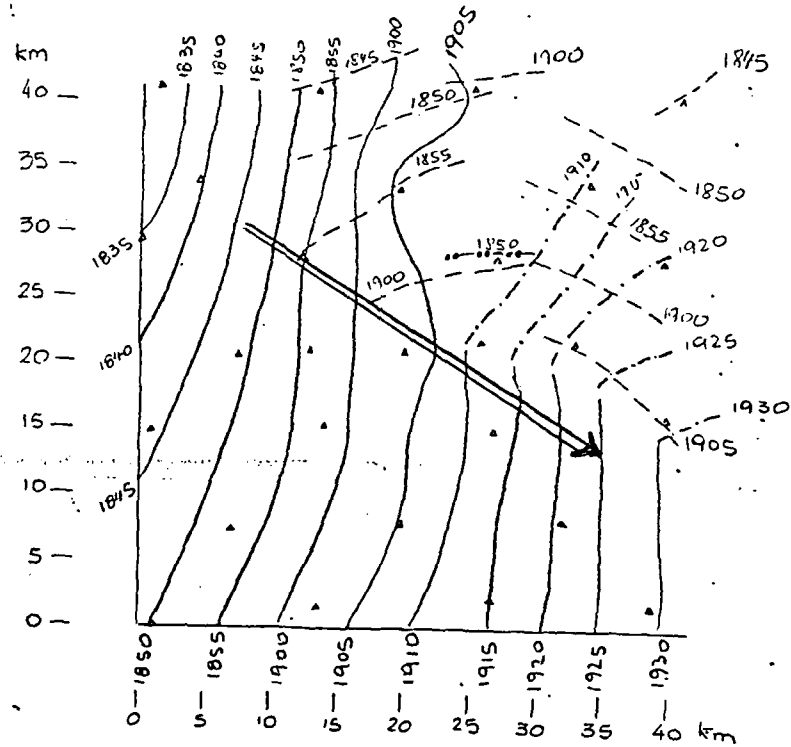


Figure B-37. Isochrones of wind shifts and track of mesocyclone, the latter given by the long arrow. Full lines indicate wind shift moving in predominantly from the west; dashed lines indicate wind shift moving largely toward the south. Dot-dash lines, beginning at 1910 CDT, reflect merging of northern branch of outflow from west with outflow from northeast. Dashed and double-dot line corresponds to a strong, southward moving gust front of limited spatial extent at 1850 CDT.

The 5 min-average relative vorticity reached peak values of $1.4 \times 10^{-3} \text{ s}^{-1}$ at 1915 (Fig. B-36c). High values of the 5 min-averaged convergence and divergence were also attained, reaching values of $1.5 \times 10^{-3} \text{ s}^{-1}$ for the convergence and $1.4 \times 10^{-3} \text{ s}^{-1}$ for the divergence. Peak values of convergence ($1.6 \times 10^{-3} \text{ s}^{-1}$) are reached at 1910 with a general strengthening of the divergence fields around 1910 CDT. At 1850 the maximum of convergence was located south of the mesocyclone center.

By 1930 the strong convective activity had left the network area. The squall line had substantially increased in width in the radar reflectivities pattern (Fig. B-32d).

Storm W

As indicated above, the convective activity after 1700 over the PAM network was under the influence of two convective scale systems, storm W and storm N, in a squall line that showed an evolution in its overall structure as revealed by radar reflectivity echoes. Storm N was the major convective system over the PAM network until 1830 when the outflow from storm W arrived in the network.

An analysis was made of the location of the wind shift lines associated with the outflow of storms W and N. The westerly outflow presented a clearly defined leading wind shift line; the northerly outflow consisted of an amalgamation of wind shifts, gust fronts, and presumably also waves that produced a complex pattern that at times became erratic. Despite that complexity there is a clear image of a southward advancing surge of outflows from different origins. The main wind shift lines shows a well defined passage, both in wind speed and direction, over the anemometers, good correspondence with both the convergence field over the network and the evolution of particular features in the radar reflectivity pattern.

Figure B-37 shows the W-E direction of movement of the storm W outflow, as well as the predominantly N-S direction of movement of the wind shift lines of the storm N outflow. It is evident that the outflow of storm N actually consisted of air descending at two different locations, from cells N1 and N2 both constituents of N. The existence of two convective cells in the northerly outflow is supported by the radar reflectivity pattern. Among the northerly outflows, the significant features are the outflows from NNW entering the network at 1845 and 1900 CDT, coming from the direction where cell N1 was located. The wind shift at 1846 over station P2 in the inner network was not strong: the gust front reached speeds of 4 m/s and the total decrease in θ_e was 3°K . Twelve kilometers toward the east, station P3 detected the NNW outflow at 1849 CDT with strong winds. Station P3 shows that 5 min-averages of wind speed reached 22 ms^{-1} , with winds stronger than 10 ms^{-1} lasting 8 minutes. Peak gust was 34 ms^{-1} . These strong winds, without any line configuration, would appear to correspond to downbursts observed by Fujita and Wakimoto (1981). They propose that such strong winds could often be produced by the collapse of storm tops protruding into the stratosphere. The θ_e values associated with the strong winds detected at station P3 began at 342°K and decreased to a minimum of 330°K , that is 4°K above the minimum value found at

the cold/dry layer in the mid-troposphere measured by the Salem sounding. However, at 1900, at the same station, a renewal of the severe winds was observed with θ_e values as low as the minimum values observed 5 hours before in the layer 700/760 mb. The configuration of storm N outflow isochrones shows a concave shape that has been observed in cases of two interacting outflows advancing in the same direction (Chalon et al., 1976). The radar reflectivity and ground data preclude considering cell N1 as being part of storm W.

Storm W outflow wind shift line passed over the station P1 at 1830. Prior to convection the θ_e value was 369°K, typical of the values of the surface environmental air ahead of the squall line.

A pool of outflow air from the storm N was already on the ground before the arrival of storm W. At 1845 the outflow from cells N1 and N2 was renewed. The southward advance of the outflow from storm N, starting at 1845, took place in an environment already containing dense outflow air from a chain of strong downdrafts produced earlier by the same storm. Before the outflow from storm W arrived, the field of vorticity at 1815 (Fig. B-36a) depicted a weak annular zone of cyclonic vorticity and a cut-off cyclonic vorticity area elongated in a N-S direction over the eastern side of the network. The field of divergence shows that, at 1815, there were zones of convergence on the north and east sides of the network (Fig. B-36b). These features are in agreement with the arch-shaped configuration of the squall line, observed both in radar echo pattern and satellite pictures.

Figure B-38 shows a strong convergent zone at the NW of the network, with a belt of weak anticyclonic vorticity on the west side. Figure B-37 indicates that the wind shift line of the storm W outflow at 1835 had only entered the area on the NW corner, although it was rapidly advancing over the network.

The radar reflectivity pattern at 1840 (Fig. B-32a) provides an overall picture of the squall line spatial location and its presence over the PAM network. Strong echoes are located over the NE corner of the network. Comparison with the radar echoes at 1850, Fig. B-32b, indicates that during the 10 min interval a rapid spatial expansion of the echo region west of the network occurs. The echo at 1840 located at $y=80$ km and $x=95$ km had grown and displaced to produce the echo protuberance located at $y=70$ km and $x=105$ km at 1850.

The divergence of storm W reached a maximum value of $1.8 \times 10^{-3} \text{ s}^{-1}$ at 1910. Convergence attained values of $-1.5 \times 10^{-3} \text{ s}^{-1}$, in two centers at 1915 (Fig. B-38d). The wind field maintained the mesocyclonic features associated with the cyclonic vorticity center which reached a maximum value of $1.4 \times 10^{-3} \text{ s}^{-1}$. By 1945 the severe features of the storm were no longer present over the network.

Mesocyclone

An important feature of this severe storm event is the presence of a mesocyclone. Cyclonic curvature of the streamlines began to appear at 1840 (Fig. B-33a) and it is clearly visible in the wind field at 1900. The mesocyclonic circulation had a displacement speed of 13.9 m/s from 328°.

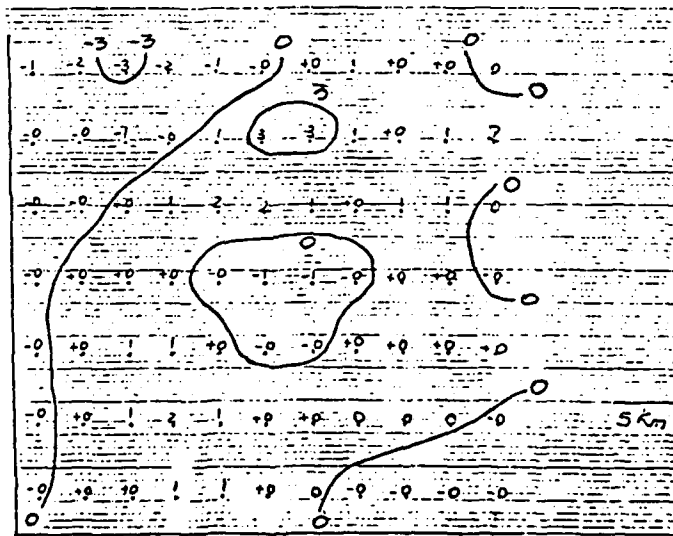
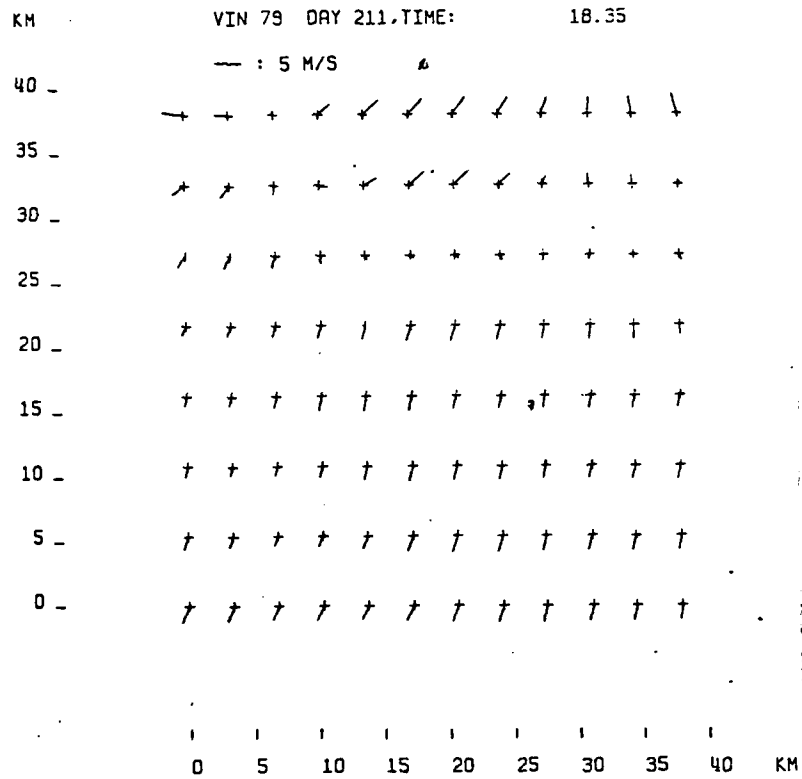


Figure B-38. Wind field (top) and vorticity (bottom) at 1835 CDT over inner weather network.

Figure B-37 shows the path of the mesocyclone and the location of several wind shift lines. The mesocyclone moves along a line of collision of storm outflows. Strong cyclonic curvature of the streamlines at 1915 (Fig. B-33f) exists over the center of the network similar to the pre-tornadic condition summarized by Brandes (1981) for the Del City-Elmond thunderstorm. This pattern was visible at 1910 and 1920, and is best defined for the period ending at 1915. The relative inflow with respect to the surface mesocyclone was from ahead and consisted of air with large values of mixing ratio and θ_e .

Table B-1 shows the 5 min mean maximum values of convergence and vorticity. Peak values of convergence and vorticity increased with time from 1835 to 1925. Mean areal values of convergence and vorticity also became larger. The values indicate a consistent pattern of intensification from 1845, with a marked strengthening of the surface kinematic fields at 1855. The zone of collision between the outflows from storms W and N was a zone of preferred location for strong convergence. This is similar to the observations of Fankhauser (1976) from hailstorms in Colorado, and those of Gurka (1976) using satellite information. Holle and Meier (1980) have studied the formation of a cumulonimbus produced by the collision of two outflows. Their analyses indicate that a small tornado was seen beneath the storm.

The direction of motion and intensity of the convective cell that produced the mesocyclone appears to be substantially influenced by the surface velocity field. Figure B-39 shows a sketch of the location and path of the radar echo of cell α , produced and maintained by the outflow collision. Also shown are radar echo, β , due to an intensification of the multicell storm W and radar echoes ϵ and m that after being generated by the gust front moved northward and merged with the main body of the squall line. The radar echoes from cell α and cell β moved parallel to the line of outflow collision.

Figure B-40 shows the area (hatched) in the PAM network over which the mean value of radar reflectivity was at least 50 dbz during the time interval 1840 to 1925. Also shown are the locations of the $-6 \times 10^{-4} \text{ s}^{-1}$ contour line of convergence between 1840 and 1920. Within the spatial resolution allowed by the 5x5 km grids it is observed that the presence of a band of high radar reflectivity from $y=20-25 \text{ km}$, $x=5-10 \text{ km}$ to $y=5-10 \text{ km}$, $x=20-25 \text{ km}$. This direction is parallel to the movement of the convergence zone associated with the line of outflow collision.

Summary

The analysis made so far on the convective regime that passed over the PAM network on July 30, 1979, indicates that a strong convective cell was produced by a collision of outflows. A surface mesocyclonic circulation that reached its maximum strength over the PAM network was observed in association with that convective cell.

The mesocyclone attained values of vorticity comparable to those observed in tornadic storms in Oklahoma for a surface network with similar space resolution. The presence of the near surface mesocyclone was associated with a strong downdraft that showed θ_e values similar to minimum θ_e values found in the troposphere in the layer 700-760 mb.

Table B-1. Mean convergence in area enclosed by indicated isocline.

Time	$> 3 \times 10^{-4} $	A (km ²)	$> 6 \times 10^{-4} $	A (km ²)	$> 9 \times 10^{-4} $	A (km ²)	Peak \times 10^{-4} s^{-1}
1835	-6.7	(112)	-8	(75)	-9.5	(37)	-10
1840	-7.1	(206)	-8.1	(131)	-10.6	(56)	-10
1845	-6.4	(337)	-7.7	(206)	-11	(19)	-11
1850	-7.0	(300)	-9.2	(150)	-10.6	(75)	-11.7
	-8.9	(150)	-13.2	(75)	-13.2	(75)	-16.1
1855	-6.7	(488)	-8.3	(319)	-9.8	(94)	-12
1900	-6.8	(431)	-8.5	(262)	-10.4	(75)	-11.5
1905	-6.8	(431)	-8.4	(262)	-9.6	(150)	-11
1910	-7.6	(450)	-9.7	(262)	-10.9	(169)	-12.3
1915	-8.6	(450)	-9.6	(375)	-11.9	(206)	-15
1920	-9.3	(375)	-11.5	(262)	-13.2	(187)	-17.1
1925	Partially gone from network						-19

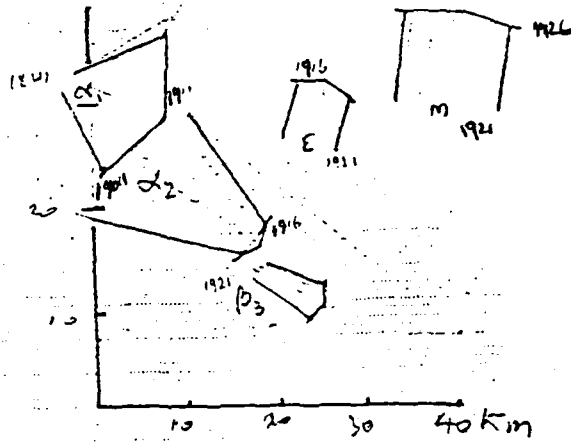


Figure B-39. Envelope at 40 dbz reflectivity contour (3.7° elevation). Tip of arrow indicates last location of detectable 40 dbz contour and direction of movement between times indicated. (See text for echo identification).

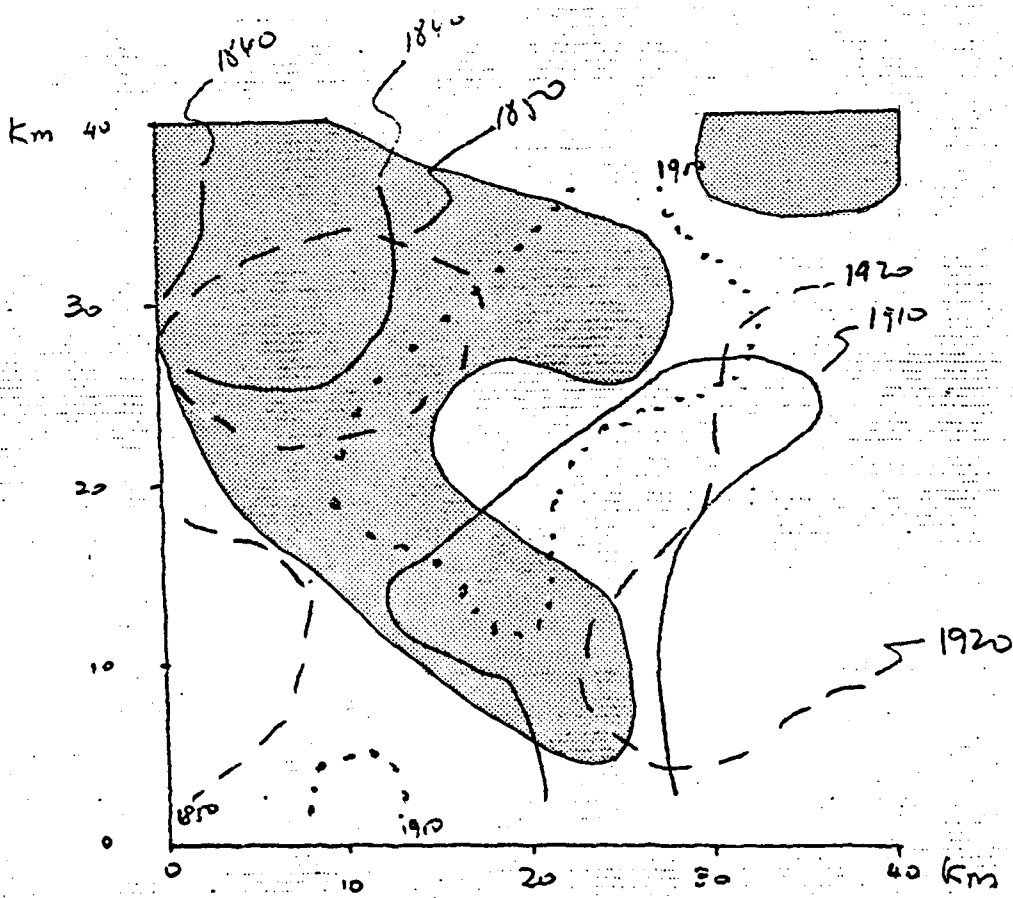


Figure B-40. Locations of $6 \times 10^{-4} \text{ s}^{-1}$ contour of convergence at indicated times (CDT) and area (shaded) over which mean value of radar reflectivity equalled or exceeded 50 dbz, in interval 1840-1925 CDT.

The main findings may be summarized as follows.

1. A mesocyclone is present in the subnetwork scale velocity fields of the squall line which passed over the VIN network on 30 July 1979.
2. The velocity (wind shift) and thermodynamic fields support the existence of near surface storm outflow and collision.
3. There is further evidence of an association between the outflow collision and the intensification of the mesocyclone.
4. Evidence of downdraft generation by a dry layer aloft suggesting undilute descent is present in the surface thermodynamic fields.

D. Surface Kinematics and Cloud Evolution (ISWS)

Introduction

Rainfall was recorded in the VIN network almost continuously from shortly after 1500 CDT on 30 July to 0300 CDT on 31 July. It occurred in four well defined storm periods: 1) an initial one from 1500 to about 1730 CDT, during which the rain was due to developing multicellular shower clouds, 2) 1730 to 2055, when the precipitation was from a major squall line, 3) 2000 to 2310, showers embedded in the rear rain shield of the squall line, and 4) post 2300, rainout from the dissipating squall. Although there was some overlap in time, the four storm periods were adequately defined areally to separate the rainfall. Most of the rainfall occurred during first two storm periods (Fig. B-2).

The analysis described below relates to the evolution of semi-isolated, small cloud masses prior to 1730, as delineated by reflectivity measurements from the CHILL radar, and the surface kinematic fields calculated from the wind network shown in Fig. B-16. The focus of the study was on the cloud development and the interaction between the cloud-scale and network-scale circulations.

The 5-min averaged winds were objectively analyzed using the same technique that was used in the regional analysis described in Section 3 of this Appendix. The fields of velocity, moisture, and heat divergence were calculated for each 5-min period beginning at 1300 CDT. As in the case of the regional analysis, the patterns of moisture and heat divergence are so similar to that of velocity divergence that only the latter are presented below. The 5-min isohyets for the full raingage network were also based on objective interpolation.

Two presentations were generated from the digital radar data: 1) a "composited PPI" in which a variety of parameters (e.g., maximum reflectivity, top of echo, etc.) were sought for vertical columns of specified cross section and 2) a CAPPI based on 3-dimensional interpolation of the full volume scan. Most of the radar maps in the following figures are of the first type, the parameter

being the maximum reflectivity in columns reaching from the surface to the top of the volume scan. Thus, the maps are a compression of the total volume scan into a PPI presentation of peak reflectivity.

Evolution of the Cloud and Divergence Fields: 1300-1730 CDT

The rainfall in the VIN network during the first storm period came primarily from clouds developing within the network. It started shortly after 1500 in the northeast corner from a new cloud forming on the west edge (upwind for cloud layer winds) of the eastern cloud cluster of the incipient line (see Fig. B-10a). Within 5 minutes, an echo developed on the western edge of the network as well (barely visible in fig. B-10a). As will be shown below, this small cloud was soon joined by other small developments to its east. The total cloud mass within the network grew very rapidly in areal extent, with individual clouds expanding due to new cell development and merger of neighbors. However the joining of adjacent echoes was only at the weaker reflectivity levels and echoes were all multicellular, with cell size commonly 2-5 km in diameter. Movement was toward the east at about 25 km/hr, with increasing consolidation as the echo mass moved eastward. Eventually the clouds which developed within the network merged with others to the east to become part of the eastern cloud cluster (Fig. B-10, b-d).

The precipitation from these network clouds tended to come as short bursts of high intensity rain, occurring at a single station in any given 5-minute period. (Station spacing in the raingage network was about 5 km, greater than the average cell size.) The rain rates were frequently very high, reaching 9 cm hr^{-1} for 5-minute accumulations and over 4.5 cm hr^{-1} for 15-minute accumulations.

Persistent areas of convergent flow were detected in the network for at least 2 hours before significant radar echoes developed. This persistent convergence occurred in a broken band extending from southwest to northeast across the network (Fig. B-41), nearly parallel to and downwind from the Sangamon River in the western 2/3 of the network, and in the valley in the northeast. Within this band, there were usually two or three centers of locally strong convergence, with maximum grid point values in excess of $2 * 10^{-4} \text{ sec}^{-1}$. During the pre-rain period (1300-1500 CDT) the locations and magnitudes of these centers tended to vary somewhat, with the centers just to the northwest of Decatur and over the Friends Creek¹ watershed less variable than the one in the northeast. The early storm clouds developed in and downwind of this band of convergent flow.

These localized regions of convergent flow are believed to be due to the topographic features in the Sangamon Valley and/or land use. Although the relief in the network is less than 200 ft, it tends to be concentrated along the streams where there is also an increase of roughness due to the wooded areas located there. The character of this roughness differs radically from

¹Friends Creek watershed is shown in Fig. B-16 by the short dashed line.

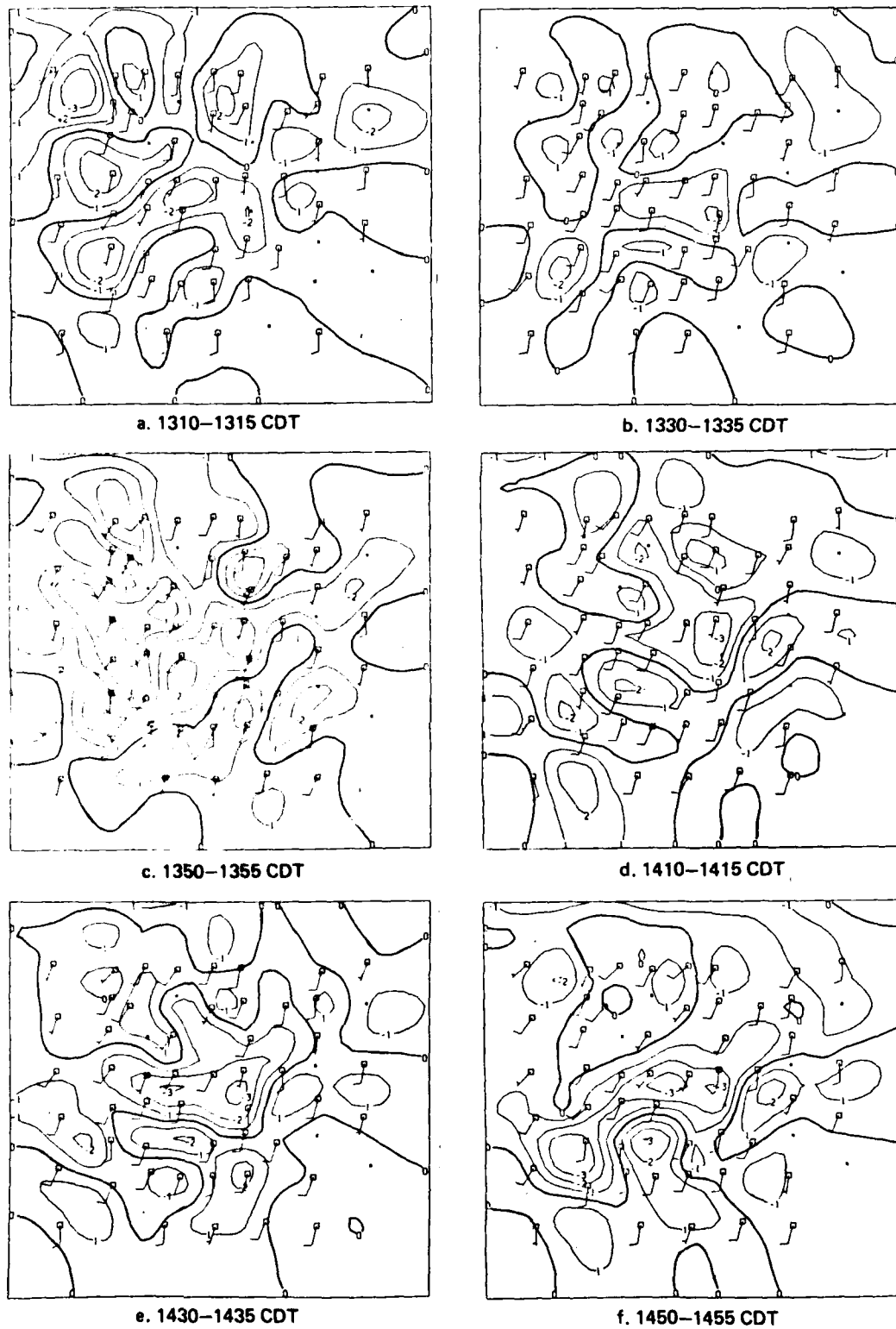


Figure B-41. Fields of velocity divergence (10^{-4} s^{-1}) in the VIN wind network prior to the start of rain. Wind barbs indicate direction from which wind is blowing and 1 full feather indicates 5 m s^{-1} . Boxes are 80 km from west to east.

that of the surrounding agricultural areas, with their uniform cropping over many acres of very close stands of corn and/or soybeans. By the end of July the fields present a nearly uniform surface to the air stream, whereas the wooded areas are more open with variable canopy height.

The pre-rain convergence was not merely a surface phenomena, but occurred throughout most, if not all, of the sub-cloud layer. The net inflow into the triangle defined by the three pibal stations was greatest, not at the surface, but aloft prior to the rain (Fig. B-42). The height at which the maximum convergence occurred decreased with time from about 350 m AGL (600-650 m MSL) 90 minutes before the rain to about 100 m AGL (350-400 m MSL) at the time the rain started. The maximum convergence aloft at 1400 CDT was almost as great as the maximum grid point value at the surface despite the fact that the latter was calculated for a much smaller area (100 km^2) than that represented by the pibal triangle (750 km^2) which included regions of divergent as well as convergent flow.

The cloud fields, as detected by the time-lapse cameras (Section 4 A of this Appendix), underwent a significant change in character between 1330 and 1400, as developing cumulus and incipient congestus replaced scattered stratocumulus. This increase in cloud activity was not reflected at the surface where the divergence field did not change significantly between 1300 and 1400 (Fig. B-41 a-c). However the inflow into the pibal triangle at the upper levels did increase markedly as the clouds developed between 1330 and 1430. After 1400, with the development of non-raining congestus, the strength of the surface convergence increased in the two most persistent regions, the one SW of Decatur and the other in the center of the network Fig. (B-41d,e). Maximum grid point values after about 1430 were fairly consistently above $3 * 10^{-4} \text{ s}^{-1}$, whereas earlier they had varied most commonly between 2.5 and $3 * 10^{-4} \text{ s}^{-1}$.

By 1445 CDT new developing congestus towers in the far NE corner of the network were detected in the time lapse film and light rain was recorded in this area starting at about 1450. Except for the precipitation echo in this location, only scattered, small and weak ($< 20 \text{ dbz}$) echoes of short duration were detected over the network prior to 1510 CDT. By 1510 the reflectivity in this precipitation echo was up to 45 dbz and very light rain was still falling. This cloud was located just downwind of the convergence cell at the northeast end of the persistent band of convergent flow (Fig. B-43b). As the peak reflectivity increased to 50 dbz and the echo grew in area between 1510 and 1520 the convergence here strengthened (Fig. B-43 b-d), with maximum grid point values increasing from 2.3 to $3.3 * 10^{-4} \text{ s}^{-1}$. Although still a relatively shallow echo, with top at about 8 km, it continued to grow and the rain continued for the next 25-30 minutes.

Three or four small echoes were detected at 1510 also, but only the two in the extreme west lasted for more than 5 or 10 minutes. The small echo near the western border grew very rapidly and by 1525 was joined by near neighbors to the SSE (Fig. B-43d). The echo cover increased significantly between 1515 and 1525, as a number of small, relatively weak echoes (reflectivity $< 35 \text{ dbz}$) with

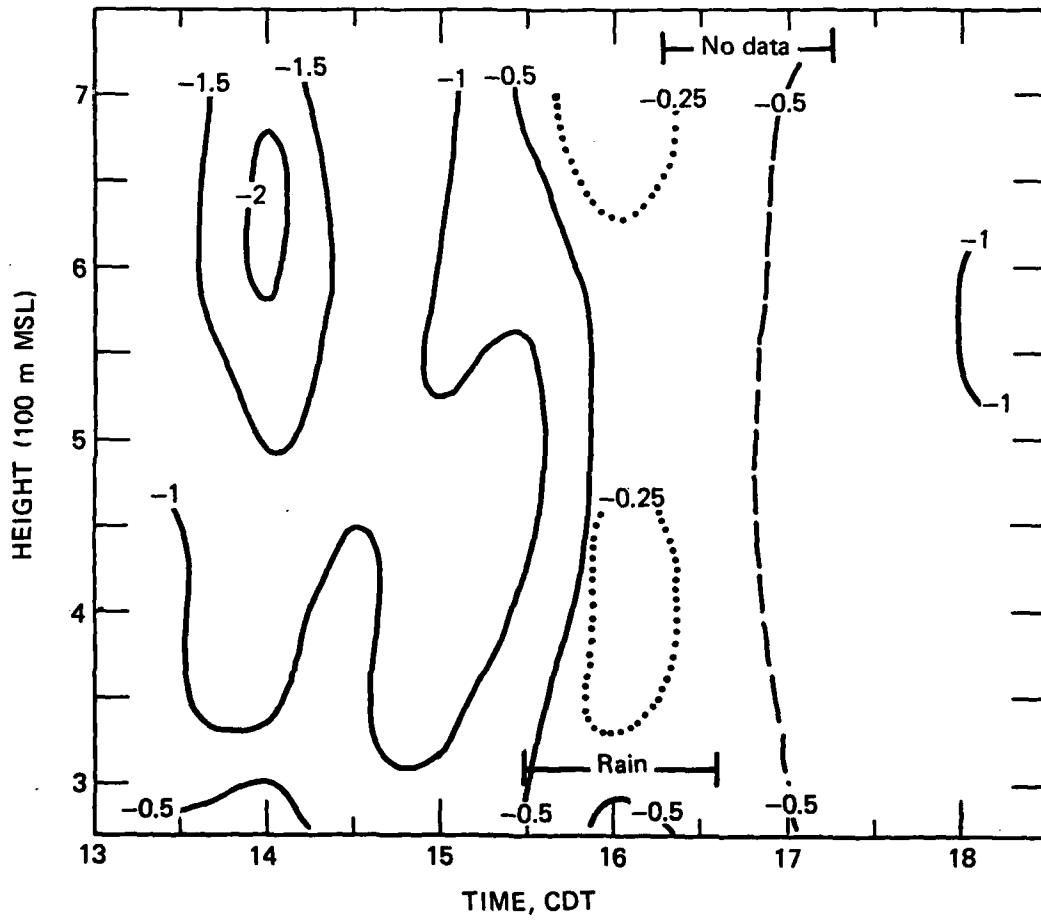


Figure B-42. Time - height cross-section of velocity divergence (10^{-4} s^{-1}) for triangular area defined by the three pilot balloon stations. Dashed contour is estimated because of missing data. Surface elevation is about 275 m MSL.

tops below 5 km developed between the cloud on the western border of the network and the older echo in the northeast corner. By 1530, there was a band of echoes nearly parallel to and downwind from the pre-rain band of convergent flow which was still evident in the divergence field (Fig. B-43e). The echo in the far west had reached reflectivity of 50 dbz and attained a top height of 8 km. Light rain was recorded at the surface below this echo complex.

The westernmost echo continued to grow in coverage as new cells developed both on the north and south ends. By 1537 (Fig. B-43f) this small line of cells (A) had merged below 4 km. Peak reflectivities in two of the cells were over 55 dbz, and the top of the complex had reached 9 km. The showers from this cloud were brief and small, lasting only 5 minutes and occurring at a single station in any given 5-min interval. However, they were intense, with rates of about 2 to 2.5 cm hr⁻¹ for 5 min accumulations ending at 1535 and 1540.

Echo B, about 10 km west of the first shower in the NE rapidly intensified and expanded between the time it first appeared at 1523 and 1535 (Fig. B-43 d-f). It developed originally directly downwind, but some distance from the persistent convergent flow in the center of the network. By 1535, this cloud had significantly affected the surface winds and the convergence upwind from it had increased markedly. Rain started shortly after 1540 and reached an intensity of 2.5 cm hr⁻¹ by 1545. The cloud continued to increase in intensity, to over 55 dbz at 1550, and the rain rate increased to 7 cm hr⁻¹. The surface wind field continued to react to this intensifying system and to new clouds in its vicinity and a region of convergent flow developed between echo B and its neighbors to the north and west (Fig. 43 g).

The divergence pattern began to change in the western third of the network as well shortly after 1530, as echo mass (A) intensified and produced rain showers. The convergence northwest of Decatur weakened, (Fig. B-43f) to be replaced by divergent or non-divergent flow by 1545 as the convergence upwind of the cloud band increased. The modification of the wind field continued rapidly in response to cloud-scale circulations and by 1550 (Fig. B-43g) a SW-NE band of convergent flow no longer existed. A region of convergence was beginning to line up WNW-ESE just upwind of echo complex A at 1545-1550, with maximum grid point values greater than $4 * 10^{-4} \text{ s}^{-1}$. This close association of surface convergence and echo became even stronger within the next 10 minutes and was to continue for the next hour as cloud complex A moved east. The change in the wind field to the SW of echo A was paralleled by changing to its north. The divergence northeast of the northern cell of A increased twofold between 1530 and 1540 and doubled again between 1540 and 1550 (Fig. B-43g, h).

The impact of the cloud circulations on the surface divergence is clearly seen in the average flow between 1555 and 1600 CDT (Fig. B-43h). The WNW-ESE zone of convergent flow upwind of cloud mass A was well established with grid point convergence up to $4.5 * 10^{-4} \text{ s}^{-1}$. Outflow from the northwest cell, and to a lesser extent from the one to the south as well, resulted in strong divergence (over $6 * 10^{-4} \text{ s}^{-1}$) beneath the cloud, and a new small area of convergence downwind. Although this area of convergence lasted for at least 10 min, there was no significant cloud growth associated with it. The major new development was in the center of the network (cloud C).

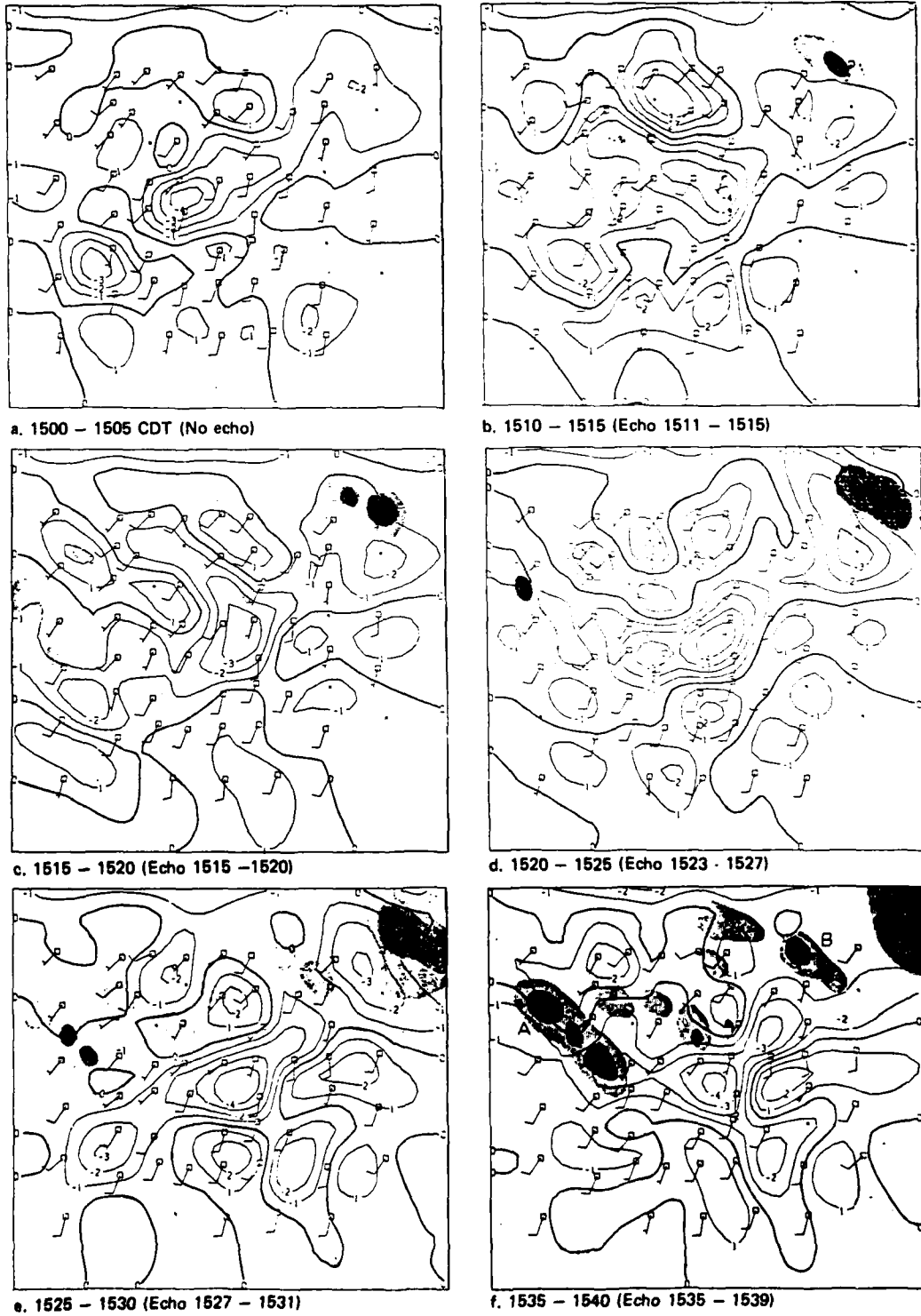
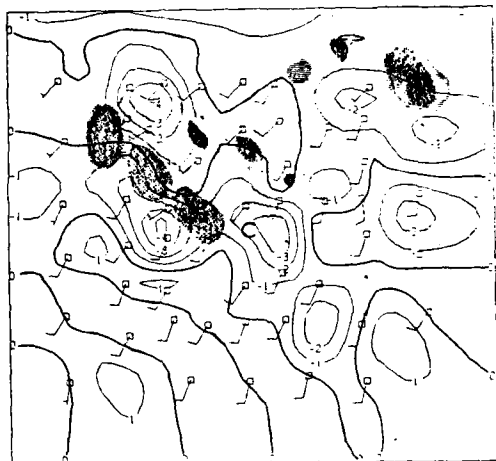
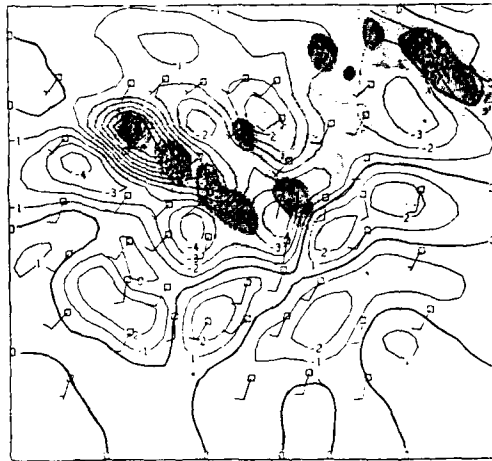


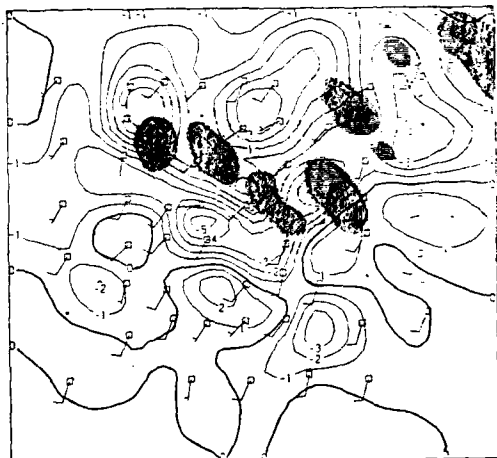
Figure B-43. Fields of velocity divergence (10^{-4} s^{-1}) from 1500 to 1650 CDT, plotted as in Figure B-41. Shading shows radar echo with reflectivity >20 dbz; darker shading indicates reflectivity >40 dbz.



g. 1545 - 1550 (Echo 1547 - 1551)



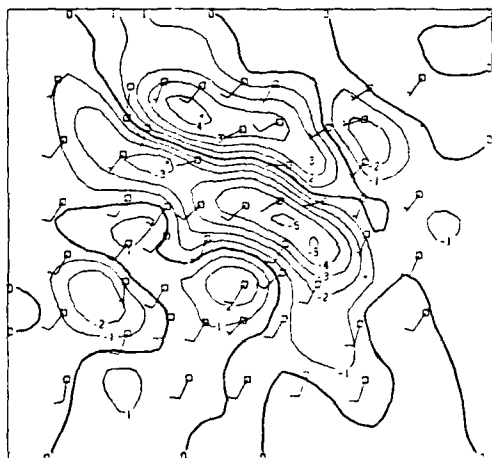
h. 1555 - 1600 (Echo 1555 - 1558)



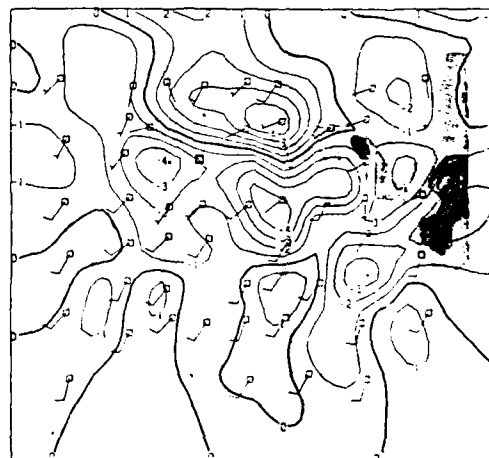
i. 1605 - 1610 (Echo 1607 - 1610)



j. 1610 - 1615 (Echo 1611 - 1614)



k. 1625 - 1630 (No radar data)



l. 1645 - 1650 (Echo 1646 - 1650)

Figure B-43, continued.

Echo C had first appeared at 1543 as two very small clouds, with tops around 3 km and maximum reflectivity just above 20 dbz. These two rapidly merged and within 4 minutes had grown to 6 km, with increase in reflectivity to 30 dbz.

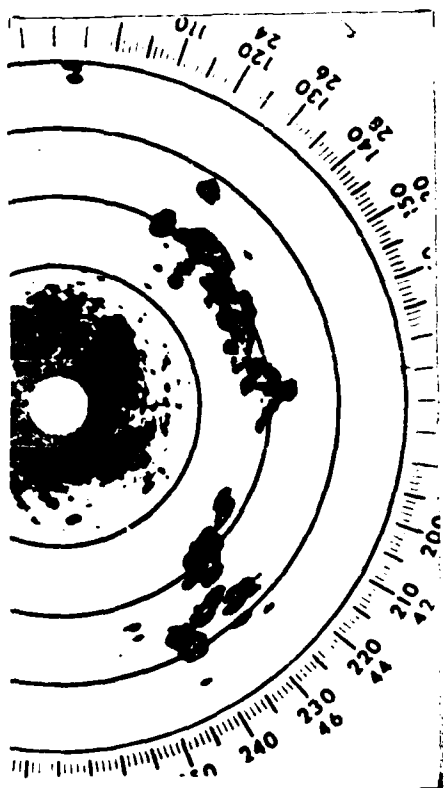
The vertical rate of growth slowed in the next four minutes, but the strength of the echo increased unabated, reaching 45 dbz by 1551, less than 10 minutes after the original small echoes appeared. This cloud was in an especially favored condition, just downwind of strongly convergent flow from a fresh source of low level air to the south. (Echo B had developed in a similarly favored location and it too had intensified rapidly.)

Echo C merged with cloud mass A, underwent accelerated growth, with echo top growing from about 7 km at 1557 to 13 km at 1609, and increased in strength to over 60 dbz. The small convergence cell upwind of this cloud shifted eastward with it, just as the band of convergent winds upwind of echo A, remained linked to that NNW-SSE line of cells (Fig. B-43 h-j). As the system moved east, the convergent flow associated with it "linked up" with a small region lying to the south (Fig. B-43i), which had been a more-or-less persistent feature of the divergence field for about an hour or more. A new "appendage" rapidly developed on the southern edge of merged echo A-C (Fig. B-43j), which was to rapidly develop into a major new cloud cell producing heavy rain and strong winds as it moved to the eastern edge of the network.

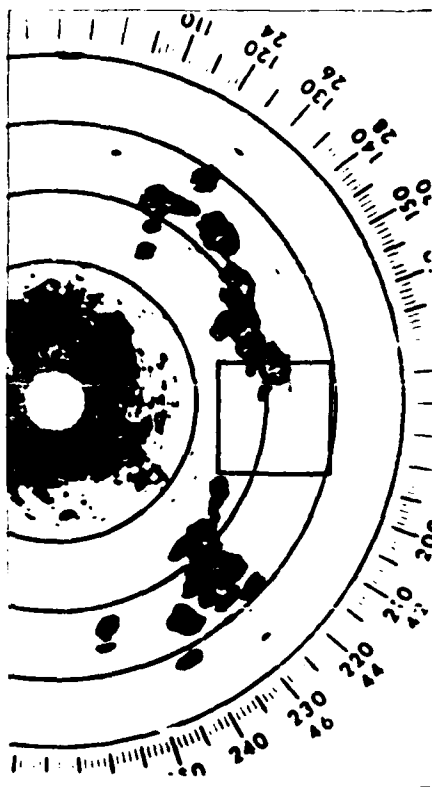
This cell (D) was first detected at about 1609 CDT, as a small ($< 3 \text{ km}^2$), shallow ($< 1 \text{ km}$), weak ($< 18 \text{ dbz}$) echo at 5 km AGL. It grew very rapidly and by the time of the next volume scan, 4 minutes later, its top was over 8 km, its depth had increased to nearly 6 km, and its area to 20 km^2 . Peak reflectivity at 1613 was 50 dbz, occurring at 6 km where the areal extent was greatest. The development of cloud D had been favored by nearly continuous convergence of fresh low level air from the south for some 40 minutes. Thus the mixed layer increased in depth and moist air was transported upward into the cloud layer. The first rain from cell D was recorded at 1620, and the 5-min rain rate reached 3 cm hr^{-1} by 1625, 16 min after the initial appearance of the echo.

Unfortunately surges on the power line due to the cloud electrical fields resulted in electronic damage to the CHILL processor about 1616 and only fragments of radar data are available for the next 40 minutes. The general evolution of complex A-C-D and the areal expansion of the southern cell D can be followed in the Marseilles WSR-57 radar-scope photographs (Fig. B-44). By 1630 the complex A-C-D had joined the eastern cloud cluster and the youngest echo D was the major cell on the SW end of the cluster. Rain fell continuously from this cloud mass, but primarily from echoes C and D, with 5-min rain rates periodically reaching very high values. Prior to 1650 rain rates in showers from D were 2.5 to 3 cm hr^{-1} .

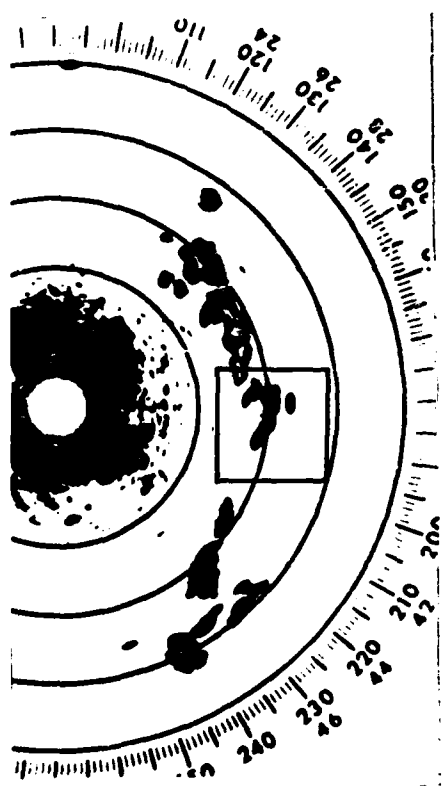
By 1646 when CHILL data were again available, echo D had partially moved out of the area of the wind analysis. Reflectivity of the portion still in the network reached 60 dbz, and the echo top was above 11 km (the maximum height scanned at the range of the echo). From 1650 CDT until the cloud moved east of the raingage network, measured 5-min rain rates exceeded 6 cm hr^{-1} .



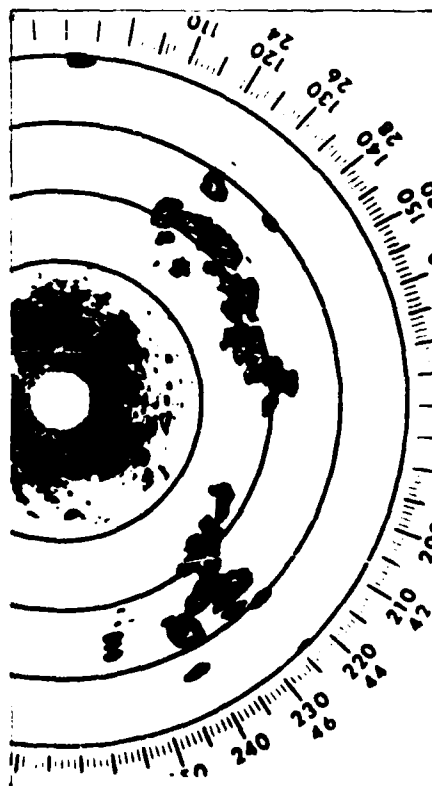
b. 1631 CDT



d. 1656 CDT



a. 1618 CDT



c. 1642 CDT

Figure B-44. Precipitation echoes as recorded by NWS radar at Marseilles, IL. Range markers are for 25 n.m. Box approximately outlines VIN network.

As the cloud moved over the radar, the cloud base was only 200 or 250 m above ground, with a well defined rotary motion, and small funnels dipping down from the base.

Echo line A was dissipating at 1646 with reflectivity levels of 40 dbz or less except in a small core where it peaked at 50 dbz. This decaying echo and a small weak one to the WNW were located between cool outflow air remaining from the earlier rain and a convergent air stream from the south (Fig. B-43l). Nevertheless, no significant cloud development occurred. Upper air data are not available in the immediate area but it is likely that subsidence aloft around the storm inhibited vertical development.

As can be seen from Fig. B-43k and l, the surface wind field was dominated by the cloud-scale circulations after 1615 and the area of divergent and convergent flow moved eastward with the clouds with which they were associated. The divergence in the NW, associated with outflow from the cells on that end of storm A, persisted to 1640, 15 to 20 minutes after the rain ended in that area. However as the clouds moved east, the background convergent flow northwest of Decatur very rapidly returned to its original magnitude (Fig. B-43h) and the surface winds over Friend's Creek water shed became convergent again (Fig. B-43l). Despite this, the wind field in the network continued to reflect the influence of the storm that had passed through until at least 1715¹.

It is evident from this analysis that persistently convergent flow in the surface layer played a role in determining the general area in which the early convection would develop. It is also evident that once the convective clouds had reached adequate size and strength and were producing significant rainfall, the cloud-scale circulations interacted with and modified the background surface wind field. When the clouds reached thunderstorm size, the cloud circulation dominated the surrounding windfield. Very rapid new cloud development occurred when convergence zones associated with the cloud circulations moved into juxtaposition with and downwind of a persistent region of convergent flow.

Vertical Fluxes and Cloud and Precipitation Development

An investigation of the relationship between the vertical transport of mass and moisture and the evolution of the clouds and precipitation was made using the same methods employed in the regional analysis (Section 3 of this Appendix). The basic data were the 5-min average winds and the 5-min rainfall accumulations from the VIN network records. Echo volumes were calculated from CAPPI analysis, with 1 km resolution, of each recorded volume scan made by the CHILL. Net inflow and vertical transport were calculated for the northern three-fourths of the analyzed area shown in Figs. B-41 and B-43. The upward transport was also estimated for only those regions within this limited area in which there was convergent flow.

¹Lightning struck the power pole at the radar trailer at 1715 causing severe damage and the CHILL was non-operational after this time. The PAM base station electronics was also affected by the lightning and surface data are not available for about the following 35 minutes.

These values of mass inflow and vertical transport, calculated for a 4 m depth in the surface layer, are plotted for each 5-min period (Fig. B-45a, B-46a) along with echo volumes (Fig. B-45b,c) and rainfall (Fig. B-46b). Note that in Figs. B-45a and B-46a, the difference between the two curves represents the net downward transport. Note also that the decrease in echo volumes and precipitation after 1645, are largely due to movement of the clouds off the network and not due to cloud dissipation.

It is quite obvious that there was a net inflow into the area for a considerable length of time prior to any significant cloud development, actually going back at least two hours to 1300 CDT. Thus, there was a long period during which the moist boundary layer deepened. Starting at 1400, there was a generally increasing trend with time of the "local" upward mass transport as indicated by the curve for the convergent regions. This started at about the time that the cloud fields were changing from cumulus to cumulus congestus. The increase in upward transport occurred for the area as a whole, but only until around 1510 when echo volumes began to increase rapidly and rain began to fall in the area. Then local areas of divergent flow started to develop and increase in magnitude sufficiently to cancel the increase in the upward transport in the convergence cells. This is supported by the upward trends in both echo volume and rainfall coverage from 1510 to 1615-1630. The return of an increasing temporal trend in net upward transport for the area after 1630 is probably a reflection of a decrease in precipitating cloud cover as the main cloud masses moved eastward out of the network.

There is no clear-cut relationship between the evolution of echo volume and vertical mass transport, except as indicated above. However, the near temporal coincidence of the increase in upward transport in regions of convergent flow at about 1550 and the increases within 5 or 10 minutes, in the echo volumes above 8 and 9 km (Fig. B-45c) and the echo volume with reflectivity ≥ 50 dbz (Fig. B-45b) suggests that intensification of local areas of convergence may precede and induce rapid vertical cloud development. This is supported by the chronological discussion above and by a comparison of the divergence fields in Figs. B-43f and g.

Three "cycles" of increase and decrease can be detected, superimposed on the generally increasing trend in the upward transport in the convergent regions. These occur from 1435 to 1545, 1545 to 1625 and 1625 to 1715. Three cycles can also be seen in 5-min accumulations of rain mass (Fig. 46b): from start of rain at about 1510 to 1605, 1605 to 1645 and 1645 to the time the rain moved east off the network. If there is, as is hypothesized, an important link between surface convergence and rainfall, these analyses would suggest a lag of about 30-40 minutes for initial development of precipitation and a 20-min lag when cloud convection becomes active. These times are in general accord with the thunderstorm model of Byers and Braham as well as with the chronology based on Figure B-43 described above.

An estimate of cloud system "efficiency" is more questionable on the network scale than on the regional scale, since some of the rain from the clouds developing within the network fell outside and was not measured. Nevertheless, some general conclusions may be drawn from the accumulations of vertical moisture transport and rainfall in Fig. B-47. In this analysis, as in that on the regional scale, a uniform inflow is assumed through a layer 800 m deep.

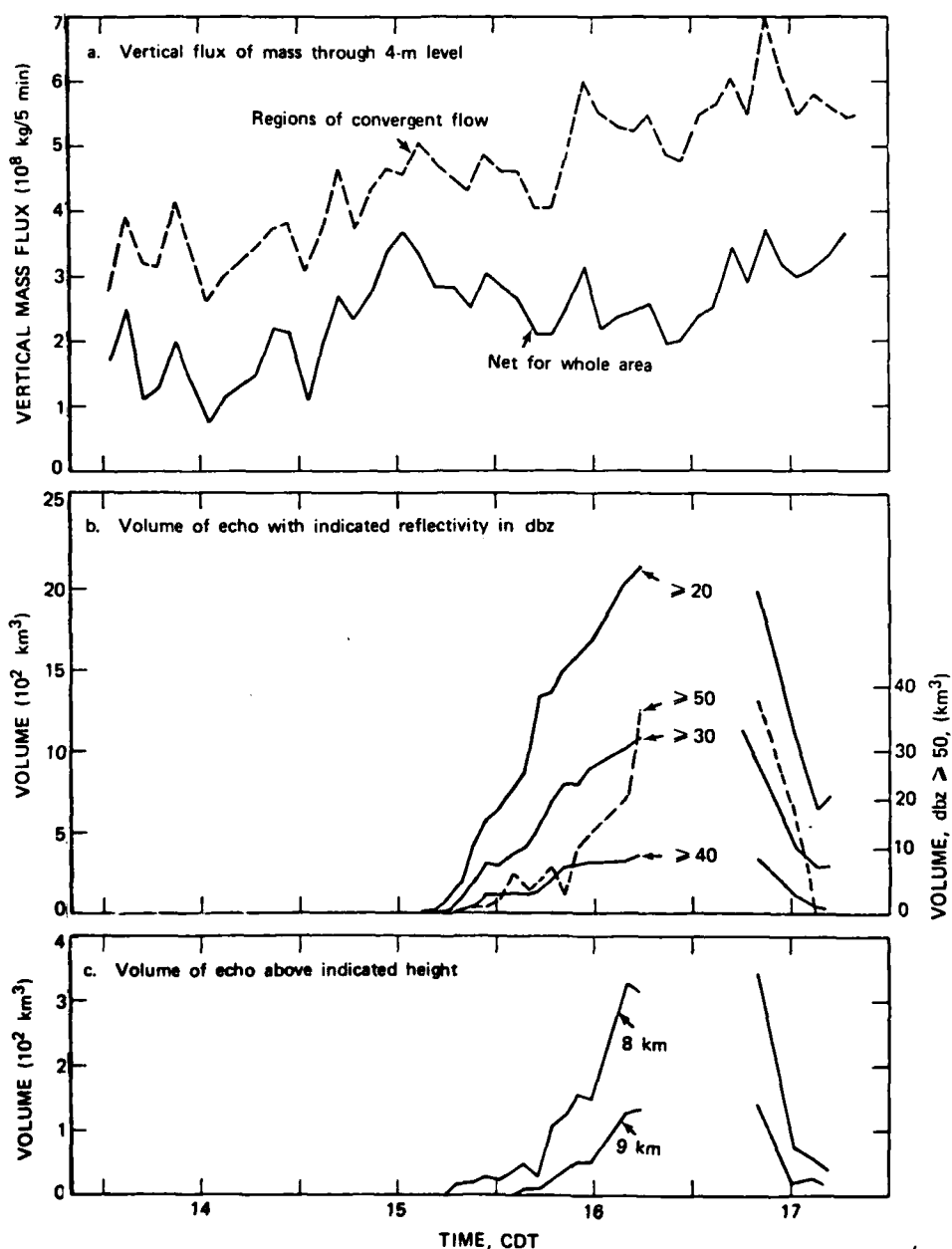


Figure B-45. Time profiles of (a) vertical flux of mass through anemometer level (b) volume of echo with reflectivity greater than or equal to indicated value and (c) volume of echo above 8 and 9 km. Note in (b) that curve for volume of echo with reflectivity ≥ 50 dbz has different scale than others. Area considered is northern 75% of that shown in Fig. B-43.

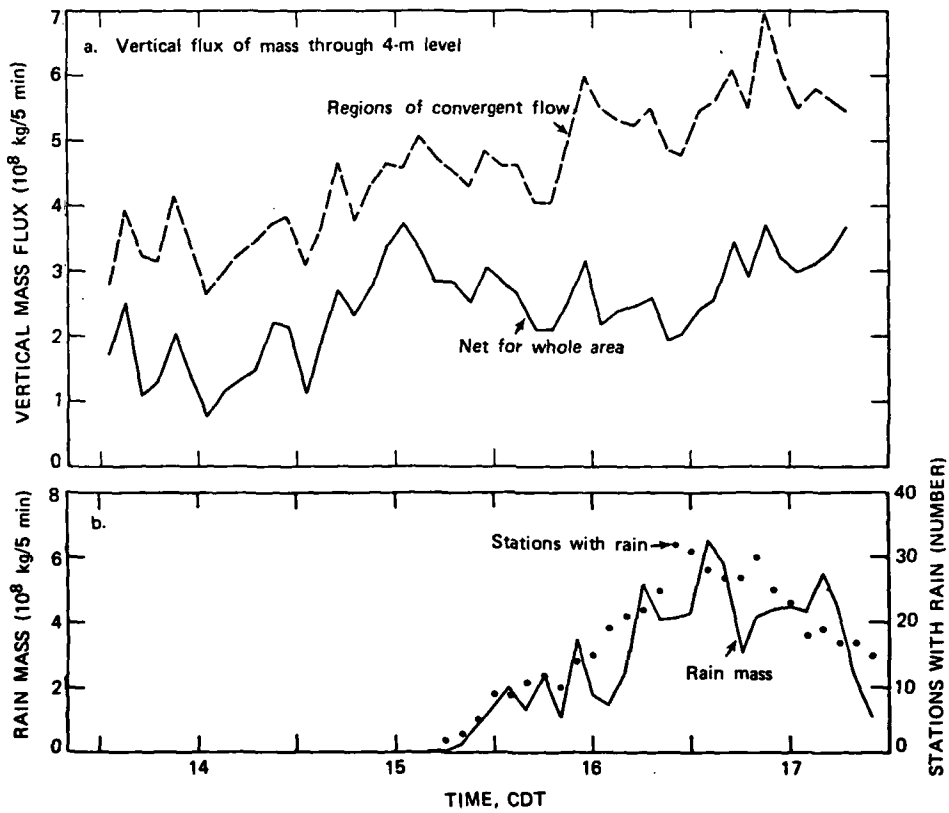


Figure B-46. Time profiles of (a) vertical flux of mass through anemometer level (as as Fig. B-45a) and (b) rain mass and rain coverage.

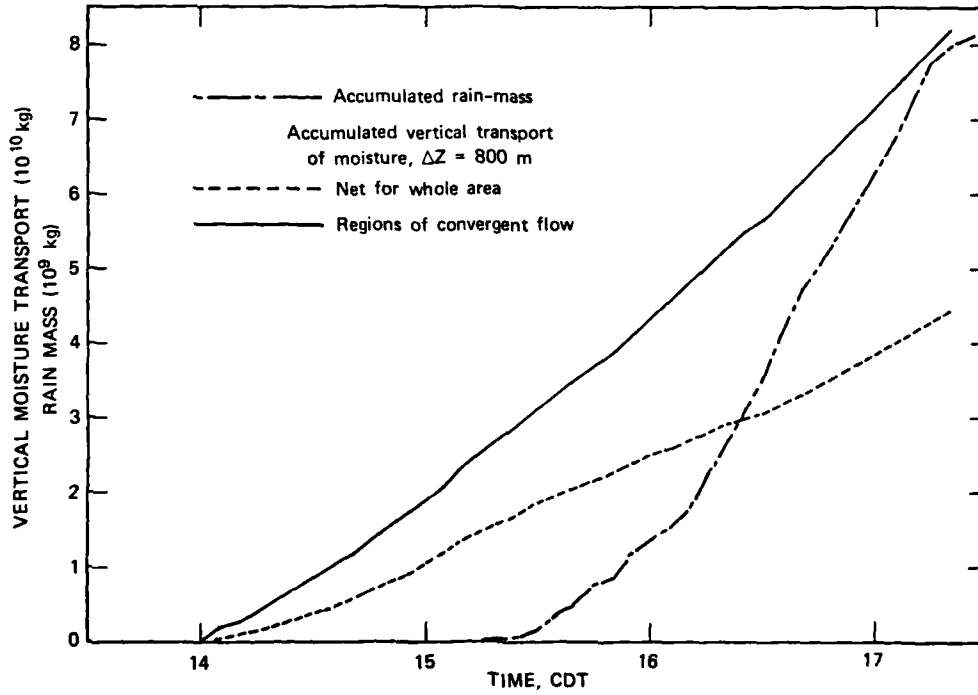


Figure B-47. Time profiles of accumulation of rain mass and vertical transport of moisture through 800 m for the northern three-fourths of the area covered in Fig. B-43 (dashed) and for the regions of convergent flow in that area (solid).

It is quite evident from a general inspection of the curves in Fig. B-47 that for the area considered, the "efficiency" of water usage, defined as fraction of moisture inflow returned to surface as rain, increased the longer it rained, and that the system was more efficient after 1610 than before. This is shortly after echoes began to grow to heights above 9 km. During the period when most of the rain was within the network, the cloud system returned about 10% of the low level vapor on which it fed, considering only the convergence areas, and about 18% for the area as a whole. If one considers the lag mentioned above as "processing time", these figures become slightly higher, 11% and 21% respectively. The maximum efficiency for areal moisture usage (assuming 20 min lags) for the rains prior to 1610 is 4.4% for convergence regions and 7.8% for the area as a whole.

Although not efficient in producing rain from the supply of low level moisture, these early clouds play an important role in transporting this moisture through a deeper layer and providing a more favorable environment for later cloud development.

5. SUMMARY

The heavy rainstorm which occurred over central and southern Illinois on 30 July 1979 developed slowly in a nearly stationary location in the warm sector of a wave cyclone. Unlike most of the prefrontal squall lines which occur in such systems, this storm was oriented nearly perpendicular to the cold front and, when fully developed, moved in a direction 30-45° to the right of the frontal movement. The evolution of this storm from two, well separated, isolated cloud clusters to a continuous line extending across the full width of Illinois appears to have been the result of complex interactions between processes occurring on a range of scales from synoptic to cloud scale.

The synoptic circulation provided the following conditions:

1. A warm, moist, conditionally unstable, tropical air mass.
2. Continued moisture advection throughout the morning and early afternoon.
3. Increasing instability due to warm air advection in the lower troposphere and cool air advection at higher elevations.
4. Moderate to weak winds ($<20 \text{ m s}^{-1}$) through most of the troposphere with relatively little directional shear.
5. Jet stream at 300 and 200 mb lying to the west, curving anticyclonically NE to Lake Superior with high level divergence over Illinois.

Thus atmospheric conditions were generally favorable for deep convection but no dynamic trigger could be identified on the synoptic scale.

Certain subsynoptic and meso- β scale (20-200 km) conditions in the morning and early afternoon were favorable for cloud development and release of the convective instability.

6. The circulation and cloud layers behind an MCC which crossed northern Illinois in the early morning hours resulted in cool, dry air over northern Illinois, thus establishing subsynoptic gradients in temperature and moisture in an otherwise homogeneous air mass.
7. Mesoscale perturbations in the low level winds over central Illinois resulted in two regions of convergent flow, one in east central Illinois and the other in west central Illinois.

The cloud line which was the precursor of the solid squall evolved, over a period of 4 hours, on the north side of the gradients in temperature and moisture mentioned in 6). The initial clouds were in two clusters, each downwind of the regions of convergent flow described in 7). These clusters slowly expanded into small E-W lines, but remained well separated for about 2 1/2 hours. Eventually the outflows from the precipitating clouds in the two lines

had sufficiently modified the low-level winds that the two regions of convergent flow merged. Almost simultaneously a cloud bridge formed between the two lines and a continuous cloud "line" extended from western Illinois to western Indiana. Subsequently the meso- β wind field was dominated by the storm circulation until the cold front and its associated pressure field entered Illinois.

The VIN network data indicated that local areas of convergence on the meso- α scale may, under circumstances with no strong larger-scale dynamic trigger, determine the location of new convection.

8. A persistent WSW-ENE band of convergence, parallel to the Sangamon River, was the southern border of early cloud development in the network.
9. Cloud-scale wind and pressure perturbations interacting with, and/or enhancing, this background convergent flow determined the evolution of the early clouds in the VIN network.

The persistent convergent flow provided a mechanism for a deepening of the moist layer and a favorable environment for convective cloud development. As the cloud began to precipitate, there was first an enhancement then a diminishment of the cells in the band of background convergent. When the small clouds merged and became more extensive, they established circulations in the low level flow which remained linked to, and moved with them. The background convergence cells tended to return to their original configurations and magnitudes as the clouds moved away.

The second period of rain in the VIN network came from the solid squall line. As this line evolved, it had a wave-like form. Initially the network was nestled in the apex of the wave. For the first 30 to 60 minutes, the winds were strongly affected by the outflow and associated gust fronts from precipitating cells to the north and west. This resulted in very strong mass inflow into the area and very rapid cloud growth. The convergence was greatest at the intersection of the two gust fronts which were advancing into the network at nearly right angles to each other. A mesocyclone associated with the gust front advancing from the west developed vorticity comparable in magnitude to that measured in tornadic storms. The center of this mesocyclone progressed ESE approximately along the intersection of the two advancing gust fronts.

The surface temperature and moisture fields also reflected the strong downdrafts which were associated with the individual cells in the advancing squall line. The surface values of θ_e were similar to minimum θ_e values in the layer from 700 to 760 mb; providing evidence of downdraft generation in this layer and possibly undiluted descent.

This second (and major) period of rains in the VIN network imposed a strong sinusoidal signature on the time profile of mass inflow into area, with very strong inflow prior to and during the early stages of the rain and strong outflow as the rain reached its maximum and moved out of the network. On the other hand, the early rain, which occurred during the early developmental period of the storm, did not impose this "typical" signature on the inflow

into the network. A reexamination of the inflow for a smaller area (the northern 75% of the network) which encompassed the convergence band and the clouds and associated rainfall indicates that there was a net inflow for at least 2 hours prior to the first rain. The mass and moisture inflow continually increased from the time that the cloud fields were changing from cumulus to cumulus congestus until local areas of divergent flow due to cloud outflow cancelled the increase in upward transport in regions of convergence.

A quantitative positive relationship was found between the temporal evolution of echo volume and the evolution of the upward transport in the local areas of convergent flow, particularly for the growth of the volume of echo above 8 or 9 km and of the echo volume with reflectivity above 50 dbz. A comparison of the temporal curves suggests that intensification of local areas of convergence may precede and induce rapid vertical cloud development. Superimposed on a generally increasing trend in upward transport in the regions of convergent flow were cycles of increases and decrease with periods of 40 to 60 minutes. Similar cycles were found in 5-minute accumulations of rain mass but with a lag of 20 to 30 minutes, a reasonable processing time for conversion of low level moisture conversion into rainfall.

Crude estimates of the precipitation efficiency of the early storm clouds in the VIN network indicate that the efficiency increased with time as the rain continued. For the full 2 1/2 hours that rain was falling within the network from the developing cloud, the rain mass was roughly 15% of the moisture fed into the cloud layer, whereas for the first half of the period only about 7% of the moisture was returned to the surface. Although not efficient in producing rain, these early clouds play an important role in transporting low level moisture into the cloud layer, and providing latent energy as for later cloud development. (These quoted values may be underestimates of the true efficiency, since the clouds were still precipitating as they moved off the eastern border of the network.)

Although the early clouds were not particularly efficient as far as producing rain, similar crude estimates indicate that the storm as a whole was highly efficient, with surface rain mass reaching 35-40% of the sub-cloud moisture transported upward in the storm area. Considering the continual supply of gulf moisture and containment of the rainstorm the area from which low level moisture was fed, these values, while sizable, do not seem unreasonable.

References

- Achtemeier, G. L., B. Ackerman, S. A. Changnon, P. Schickedanz, and R. G. Semonin, 1978: Illinois precipitation enhancement program (Phase 1) and design and evaluation techniques for High Plains Experiment. Atmospheric Sciences Section, Illinois State Water Survey, Final Report, Contract 14-06-D-7197, 210 pp.
- Barnes, 1978: Oklahoma thunderstorms on 29-30 April 1970. Part I: Morphology of a tornadic storm. Mon. Wea. Rev., 106, 673-684.
- Brandes, E., 1981: Fine structure of the Del City-Edmond tornadic mesocirculation. Mon Wea. Rev., 109, 635-647.
- Brock, F. V., and P. K. Govind, 1977: Portable automated mesonet in operation. J. Appl. Meteor., 16: 299-310.
- Chalon, J., J. Fankhauser, and P. Eccles, 1976: Structure of an evolving hailstorm, Part I: General characteristics and cellular structure. Mon. Wea. Rev., 104, 564-575.
- Cooper, H. J., M. Garstang, and J. Simpson, 1982: The diurnal interaction between convection and peninsular scale forcing over south Florida. Mon. Wea. Rev., 110, 486-503.
- Cressman, G. P., 1959: An operational objective analysis system. Mon. Wea. Rev., 87: 367-374.
- Fankhauser, J., 1976: Structure of an evolving hailstorm, Part II: Thermodynamic structure and airflow in the near environment. Mon. Wea. Rev., 104, 576-587.
- Fujita, T., and R. Wakimoto, 1981: Five scales of airflow associated with a series of downbursts on 16 July 1980. Mon. Wea. Rev., 109, 1438-1456.
- Gurka, J., 1976: Satellite and surface observations of strong wind zones accompanying thunderstorms. Mon. Wea. Rev., 104, 1484-1493.
- Holle, R., and M. Maier, 1980: Tornado formation from downdraft interaction in the FACE mesonet. Mon. Wea. Rev., 108, 1010-1028.
- Lemon, L. R., and C. Doswell, 1979: Severe thunderstorm evolution and mesocyclone structure as related to tornadogenesis. Mon. Wea. Rev., 107, 1184-1197.

Watson, A. I., and R. L. Holle, 1982: The relationship between low-level convergence and convective precipitation in Illinois and south Florida. Tech. Rept. No. 7, NOAA Environmental Research Laboratories, Office of Weather Research and Modification, Boulder, CO, and Illinois State Water Survey, Champaign-Urbana, IL.

Watson, A. I., R. L. Holle, J. B. Cunning, P. T. Gannon, and D. O. Blanchard, 1981: Low-level convergence and the prediction of convective precipitation in south Florida. Tech. Rept. No. 4, NOAA Environmental Research Laboratories, Office of Weather Research and Modification, Boulder, CO, and Illinois State Water Survey, Champaign-Urbana, IL. 228 pp.

**LATE
LME**